



Department of Information Science and Technology

SAGA – Smart Gateway for Adaptive Environments

Mariana Catela Jacob Rodrigues

A Dissertation presented in partial fulfillment of the Requirements for the Degree of

Master in Telecommunications and Computer Engineering

Supervisor

Prof. Dr. Francisco António Bucho Cercas, Full Professor,
ISCTE-IUL

Co-Supervisor

Prof. Dr. Octavian Adrian Postolache, Associate Professor,
ISCTE-IUL

September, 2019

Acknowledgements

I would like to express my sincere thanks and appreciation to professor Francisco Cercas for all the essential support, encouragement, fundamental advices and kind supervision.

I'm grateful of having professor Octavian Postolache as my supervisor and for all the constant support, kind help and guidance he has provided throughout the elaboration of this thesis.

It is a great honor to work under both your supervision.

I would also like to thank Mr. José Gouveia from Instituto de Telecomunicações of Instituto Superior Técnico for helping with the conception of the final assemblies of the system's sensor nodes.

A great thanks to Instituto de Telecomunicações of ISCTE-IUL for providing all necessary hardware material and resources for this thesis preparation.

I must express my gratitude to my family for all their encouragement, support and motivation, that substantially helped me going through this period, as well as for the precious help and encouragement of my friends and colleagues.

The work was supported by Fundação para a Ciência e Tecnologia, Project TailorPhy - PTDC/DTP-DES/6776/2014, Project UID/EEA/50008/2019 and Instituto de Telecomunicações.

Resumo

A criação de ambientes adaptativos tem o principal objetivo de providenciar o bem-estar a um indivíduo, melhorar as condições do ambiente em seu redor e de facilitar/automatizar qualquer atividade. De forma a implementar tais sistemas, a utilização de dispositivos com capacidade de intercomunicação e de recolha de parâmetros relacionados com o ambiente em redor do utilizador é essencial. Com a utilização de redes de sensores sem fios, é possível monitorizar os diversos índices de qualidade de um ambiente interior e dessa forma melhorar a qualidade de vida.

Nesta dissertação será apresentado um sistema baseado numa rede de sensores sem fios que permite analisar e melhorar a qualidade ambiental de espaços interiores e avaliar o estado de saúde de um indivíduo. O sistema adquire e atua sobre parâmetros relacionados com a qualidade do ar e qualidade de iluminação, assim como dados fisiológicos de um utilizador, através da utilização de nós de sensores e atuadores distribuídos pelo ambiente. Foram implementados diversos protocolos de comunicação sem fios para possibilitar a intercomunicação com outros elementos da rede, nomeadamente o nó coordenador/*gateway*. Foram configurados diversos mecanismos de alerta de forma a avisar o utilizador para a presença de fatores que possam colocar em risco a sua saúde, nomeadamente a presença de poluentes e condições térmicas que possam desencadear desconforto respiratório.

De forma a proporcionar uma análise de dados em tempo real, controlo do sistema e dispor de mecanismos de alerta adicionais, foi desenvolvida uma aplicação Web dedicada a este sistema. Através desta, o utilizador poderá tornar o ambiente adaptável às suas características e de acordo com as suas preferências, através da configuração de perfis.

Todo o processo de desenvolvimento do sistema, *hardware*, *software*, testes experimentais e contribuições serão incluídos nesta dissertação.

Palavras-Chave: Ambientes Adaptativos, Redes de Sensores sem Fios; Internet das Coisas; Qualidade do Ar; Qualidade de Iluminação; Medicina Ambiental; Desconforto Respiratório; Aplicação Web.

Abstract

The development of adaptive environments has the main objective of providing well-being to an individual, improving the environmental conditions of indoor environments and facilitating/automating any activity. In order to implement such systems, the use of devices capable of intercommunication and acquisition of environment-related parameters around the user is essential. Using wireless sensor networks, it is possible to monitor the various quality indices of indoor environments that can be used to develop strategies to improve quality of life of the users in personalized way.

In this dissertation, a system based on a wireless sensor network that analyses and improves the environmental quality of indoor spaces, as well as evaluating the health status of an individual is presented. The system acquires and acts upon air quality and illumination quality-related parameters, as well as physiological data of a user, using sensor nodes and actuators distributed throughout the environment. Several wireless communication protocols have been implemented to enable intercommunication between the several elements present in the sensor network, such as actuators, sensor nodes and a coordinating / gateway node. Several warning mechanisms have been configured to alert the user to the presence of factors that may endanger their health, namely the presence of pollutants and thermal conditions that may trigger respiratory distress.

In order to provide real-time system control including additional warning mechanisms, data analysis, a dedicated web application has been developed for this system. The user can control the environment according with his own needs and preferences through profiles configuration.

The whole process of system development, hardware, software, experimental tests and contributions are included in this dissertation.

Keywords: Adaptive Environments; Wireless Sensor Network (WSN); Internet of Things (IoT); Indoor Air Quality; Indoor Lighting Quality; Environmental Medicine; Respiratory Impairment; Cardiac Assessment; Web Application.

Contents

Acknowledgements	i
Resumo	iii
Abstract	v
Contents	vii
List of Tables	xi
List of Figures	xiii
List of Acronyms	xvii
Chapter 1	1
Introduction	1
1.1. Motivation.....	1
1.2. Objectives	3
1.3. Scientific Contributions	4
1.4. Structure of the Dissertation	5
Chapter 2	7
State of the Art	7
2.1. Environmental and human health assessment	7
2.1.1. Indoor Environmental Quality	7
2.1.1.1. Indoor Air Quality	8
2.1.1.2. Indoor Lighting Quality and Noise Health Effects.....	10
2.1.2. Cardiac Activity Monitoring using Ballistocardiography (BCG) and Photoplethysmography (PPG)	11
2.2. Internet of Things.....	13
2.3. Wireless Sensor Networks.....	15
2.4. Wireless Communication Protocols.....	17
2.4.1. 802.15.1 (Bluetooth).....	18
2.4.2. 802.11 (Wi-Fi).....	19
2.4.3. 802.15.4 (ZigBee).....	20
2.4.4. Long Range Communication.....	20

Chapter 3	21
System Hardware	21
3.1. System Architecture.....	21
3.2. Sensor Nodes	23
3.2.1. Embedded Computation	23
3.2.2. Node 1 – Thermal Conditions Measuring Node	30
3.2.3. Node 2 – Gas Sensing Node	34
3.2.4. Node 3 – Particulate Matter Measuring Node	44
3.2.5. Node 4.....	46
3.2.6. Node 5 – Cardiac Activity Monitoring Node	47
3.3. Actuator Nodes	50
3.3.1. Smart Lighting.....	50
3.3.2. Indoor thermal conditions.....	52
3.4. Coordinator Node / Gateway	53
Chapter 4	55
System Software	55
4.1. Embedded software.....	55
4.1.1. Sensor nodes data transmission	57
4.1.2. Sensor data reading and processing.....	58
4.1.2.1. Node 1 and Node 4 - Thermal Conditions Measuring Nodes	58
4.1.2.2. Node 2 - Gas Sensing Node.....	59
4.1.2.3. Node 3 – Particulate Matter Measuring Node	60
4.1.2.4. Node 5 – Cardiac Activity Monitoring Node	62
4.1.2.5. Deep sleep mode implementation on the ESP-32	63
4.2. Smart gateway.....	65
4.2.1. Actuators control	66
4.3. Data Storage.....	70
4.4. Web application	73

Chapter 5	83
Results	83
5.1. Data analysis of the sensor nodes	83
5.2. Power consumption	94
5.2.1. Node 1.....	94
5.2.2. Node 2.....	96
5.2.3. Node 3.....	97
5.2.4. Node 4.....	98
 Chapter 6	 99
Conclusions and Future Work	99
6.1. Conclusions	99
6.2. Future Work.....	100
References	101
Appendix A	107
Published Papers.....	107
Appendix B	103
Best Paper Award	103
Appendix C	121
Gas Sensors Datasheets	121

List of Tables

Table 2.1. Comparison of Bluetooth, Zigbee and Wi-Fi protocols	17
Table 3.1. Comparison between the ESP8266, the ESP32 and the Arduino Uno.....	24
Table 3.2. ESP-32 power consumption during Active mode.....	27
Table 3.3. ESP-32 power consumption during Modem and Light sleep modes	28
Table 3.4. ESP-32 power consumption during Deep sleep modes.....	29
Table 3.5. Types of Gas detected by each sensor.....	35
Table 3.6. Gas concentration in ppm and its associated volume of gas	39
Table 3.7. Sensitivity characteristic of MQ-135 for Alcohol.....	40
Table 3.8. Sensitivity characteristic of MQ-4 for CH ₄	42
Table 3.9. Sensitivity characteristic of MQ-9 for LPG.....	42
Table 3.10. Comparison between Philips Hue and Xiaomi Yeelight.....	51
Table 5.1. PM Concentration levels and the associated levels of air pollution.....	88

List of Figures

Figure 2.1. IEQ components	8
Figure 2.2. The different triggers of asthma distress.....	9
Figure 2.3. Natural light colour temperature changes throughout the day. Source [19].....	10
Figure 2.4. Electrocardiogram (ECG) and Ballistocardiogram (BCG) signals. Source: [11]	11
Figure 2.5. Electrocardiogram (ECG) and photoplethysmogram (PPG) signals	12
Figure 2.6. Global IoT market share by sub-sector. Source: [29].....	13
Figure 2.7. IoT typical architecture. Adapted from [33]	15
Figure 2.8. Wireless Sensor Network (WSN).....	15
Figure 2.9. WSN topologies: (a) Star Topology; (b) Mesh Topology; (c) Tree Topology.....	16
Figure 2.10. Bluetooth piconet possible configurations.....	18
Figure 2.11. IEEE 802.11 Architecture	19
Figure 3.1. System Architecture with a device layer composed of three actuator nodes and four sensor nodes.....	22
Figure 3.2. a) ESP8266 and b) ESP32.....	23
Figure 3.3. Functional Block Diagram of the ESP32's chip. Source: [47]	26
Figure 3.4. Active features of ESP-32 during Active mode.....	27
Figure 3.5 Active features of ESP-32 during Modem and Light Sleep mode.....	28
Figure 3.6. Active features of ESP-32 during Deep Sleep mode	29
Figure 3.7. Environmental parameters measured by Node 1	30
Figure 3.8. Temperature and Relative humidity sensor - Si7021	31
Figure 3.9. Light Dependent Resistor (LDR) exemplar	32
Figure 3.10. Photocell resistance dependency with the incident illumination	32
Figure 3.11. Electret Microphone Amplifier - MAX9814	32
Figure 3.12. Schematic circuit of Node 1	33
Figure 3.13. First prototype of Node 1	33
Figure 3.14. PCB schematic of Node 1	33
Figure 3.15. Node 1	34
Figure 3.16. Exemplar of a MQ series Gas Sensor	35
Figure 3.17. Gas sensing unit circuit (V_c – circuit voltage, H – heater, V_{out} – gas sensor output, R_L – load resistance).....	36
Figure 3.18. Node 2 circuit schematic	36
Figure 3.19. First prototype of Node 2	37
Figure 3.20. PCB schematic of Node 2	37
Figure 3.21. Node 2	37
Figure 3.22. Figaro gas test chamber.....	38
Figure 3.23. Sensitivity characteristics of the MQ-135 for CO_2 , CO, Alcohol, NH_4 , Toluene and Acetone	40
Figure 3.24. Sensitivity characteristics of the MQ-135 gas sensor in the presence of Alcohol	40
Figure 3.25. Sensitivity characteristics of the MQ-4 for LPG, CH_4 , H_2 , CO, Alcohol and Smoke	41
Figure 3.26. Sensitivity characteristics of the MQ-9 for LPG, CO and CH_4	41
Figure 3.27. Sensitivity characteristic of the MQ-4 gas sensor in the presence of CH_4	42
Figure 3.28. Sensitivity characteristic of the MQ-9 gas sensor in the presence of LPG	43

Figure 3.29. Shinyei PPD42NS and its inner components	44
Figure 3.30. De-construction of the Shinyei PPD42NS. Source: [60]	45
Figure 3.31. Node 3, with a Shinyei PPD42NS particle counter	45
Figure 3.32. Node 4 circuit schematic	46
Figure 3.33. PCB schematic of Node 4	46
Figure 3.34. Node 4	46
Figure 3.35. EMFIT sensor of the L-series	47
Figure 3.36. BCG charge amplifier scheme	48
Figure 3.37. Pulse sensor for PPG	48
Figure 3.38. Physiological parameters measurement system with BCG and PPG sensing units embedded on a chair	49
Figure 3.39. Scheme of interaction between the coordinator node and the actuator nodes	50
Figure 3.40. Xiaomi's Yeelight LED Light Bulb	52
Figure 3.41. Xiaomi's Yeelight Lightstrip (Color)	52
Figure 3.42. Smart gateway - Raspberry Pi 3 B+	53
Figure 4.1. Interaction flow between the Sensor node and Coordinator node	56
Figure 4.2. Callback function to detect new client connection events	57
Figure 4.3. Sound sensor signal conversion	59
Figure 4.4. Conversion of gas sensor's readings into gas concentration levels	60
Figure 4.5. Lo Pulse Occupancy time example. Source [63]	60
Figure 4.6. PPD42NS characteristic graph. Source [63]	61
Figure 4.7. PPD42NS estimation of the particle's concentration per 0.01cf	61
Figure 4.8. ESP-32 printed messages while deep sleep mode is configured	64
Figure 4.9. Interaction flow between the Coordinator node and Sensor nodes	65
Figure 4.10. Smart light's color temperature variance throughout the day	67
Figure 4.11. Acuator's control logic performed by the Coordinator node	68
Figure 4.12. Database structure	70
Figure 4.13. Database structure for Node 1	72
Figure 4.14. Flow of interaction between the Web application and the database	73
Figure 4.15. Login form of the web application	74
Figure 4.16. JavaScript method to authenticate a user on the web application	75
Figure 4.17. Authentication process of Firebase Authentication SDK	76
Figure 4.18. Dashboard of the web application with temperature, relative humidity, light color temperature and air quality estimation in real-time	76
Figure 4.19. Available pages on the web application	77
Figure 4.20. Dashboard and notification message viewed on the smartphone	78
Figure 4.21. Sensor nodes location and their respective data displayed on the web application	79
Figure 4.22. User Profile page with the change of thresholds and their update on the database	80
Figure 4.23. Heart Rate Measurements page with data collected from the biomedical node	81
Figure 5.1. Spatial distribution of the sensor nodes	83
Figure 5.2. Distributed temperature a) and relative humidity b) measurements during 24h.	84
Figure 5.3. Distributed temperature a) and relative humidity b) measurements for 1 week	85
Figure 5.4. Gas Concentration variation in PPM for different volumes of injected Ethanol (MQ-135 gas sensor)	86

Figure 5.5. Particulate Matter (pcs/0.01 cf) over time for the first testing scenario.....	87
Figure 5.6. Particulate Matter (pcs/0.01 cf) over time for the second testing scenario..	88
Figure 5.7. Sample of a BCG wave collected from the EMFi sensor embedded on a chair	89
Figure 5.8. BCG waves collected from the EMFi sensor embedded on a chair.....	90
Figure 5.9. EMFi sensor signals acquired by the ESP32 microcontroller.....	90
Figure 5.10. PPG waves collected from the pulse sensor.....	91
Figure 5.11. Screenshot of the “Heart Rate Measurements” webpage.....	91
Figure 5.12. Recorded heart rate data of subject n°1 for 20 minutes while resting on a chair	92
Figure 5.13. Real-time heart rate statistics of subject n°1	93
Figure 5.14. Recorded heart rate data of subject n°2 for 25 minutes	93
Figure 5.15. Real-time heart rate statistics of subject n°2	94
Figure 5.16. Current consumption of of Node 1 while: (1) Waiting for connection, (2) Transmitting data, (3) Deep Sleep mode	95
Figure 5.17. Current values of Node 1 while: (1) Waiting for connection, (2) Transmitting data, (3) Deep Sleep mode	95
Figure 5.18. Current consumption of Node 2 while: (1) on Deep Sleep Mode, (2) Waiting for connection, (3) Transmitting data, (4) Current variations when in presence of Ethanol	96
Figure 5.19. Current values of Node 2 while: (1) on Deep Sleep Mode, (2) Waiting for connection, (3) Transmitting data.....	96
Figure 5.20. Current consumption of Node 3 while: (1) on Deep Sleep Mode, (2) Transmitting data.....	97
Figure 5.21. Current values of Node 3 while: (1) on Deep Sleep Mode, (2) Transmitting data	97
Figure 5.22. Current consumption of Node 4 while: (1) on Deep Sleep Mode, (2) Waiting for connection, (3) Transmitting data	98
Figure 5.23. Current values of Node 4 while: (1) on Deep Sleep Mode, (2) Waiting for connection, (3) Transmitting data.....	98

List of Acronyms

ADC	Analog to Digital Converter
AES	Advanced Encryption Standard
AGC	Automatic Gain Control
BCG	Ballistocardiography
BLE	Bluetooth Low Energy
BPM	Bits Per Minute
BSS	Basic Service Set
CAN	Controller Area Network
COPD	Chronic obstructive pulmonary disease
CPU	Central Processing Unit
CSS	Chirp Spread Spectrum
DAC	Digital to Analog Converter
DS	Distribution System
ECC	Error-Correcting Code
ECG	Electrocardiogram
EMFi	Electromechanical Film
EPA	Environmental Protection Agency
ESS	Extended Service Set
FFD	Full-Function Device
GPIO	General-Purpose Input/Output
GUI	Graphical User Interface
HTTP	HyperText Transfer Protocol
HR	Heart Rate
I2C	Inter-Integrated Circuit
IAQ	Indoor Air Quality
IBI	Inter-Beat Interval

IBSS	Independent Basic Service Set
IDE	Integrated Development Environment
IEEE	Institute of Electrical and Electronics Engineers
IEQ	Indoor Environmental Quality
IIR	Infinite Impulse Response
IoT	Internet of Things
IR	Infrared Radiation
ISM	Industrial, Scientific and Medical radio band
LAN	Local Area Network
LDR	Light Dependent Resistor
LED	Light-Emitting Diode
LPDDR2	Low-Power Double Data Rate Synchronous Dynamic Random-Access Memory
LPF	Low Pass Filter
LPO	Low Pulse Occupancy
MCU	Microcontroller Unit
MIMO	Multiple Input Multiple Output
MQTT	Message Queuing Telemetry Transport
OS	Operative System
OTA	Over-The-Air
PCB	Printed Circuit Board
PHY	Physical Interface Device
PM	Particulate Matter
PMU	Phasor Measurement Unit
PPG	Photoplethysmography
PPM	Parts Per Million
PWM	Pulse Width Modulation
QPSK	Quadrature Phase-Shift Keying Modulation
RDF	Reduce-Function Device
RWD	Responsive Web Design
RH	Relative Humidity

RNG	Random Number Generator
RTC	Real Time Clock
SDIO	Secure Digital Input Output
SHA-2	Secure Hash Algorithm 2
SoC	System on a Chip
SPI	Serial Peripheral Interface
SQL	Structured Query Language
SRAM	Static-Random Access Memory
UART	Universal Asynchronous Receiver-Transmitter
ULP	Ultra-Low Power
USB	Universal Serial Bus
WHOAQG	World Health Organization Air Quality Guidelines
WLAN	Wireless Local Area Network
WPAN	Wireless Personal Area Network
WSN	Wireless Sensor Networks

Chapter 1

Introduction

1.1. Motivation

Adaptive environments are essential in ensuring maximum comfort and well-being of an individual. Adaptable to everyone's own characteristics, these types of environments are formed by an ecosystem of devices that interact with each other, such as smart sensors, actuators and embedded systems. Wireless Sensor Networks (WSN), a technology often used within an Internet of Things (IoT) system, makes these smart environments possible, providing the user not only a better understanding of the surrounding environment but also the possibility of adapting and controlling it for its own benefits. Hence, several factors are considered in the development and implementation of an adaptive environment, namely the monitoring of Indoor Environmental Quality (IEQ) levels and some physiological parameters.

Indoor Air Quality represents one of the Indoor Environmental Quality [1] sub-domains, and it is the most crucial factor that determines the quality of indoor environments. Air pollution is considered one of the greatest environmental risks for human health and it can lead to a variety of health problems related to respiratory diseases. Chronic obstructive pulmonary diseases (COPD) and asthma are among the most common respiratory illnesses and can be prevented by monitoring certain air quality parameters. These parameters are generally air pollutants that are widely present in urban areas, such as particulate matter (PM), ozone (O₃), sulphur dioxide (SO₂), nitrogen oxides (NO_x) and carbon monoxide (CO) [2], and can be found in both indoor and outdoor environments. Air pollution needs to be considered specially in indoor environments: according to the U.S Environmental Protection Agency (EPA) [3], levels of pollutants can be exponentially higher in indoor environments than outdoors. Since population spends most of their time inside buildings, these factors are of great concern. Some of these pollutants come from inside home - indoor building materials, furnishings,

appliances, and human activities – and can potentially aggravate respiratory distress and asthma attacks. According to the study in [4] several pollutants present in the air are associated with asthma-related hospital emergencies, from which PM10, NO2 and O3 are the major contributors that potentially aggravate this respiratory illness.

There are two major approaches that reduce the pollution levels of these air contaminants: one is to increase the ventilation rate of outdoor air into the building, which will only work if outdoors air is clean enough; the other is to reduce or control the sources of pollutants, within and outside the building [1]. This second approach however proves to be quite difficult to achieve, specially the reduction of outdoor sources of pollutants in urban environments.

The monitoring of relative humidity levels is also an important step to prevent acute respiratory distress or asthma attacks. Even though relative humidity is not considered an indoor contaminant or a cause of health problems, it has many direct and indirect effects on an individual's health and comfort [5].

Some types of health-related symptoms can also be induced by the lack of some other IEQ components, such as poor lighting quality. A good lighting quality not only plays an important role in an individual's visual capacity, but also has many positive biological effects. Therefore, the development of a system with smart lighting that automatically changes the colour temperature and illuminance levels of light throughout the day is of major importance.

Having a special focus on providing tools to improve home healthcare and assisted living options, some physiological parameters and motion status can be measured in non-invasive ways. To monitor these physiological signs without the use of obtrusive procedures, embedded sensors can be placed in office chairs, wheelchairs and beds. In this way, it is possible to assure the patient's comfort and provide a user-friendly cardiovascular examination [6].

Many projects have used EMFi (Electromechanical Film) sensors for healthcare purposes, since they can acquire ballistocardiograms (BCG) in unobtrusive ways [6]-[13]. These EMFi sensors are plastic films that can convert mechanical energy to an electrical signal. The sensor's structure is based on several thin polypropylene layers separated by air voids [14]. The thickness variation of these air voids, which happens when pressure is applied on the sensor, generates electrical charges on its electrically conductive surface, that can be measured as a voltage signal at the output of a charge amplifier.

Additionally, sensors that work on the principle of photoplethysmography (PPG) also acquire physiological data in non-invasive ways. These sensors provide highly accurate data and can be used to determine the user's heart rate and heart rate variability.

There are several projects that use embedded sensors in office chairs for cardiac activity monitoring, but there are few that reconcile the monitoring of these physiological parameters with the adaptation and personalization of the surrounding environment.

1.2. Objectives

Main Objective: Considering all previously mentioned factors, the main objective of this dissertation is the development of a WSN that materializes an environmental quality (IEQ) analysis system and provide healthcare assessment by monitoring cardio-respiratory parameters of the users.

Objective 1: The WSN must perform sensory data acquisition and execution of commands for distributed actuators in the environment, through the implementation of wireless and wired communication interfaces, such as Wi-Fi, Bluetooth, USB and I2C. These sensors have the function of monitoring air quality, noise levels, illuminance levels and acquiring some physiological parameters of the user. For this purpose, the WSN will:

- Collect information from distributed sensors and other agents to alert the user to the presence of harmful pollutants and subsequently improve air quality through actuators;
- Gather information related to the indoors lighting quality and control light's colour temperature and intensity levels, to enhance its positive biological effects on the human body;
- Collect temperature and relative humidity data and change it if necessary, with the use of actuator nodes, as well as monitor noise levels and alert the user if they exceed the tolerance limits;
- Monitor the user's heart rate and change the surrounding environment with actuator nodes according to its cardiac activity.

Objective 2: Development of a user-friendly web application to provide data analysis, full remote control over the system and additional alert mechanisms. Through this application, profiles need to be created according to the individual preferences and characteristics of the user, so that the environment adapts to it as best as possible.

1.3. Scientific Contributions

The elements and results of this research resulted in two scientific articles, both published and presented at a national and international conference, respectively:

- M. J. Rodrigues, O. Postolache, and F. Cercas, “Wireless Sensor Network for Indoor Air Quality Monitoring”, *11th Conference on Telecommunications (Conftele 2019)*, Lisbon, Portugal, 2019;
- M. J. Rodrigues, O. Postolache, and F. Cercas, “Indoor Air Quality Monitoring System to Prevent the Triggering of Respiratory Distress”, *2nd International Symposium on Sensors and Instrumentation in Internet of Things Era (ISSI 2019)*, Lisbon, Portugal 2019;

The project was also presented and demonstrated in two workshops, both organized by the IEEE Instrumentation & Measurement Society Portugal Section, Instituto de Telecomunicações and ISCTE-IUL:

- “WSN for Indoor Air Quality Monitoring“, 1st Workshop on Technologies for Everyday Life, May 13th, 2019.
- “Indoor Air Quality Monitoring System to Prevent the Triggering of Respiratory Distress”, 2nd Workshop on Technologies for Everyday Life, July 26th, 2019.

1.4. Structure of the Dissertation

This dissertation is organized in 6 chapters, where the different phases for the development of this system and its experimental results are described.

- Chapter 2 includes literature review on how environmental and human health assessment can be achieved, the internet of things concept, wireless sensor networks and the different wireless communication protocols.
- Chapter 3 describes the whole system's architecture, presenting detailed descriptions of every developed node of the wireless sensor network.
- Chapter 4 includes the system's software description, with detailed information about the embedded software, smart gateway, data storage and the web application.
- Chapter 5 presents all the achieved experimental results done in real case scenarios, as well as the results of applying energy saving strategies.
- Chapter 6 summarizes the obtained results of this research and some future work that can be done to improve the system even more.

Chapter 2

State of the Art

In this chapter, the various research topics relevant to the development of this project are presented. In Section 2.1, the main reason why an indoor environmental quality monitoring system is required and what impact it has on human health is described. A method to record and monitor the user's health status, namely cardio-respiratory parameters, is also presented. In Section 2.2, the IoT concept is addressed by explaining how this technology is used and how it works. In Section 2.3, wireless sensor networks are explained, followed by Section 2.4, where the different available communication techniques used with these technologies are discussed.

2.1. Environmental and human health assessment

This section describes the different environmental factors that have a great influence on human health. Some information about the monitoring of physiological parameters that integrate health assessment systems is also provided.

2.1.1. Indoor Environmental Quality

Indoor Environmental Quality (IEQ) is an indicator of the general quality conditions of indoor environments that may have an impact on human's health. The IEQ indicator is composed of multiple sub-domains [1], as depicted in Fig. 2.1.



Figure 2.1. IEQ components

2.1.1.1. Indoor Air Quality

Air pollution is one of the greatest risks for human health. It can potentially cause numerous respiratory problems such as asthma, chronic obstructive pulmonary disease (COPD), allergies, and in a more extreme case, lung cancer. While most people are aware that outdoor air pollution has a major impact on their health, few have the idea that indoor pollution can be far more harmful. According to the United States Environmental Protection Agency (EPA) [3], indoor pollution levels can be 2 to 5 times higher than in outdoor environments. Since population usually spends approximately 90% of their time inside buildings, these factors are of great concern.

Particulate matter (PM), ozone (O₃), sulphur dioxide (SO₂), nitrogen oxides (NO_x) and carbon monoxide (CO) [2] are the most common air pollutants present in urban areas and can either be formed by both outdoor and indoor sources of pollution. Outdoor air pollutants greatly affect indoor environments, since the air exchange between these two environments is constantly done through mechanical ventilation and natural ventilation [15]. However, most of pollutants created by indoor sources have a greater impact on indoor air conditions. These pollutants usually come from as combustion sources, cleaning products, air conditioners (without maintenance), smoke, cooking oils, building materials, and many other indoor sources.

As noted above, asthma and chronic obstructive pulmonary disease (COPD) are two respiratory diseases that are potentially aggravated by poor air conditions. Asthma attacks can be triggered by exposure to allergens, such as pollen, or other biological contaminants, such as dust mites, pet dander, smoke, perfumes and strong odours [16].

In addition to these biological contaminants, CO, PM₁₀, NO₂, and O₃ are air pollutants that are largely associated with asthma-related hospital emergencies. Therefore, the monitoring and control of this air pollutants is a very important step to address these IAQ related issues.

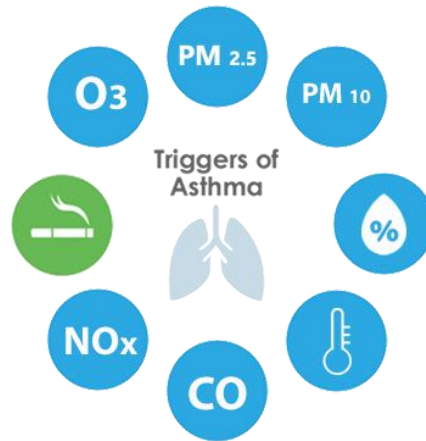


Figure 2.2. The different triggers of asthma distress

In addition to these air pollutants, relative humidity is also a major triggering factor of asthma exacerbations. Even though it is not considered an indoor contaminant, it has both direct and indirect effects on an individual's health and respiratory comfort. The direct effects are the impact of relative humidity on human physiological processes, whereas the indirect effects consist on the impact of relative humidity on infectious or allergenic organisms [5].

A relative humidity between 40%-60% is ideal for indoor environments, as it minimizes most adverse health effects. Values above 60% will turn the air harder to breath – besides narrowing and tighten the airways, humidity also makes the air stagnant and traps the pollutants and allergens, which can help trigger asthma attacks [17].

COPD exacerbations, for instance, are often triggered by viral or bacterial respiratory infections (70-80%), where the remaining 20-30% are related with exposure to environmental pollution [18], such as tobacco smoke and biomass-burning smoke.

2.1.1.2. Indoor Lighting Quality and Noise Health Effects

The symptoms described in the previous section are not necessarily caused by poor air quality. Not only indoor lighting quality plays an important role in an individual's visual ability, but also has several positive biological effects. The benefits of adapting both light levels and colour throughout the day in indoor environments are numerous. Adequate lighting levels during the day and night can regulate circadian sleep-wake rhythms and vastly improve an individual's health, productivity and comfort, as presented in the literature [19]-[21]. Circadian lighting is a concept that is becoming often present in various sectors, from healthcare to corporate. It follows the circadian rhythm, a 24-hour internal clock that cycles between sleepiness and alertness at regular intervals. Lightness and darkness have a direct impact on this sleep-wake rhythm. The eyes send signals to an area of the brain called hypothalamus, that will report if it's night-time or daytime. The hypothalamus, in turn, controls the amount of melatonin that needs to be released, associating sleepiness with darkness and alertness with lightness [22]. Given that most of the population don't have access to natural light in their working environments and at home, they are often subjected to electric light. Electric light is usually kept at certain wavelengths of blue light at great amounts of time, which can lead to negative impacts on melatonin production. Smart lighting systems have been recently helping to address these problems. Capable of changing light temperature colour and light intensity, these systems can be used to support human health and regulate sleep-wake rhythms.

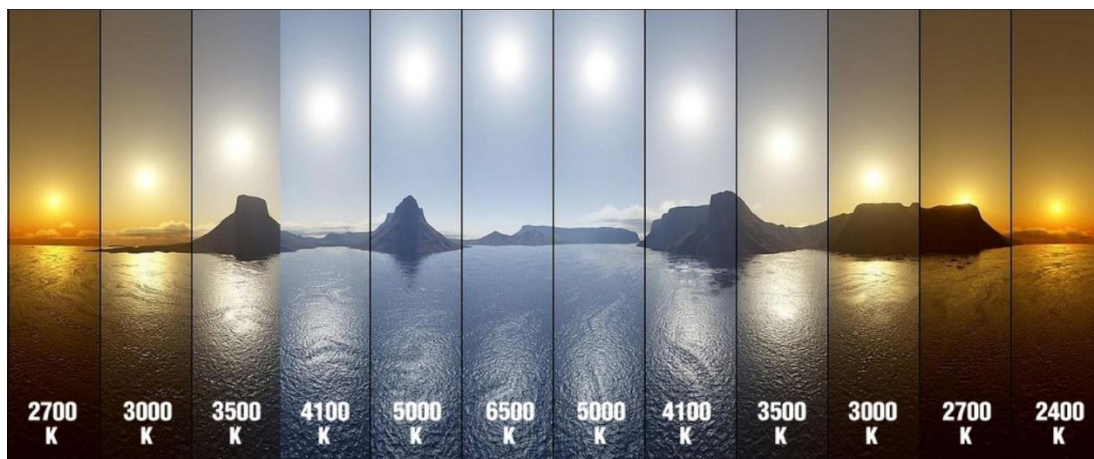


Figure 2.3. Natural light colour temperature changes throughout the day. Source [19]

With population growth, increased vehicular traffic and industrial activities, noise is increasingly present in the daily lives of millions of people. The notion of noise may vary from individual to individual, depending on their subjectivity or auditory sensitivity. Problems such as sleep disturbances, stress, difficulty in communication between people and loss of concentration are among the most frequent effects caused by this physical agent [23][24]. Monitoring noise levels is an equally important factor in ensuring the productivity, well-being and health of an individual.

2.1.2. Cardiac Activity Monitoring using Ballistocardiography (BCG) and Photoplethysmography (PPG)

Ballistocardiography (BCG) is a technique used to measure repetitive motions of the human body associated with cardiac contraction and ejection of blood in the vessels. It is one of the oldest non-invasive methods for cardiac-respiratory monitoring and can be used to get information about the activity of the heart, its condition and breathing patterns [10].

Its graphic representation consists of the action-reaction force caused by the heartbeat and the pump of blood through the aorta [11].

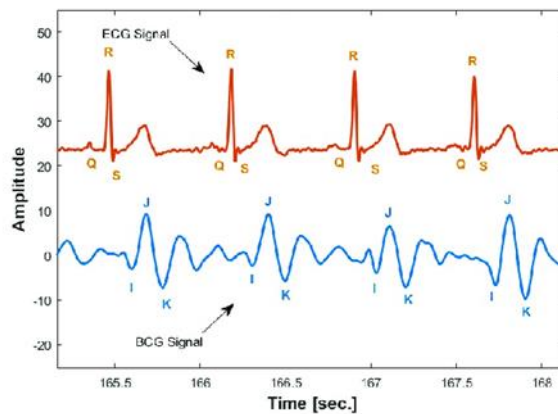


Figure 2.4. Electrocardiogram (ECG) and Ballistocardiogram (BCG) signals. Source: [11]

Figure 2.4. shows an example of the BCG waveform and its comparison with an ECG wave. The IJK wave complex from the BCG is equivalent to the QRS from an electrocardiogram. These main waves and time intervals between them reflect the physiological condition of the subject's heart and its main blood vessels. The IJK zone represents the ejection phase of the cardiac cycle and it is the most studied wave complex

[12]. Regarding the acquisition of the associated cardiac frequency, a simple peak detection, such as the J peak, or a comparison with voltage thresholds can be performed.

The monitoring of these physiological parameters can be performed by two types of BCG systems [9]: 1) a BCG monitoring system that requires a mechanical connection between the subject's body and the sensor, 2) a BCG monitoring system that does not require mechanical connection between the human body and the sensing unit. Ballistocardiograph devices that do not require mechanical contact are, for example, ultrasonic sensors [25] and Doppler radar [26]. The main devices that require mechanical contact are the piezoelectric sensors, the load cells, sternal accelerometers and electromechanical film sensors.

Considering the robustness and the numerous researches already done with electromechanical sensors, the BCG monitoring system will be based on a lightweight and flexible electromechanical film (EMFi) sensor.

Photoplethysmography (PPG) is an optical measurement method that is often used to monitor heart rate. It is considered a non-invasive method, as it uses a light source and a photodetector at the surface of skin to measure the volumetric variations of blood circulation in veins [27]. The absorption or reflection of light depends on the quantity of blood that is going through the veins and thus, in the optical path [28]. The PPG signal is related to changes in the volume of blood, which is associated with a heartbeat.

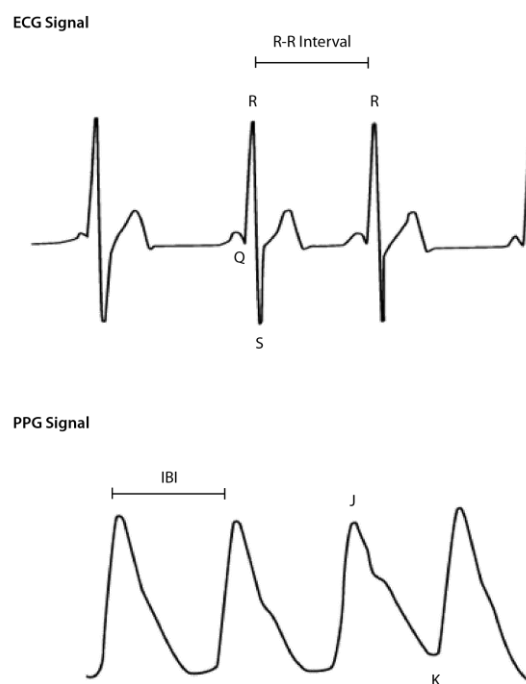


Figure 2.5. Electrocardiogram (ECG) and photoplethysmogram (PPG) signals

The mark of a heartbeat is done differently when comparing an ECG with PPG. Using an ECG, it is usually the R peak of the QRS complex that signals a heartbeat. On a PPG signal, instead of measuring R-R intervals, the interbeat intervals (IBI) are measured. Figure 2.5 shows the typical waveform of an ECG and PPG signal.

2.2. Internet of Things

Nowadays, with technological expansion delineating our future, there are numerous studies carried out in this area. As a result of technological advancements, the concept of Internet of Things (IoT) emerges.

IoT is a term used to describe an object that is connected to the Internet. More precisely, an object that communicates with other objects that are also connected to the Internet. These objects can be small sensors, smartphones, wearable devices, vehicles or appliances, such as toasters, refrigerators, washing machines and lighting. It is a theme widely explored by Industries and academia, due to its great potential in simplifying human activities and improving their living conditions.

Based in Figure 2.6, it is possible to affirm that by 2020 the global market for IoT will be dominated by three sub-sectors: Smart Cities (26%), IoT for Industry (24%) and IoT for Health (20%). Smart Homes (14%) are the fourth dominant market [29].

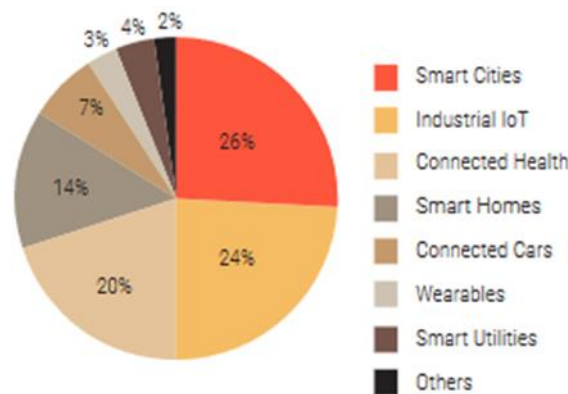


Figure 2.6. Global IoT market share by sub-sector. Source: [29]

It is estimated that in 2020 there will be about 30 billion devices using IoT [30]. This means that IoT will be vastly used in the future and it will be present in almost every environment and in everyone's lives.

An IoT system is usually composed by four different elements: sensors, gateways, cloud services and a user interface [31].

1. Smart sensors

Sensors are continuously collecting environmental data. They can be temperature and humidity sensors, air quality sensors, pressure sensors, light intensity sensors, among others. In order to communicate with each other and in order to receive their readings, they are generally connected over wireless networks such as Wi-Fi, Bluetooth, ZigBee, LoRa, etc.

2. Gateway

Gateways can be physical devices (e.g. Raspberry Pi) or software programs and have the function of allowing the flow of information between different networks through wireless communication protocols. It serves as a connection point between the Cloud and the sensor / device nodes.

Gateways can also be configured to pre-process locally the collected data from sensors before it is sent to the Cloud. In this way, the volume of data that needs to be routed to the Cloud is reduced, thus improving response times and network transmission costs [32].

3. Cloud and Data Processing

Cloud services can provide a set of tools for gathering, processing, managing and storing large amounts of data in real-time. While sensors and devices collect data and perform actions, all processing, commands and analysis are typically done in the Cloud.

4. User Interface

The collected and already processed information becomes useful to the user through the User interface. It is the visible and tangible part of the IoT system, and it is where the user can see all the information related to the system. In an air quality monitoring system, this information is typically sensory data from the distributed sensors, the current air quality, graphs with different measured pollutants at a certain time of the day, etc. It also gives the user manual control over the system.

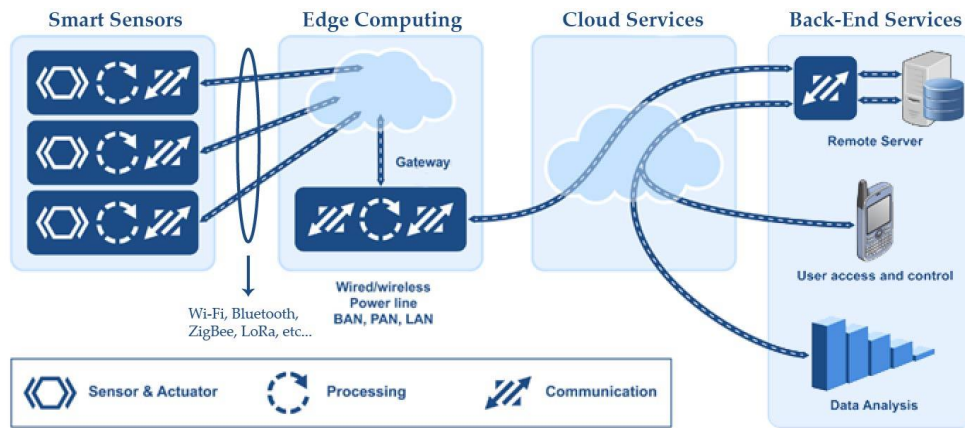


Figure 2.7. IoT typical architecture. Adapted from [33]

2.3. Wireless Sensor Networks

Wireless sensor networks (WSN) have been one of the most researched areas over the past years [34]. A WSN is defined by a set of devices usually called sensor nodes. These nodes are usually scattered in a sensor field and have the capability of collecting data and route data back to a coordinator node/gateway [35][36]. Each sensor node is characterized by four basic components: a sensing unit, with one or more sensors for data acquisition, a processing unit, a transceiver unit and a power unit. Through the transceiver unit, the nodes can communicate with each other over wireless or wired protocols, being wireless technologies considered the best choice for such devices. The coordinator node either uses the data to perform local tasks or sends it to the cloud over the internet for data processing. Figure 2.8 illustrates the typical architecture of a WSN.

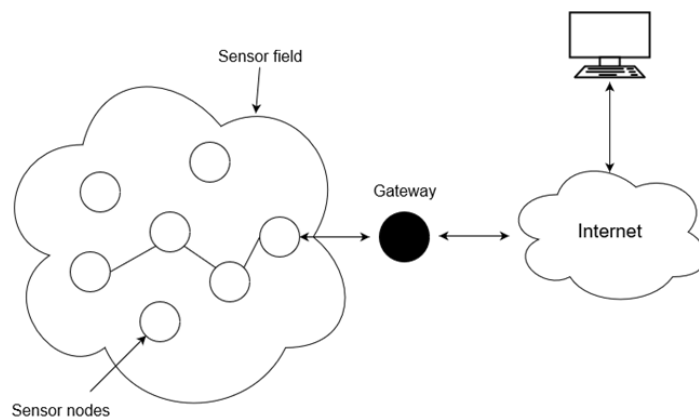


Figure 2.8. Wireless Sensor Network (WSN)

WSNs can be expressed in multiple topologies that are following mentioned: Star, Mesh, Tree topologies and many more [37].

A. Star Topology

In this topology, shown in Figure 2.9 a), each sensor node is connected to a centralized node – the coordinator node. The nodes cannot communicate directly with each other, since the entire communication must be routed through the coordinator node.

It is one of the most common WSN topologies and it is easy to design and implement. Its greatest advantage is that it can be extent by just adding new sensor nodes. However, if the coordinator node fails, the entire network will fail as well.

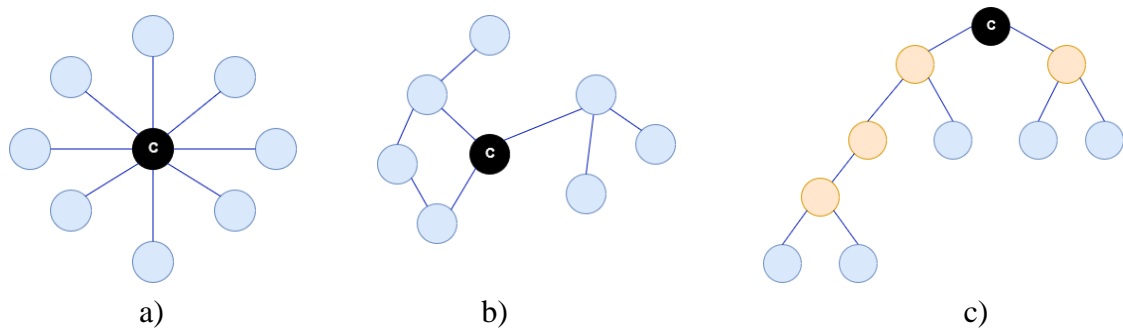


Figure 2.9. WSN topologies: (a) Star Topology; (b) Mesh Topology; (c) Tree Topology

This type of topology provides a limited coverage range. This drawback can only be addressed if more coordinator nodes are added to the sensor network, distributed in different areas.

B. Mesh Topology

In mesh topologies, messages can go through many nodes till they reach the coordinator node. Each node can be connected to any other nodes, as shown in Figure 2.9 b). Mesh networks have self-healing properties, as data can follow a different path if one node fails [38]. It also overcomes the coverage limitation of star topologies.

C. Tree Topology

Any sensor network that follows this topology is formed by a hierarchy of nodes in which the highest level of the hierarchy belongs to a “root node”. This node is connected to more than one node on the level below, and it can be considered a mixture between both Star and Peer-to-Peer network topologies, as shown in Figure 2.9 c). Due to its simple structure, it is easy to identify and isolate faults [39].

This topology can contain many levels of nodes, and, as they get larger, their management becomes more difficult.

2.4. Wireless Communication Protocols

Connectivity is the most important part of an IoT system. Elements such as radio range and power consumption are decisive when implementing a wireless sensor network. Wi-Fi, Bluetooth/BLE (Bluetooth Low Energy) and ZigBee are the WSN’s most common wireless technologies, and some of their specifications are presented in Table 2.1. A more detailed description of each wireless technology is given in section 2.4.1, 2.4.2 and 2.4.3, respectively.

Table 2.1. Comparison of Bluetooth, Zigbee and Wi-Fi protocols [40][41]

Standards	Bluetooth	ZigBee	Wi-Fi
IEEE specification	802.15.1	802.15.4	802.11n 802.11ac
Signal rate	1 Mbps	250 kbps	max 600 Mbps max 1.3 Gbps
Frequency	2.4 GHz	2.4 GHz	2.4 GHz; 5 GHz
Nominal Range	10 m	10 m	100 m; 70 m 35 m
Basic Cell	Piconet	Star	BSS
Maximum number of nodes	7	> 65000	2007
Peak current consumption	< 30 mA	1 – 10 mA	100 - 350 mA

2.4.1. 802.15.1 (Bluetooth)

Bluetooth is a standard based on a wireless radio system and designed for short-range wireless communications. It is mainly oriented to establish wireless connections between closely connected devices and it is widely used in IoT systems due to its low power consumption. When two or more devices want to connect with each other, they need to go through a pairing process. Once the pairing is succeeded, and ad hoc network is established. Bluetooth can adopt two different network topologies: a piconet topology and a scatternet topology. The piconet is the simplest topology and it consists of a wireless personal area network (WPAN) that is formed by a single Bluetooth device serving as a master and up to seven Bluetooth devices serving as slaves (Figure 2.10).

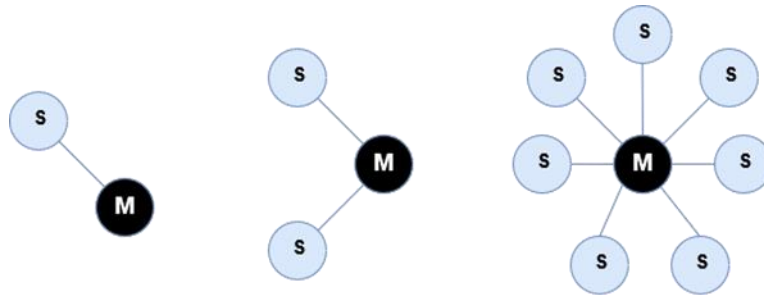


Figure 2.10. Bluetooth piconet possible configurations

Each piconet is defined by a frequency-hopping channel based on the address of the master device, and all the participating slaves are synchronized using its clock [40].

Piconets can be interconnected, thus forming a scatternet. In this topology, a *multihop* wireless network can be built. Two distant nodes can communicate with each other by using other nodes as relays. In a more complex scatternet configuration, different piconets can communicate with each other through a common node that belongs to both, and a node can either be a master in one piconet and a slave in several others [41].

Thinking on a less power consuming alternative, Bluetooth Special Interest Group (SIG) developed the Bluetooth Low Energy (BLE), which began with the release of Bluetooth 4.0 version. The most recent release, Bluetooth 5, provides improved speed and greater range than the older versions. This innovative technology is often applied in Internet of Things (IoT) systems thanks to its versatility and low power consumption [42]. It shares the same architecture as Bluetooth Classic and operates in the 2.4 GHz ISM frequency band.

2.4.2. 802.11 (Wi-Fi)

Wi-Fi is based on the IEEE 802.11 family of standards and is commonly used between devices inside a wireless local area network (WLAN). This family of specifications started in 1997 when IEEE approved the first standard for WLAN with signal rates up to 2 Mbps in the 2.4 GHz frequency band. This family continues to grow today, and their new standards bring many improvements that allow higher wireless throughput levels and higher range, as well as the use of new frequency bands. Introduced in 1999 and 2003, the IEEE 802.11b and g standards work with signal rates of 11 Mbps and 54 Mbps at 2.4 GHz, respectively [41]. Later, the increasing of data rates was brought with the IEEE 802.11n in 2009, where MIMO physical layer and new modulation and coding mechanisms were implemented. It also allowed the usage of two band frequencies – the 2.4 GHz and 5GHz – with increased data rates up to 600 Mbps [43]. By implementing multiuser MIMO, wider channels and better modulation schemes, the IEEE 802.11ac standard brought even better improvements on throughput, as it provides a multi-station WLAN throughput of at least 1 Gbps.

The IEEE 802.11 WLAN architecture is composed by a set of mobile or fixed stations called basic service sets (BSS). This standard allows stations to directly communicate with each other without the need of an access point. This operation is entitled independent basic service set (IBSS) and its configuration is shown in Figure 2.11. A BSS can also form an extended service set (ESS) by interconnecting with other BSSs. This is possible with a distribution system (DS), that allows the making of an ESS network of arbitrary size and complexity [40].

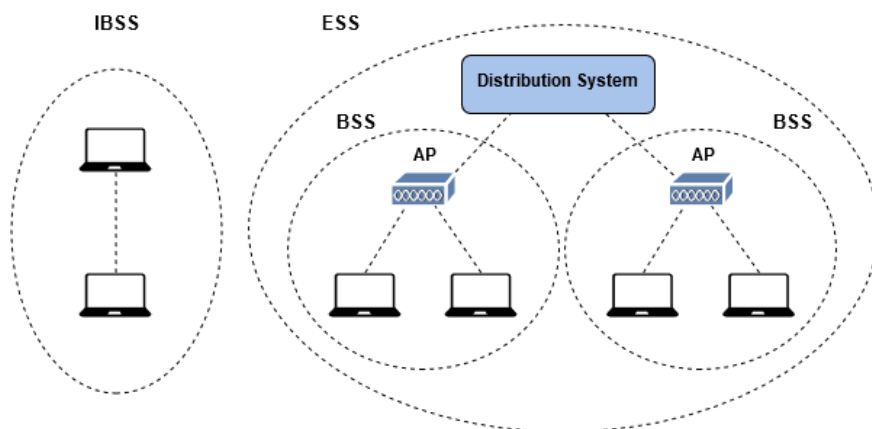


Figure 2.11. IEEE 802.11 Architecture

2.4.3. 802.15.4 (ZigBee)

ZigBee operates on the IEEE 802.15.4 specification and it is designed to use low-power radio signals for wireless personal area networks (WPAN). The protocol is used to create networks that require low data transfer rates and energy efficiency, and it can easily be integrated in IoT systems via ZigBee gateways. However, additional hardware modules are required to implement this wireless protocol. Other drawbacks include its low transmission rate (250 kbps) and some interoperability problems.

There are two different types of devices on a ZigBee network: a full-function device (FFD) and a reduce-function device (RFD). The FFD performs all tasks, can become a network coordinator and talk to other FFDs or RFDs. On the other hand, the RFD can only talk to an FFD, cannot become a network coordinator and it is intended to perform extremely simple tasks [40].

2.4.4. Long Range Communication

There are many different long range wireless protocols specially conceived for IoT technologies which provide low-power consumption, reduced operating costs and reliable communications. Some of these protocols include the three emerging technologies: SigFox, LoRa and Narrowband IoT.

SigFox offers an end-to-end connectivity solution for the Internet of Things, therefore designed for long ranges, low data rates and low power consumption. It uses BPSK modulation with ultra-narrowband technology and works on the frequency band of 868 MHz (ISM) in Europe and 902 MHz (ISM) in the United States. The data transmission range for rural areas goes between 30-50 km and 3-10 km in urban areas. Has for the data rate, it only has a maximum throughput of only 100 bps [44]. LoRa, which stands for Long Range, is based on bidirectional communications based on the chirp spread spectrum (CSS) modulation. It also uses the same unlicensed ISM bands, like SigFox, and provides shorter data transmission ranges – 5 Km for urban areas and 20 km for rural areas. The maximum LoRa data rate is 50 kbps, which is more than SigFox's range [44]. Regarding Narrowband IoT, or NB-IoT, this protocol works on licenced LTE frequency bands and employs the quadrature phase-shift keying modulation (QPSK). It offers higher transmission rates than the previous protocols – 200 kbps – and a shorter transmission range of about 1 km in urban areas and 10 km in rural areas [44].

Chapter 3

System Hardware

In this chapter, a description of the developed system hardware components will be made, describing in section 3.1. the sensors network architecture and the chosen hardware components. Being the main objective the development of a system that monitors the indoor environment and adapts it to the user's specific needs and characteristics, the system will be based on a wireless sensor network that acquires environmental data and a user's physiological state, and on several distributed actuators. The capacity of scalability of the entire system is an essential feature of a modern solution and is one of this architecture' strengths. To assure the system's flexibility and mobility, its measuring nodes can be distributed in different regions of the house according to the user's location and specific monitoring scenarios.

The user interaction with the system is performed through a graphical user interface, which is generally the top layer of any IoT system. This monitoring can be done remotely through a dedicated web application, specially developed for the system in question.

3.1. System Architecture

The proposed architecture can be divided into four parts. The first is the device layer, which include physical devices such as sensors and actuators. These components will be described in section 3.2 and 3.3, respectively. The second and third refers to the smart gateway, whose hardware will be presented in section 3.4, and to the online database, respectively. The last part represents the user interface. The block diagram of the system is presented in Figure 3.1.

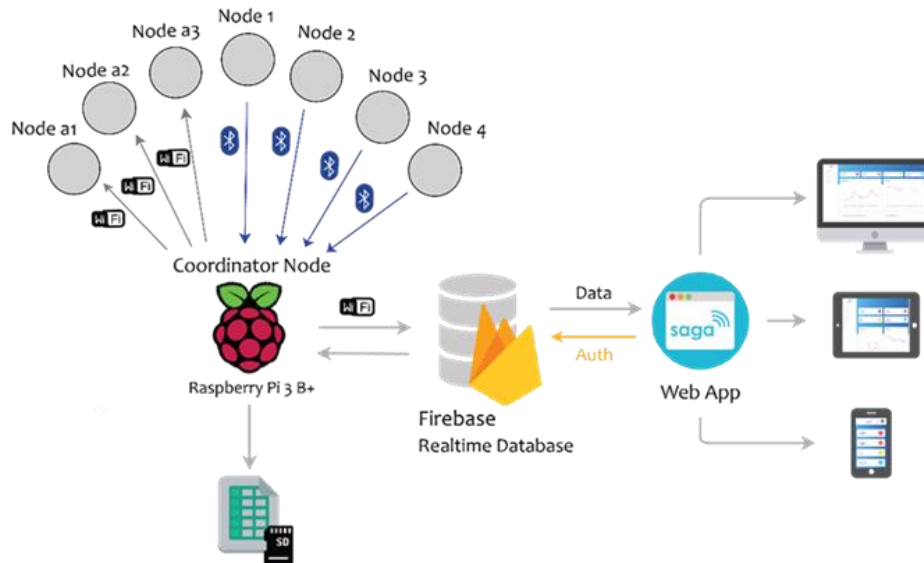


Figure 3.1. System Architecture with a device layer composed of three actuator nodes and four sensor nodes

The sensor network contains several nodes (node1, node2, ...) with different types of sensors that allow the acquisition and measurement of air quality-related parameters and physiological data.

Each node communicates with a coordinator node (a Raspberry Pi) using the Bluetooth protocol. This node collects all the received data and sends it to Firebase [45], a Google’s cloud hosted NoSQL Realtime database, over the internet. Additionally, and to avoid losing data events, the acquired data is saved on a local file, on the Raspberry Pi 3 B+ SD card.

The WSN has three actuator nodes (node a1, node a2 and node a3), each one controlled by the coordinator node through Wi-Fi: a smart lighting system to adapt both the level and the colour of indoor lighting throughout the day, alert the user when the values measured by gas, temperature and humidity sensors are potentially harmful (according with personalized thresholds stored on the database) and help changing the user’s emotional state, based on his heart rate; a humidifier to increase humidity (moisture) levels, and finally a single-room ventilation unit to displace indoor pollutants, increase thermal comfort or dehumidify the environment. Then, a unique web application named “SAGA”, and developed for this purpose, is used to analyse the recorded data; grant to the user remote control over the smart lighting system and other actuators; allow the user to modify the threshold values related to asthma, and to implement an additional alert mechanism. The web application works on multiple platforms and thanks to its responsive

web design (RWD) , it can render on a variety of devices with different screen or window sizes, enabling it to be used by anyone through its personal computer, laptop, tablet or smartphone.

3.2. Sensor Nodes

Each sensor node requires a module that collects the data from the various sensors and transmits it to an aggregation node. To do this, a self-contained, deployable unit that captures the data generated by sensors is needed. The sensor node does not have enough processing power, memory, and storage to deal with the data locally, so a low-energy radio communication network is needed to send the data to a central location. The communication link between sensors and the central hub can be based on ZigBee, Bluetooth / BLE or Wi-Fi. In this system, each sensor node performs transmissions through the Bluetooth protocol. An ESP32 microcontroller has been chosen for this purpose and its description will be made, along with comparisons between other existing platforms.

3.2.1. Embedded Computation

The ESP32 was the chosen microcontroller for each sensor node. It is a low-cost, low-power system on a chip (SoC) with Wi-Fi and Bluetooth capabilities created by Expressif Systems. His predecessor was the already popular platform for IoT applications - the ESP8266. It already had a 32-bit processor, a Wi-Fi module, and several GPIO pins. With a more powerful board in mind, Expressif developed a dual-core microprocessor with both Wi-Fi and Bluetooth/BLE modules, more GPIO pins (36 against the 17 of ESP8266), more ADC channels, and many more.

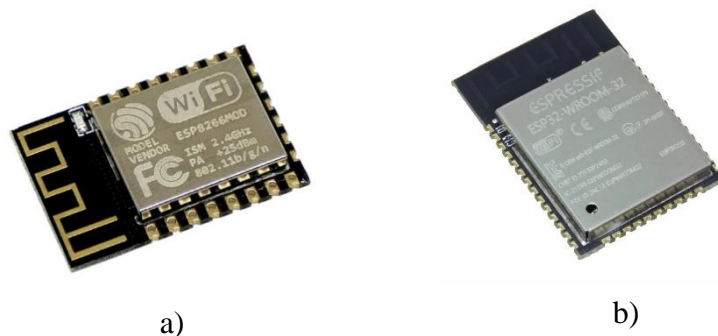


Figure 3.2. a) ESP8266 and b) ESP32

The ESP8266 was already a strong opponent on the Arduino family boards. With the ESP32's arrival, the difference between the two family boards becomes even more remarkable. The 32-bit Tensilica Xtensa dual-core low-power microprocessor and integrated flash memory allows the ESP32 to be programmed independently without the need for other microcontroller boards, as with Arduino. In addition to its superiority in numbers of GPIOs and ADCs, the ESP32 also has Wi-Fi and Bluetooth radio capabilities, whereas Arduino would require the use of external modules and extra wired connections.

The ESP32 has many types of development boards. These platforms can combine the ESP32 chip, an integrated serial USB converter and micro-usb port for power supply and programming. Like the Arduino, the ESP32 development board can be programmed using the Arduino IDE thus supporting many compatible libraries and having the ease of programming offered by the Arduino IDE interface.

Table 3.1 shows a comparison between ESP8266, the ESP32 and the Arduino Uno.

Table 3.1. Comparison between the ESP8266, the ESP32 and the Arduino Uno

Specifications	ESP8266	ESP32	Arduino Uno
MCU	Tensilica Xtensa® Single-Core 32-bit L106	Tensilica Xtensa® Dual-Core 32-bit LX6 600 DMIPS	ATmega328P
802.11 b/g/n Wi-Fi	HT20	HT40	None
802.15.1 Bluetooth	None	v4.2 BR/EDR and Bluetooth Low Energy (BLE)	None
CPU Frequency	Up to 160 MHz	Up to 240 MHz	16 MHz
SRAM	160 KBytes	520 KBytes	2 KBytes
Flash	16 MBytes	16 MBytes	32 KBytes
GPIO	17	36	14
Hardware / Software PWM	None / 8 Channels	1 / 16 Channels	None / 6 Channels
Buses	SPI, I2C, UART, I2S	SPI, I2C, UART, I2S, CAN	SPI, I2C, UART
ADC	1 (10-bit)	18 (12-bit)	6 (10-bit)
DAC	2	0	0
Programming Environments	Arduino IDE, Espressif IDF, Micropython, etc.	Arduino IDE, Espressif IDF, Micropython, etc.	Arduino IDE

The ESP32's remarkable element is its dual-core processor, with about 520 KBytes of SRAM memory, which allows the execution of more complex programs. The integration

of a Controller Area Network (CAN) bus also allows this module to interact with CAN networks, which is a communication protocol widely used in the field of automation. In addition to this feature, the ESP32 has an Ethernet MAC interface, which means that the module can be used for Ethernet LAN communications. However, it requires an external physical interface device (PHY) to connect to the physical LAN bus. Another important feature includes a built-in temperature sensor that monitors the microcontroller's temperature, a built-in sensor, touch sensitive pins and multiple power modes.

The numerous features of the ESP32's chip makes it indispensable for its use in Internet of Things (IoT). The existence of more peripherals allows its integration with more devices and components. Figure 3.3 shows the several components present in the ESP32's chip. Its various communication interfaces include the most common SPI, UART and I2C protocols, as previously mentioned, and it also includes infrared (IR), SDIO (memory card interface) and I2S support, which is an electrical serial bus interface standard used for connecting digital audio devices together [46].

The chip also offers several security mechanisms, such as secure boot, flash encryption and an acceleration module for cryptographic applications, which supports SHA-2, AES, RSA, ECC and Random Number Generator (RNG) [47]. An important point of the chip is its RTC module, which contains a PMU (Phasor Measurement Unit), an ultra-low-power 32-bit co-processor (ULP coprocessor), and 8Kbytes of recovery memory. The ULP co-processor allows you to delegate / perform some simple tasks while the main processors are off (when in sleep mode). In conjunction with the RTC memory, which is 4 times larger than the memory of the Arduino Uno, it is possible to access peripheral devices, internal timers and internal sensors during Deep-sleep mode. It is very useful for when the CPU needs to be woken up by an external timer or event, while maintaining minimal power consumption. The different ESP32 power-modes will be described next.

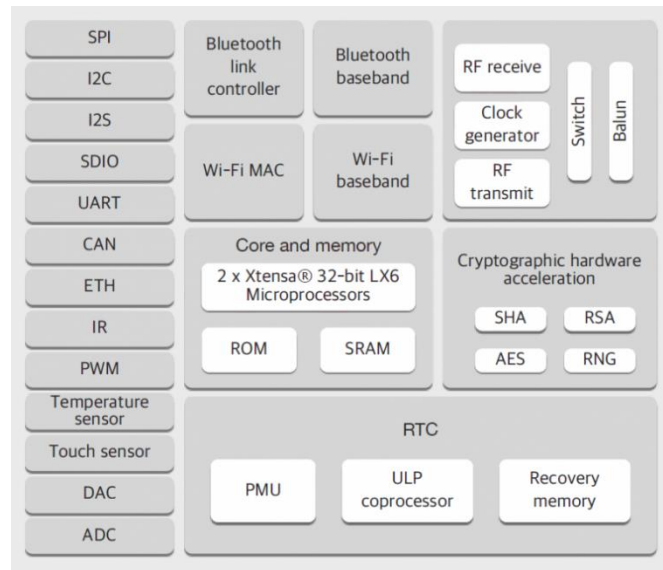


Figure 3.3. Functional Block Diagram of the ESP32's chip. Source: [47]

3.2.1.1. Power consumption and ESP32 sleep modes

In IoT systems, a node's low power consumption is crucial if batteries are used as a power supply. Battery life can be extended from days to months if power-saving states are implemented on the ESP-32 microcontroller. Fortunately, the ESP-32 has different Sleep Modes that can exponentially extend a node's battery life. The chip can switch between 5 configurable power modes [47], each one with distinct features and power saving capabilities:

- Active mode
- Modem Sleep Mode
- Light Sleep Mode
- Deep Sleep Mode
- Hibernation Mode

3.2.1.1.1. Active Mode

In Active mode, all the ESP-32 components are active: its dual core and memory, the Wi-Fi module, Bluetooth module, cryptographic accelerator, the RTC module and all peripherals. Figure 3.4 depicts the ESP-32 chip’s block diagram and its active features on this power mode.

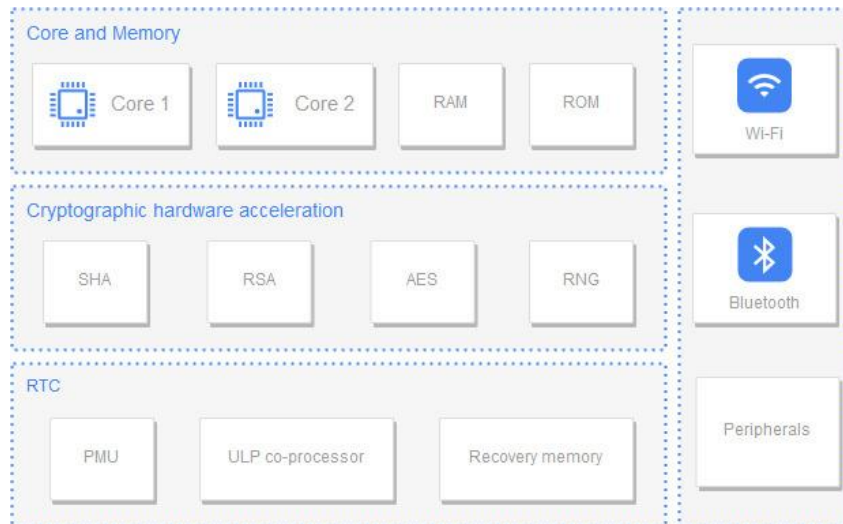


Figure 3.4. Active features of ESP-32 during Active mode

Since Wi-Fi modules, processing cores and Bluetooth modules require large energy consumption, this power mode is considered the most inefficient mode, as it will drain the most current. The following table provides information relative to the microcontroller’s power consumption during Active mode, according to the manufacturer.

Table 3.2. ESP-32 power consumption during Active mode

Mode	Power Consumption
Wi-Fi Transmission (14 dBm ~ 19.5 dBm)	180 ~ 240 mA
Wi-Fi Reception	95 ~ 100 mA
BT/BLE Transmission	130 mA
BT/BLE Reception	95 ~ 100 mA

3.2.1.1.2. Modem and Light Sleep Mode

In Modem sleep mode everything is active except the Wi-Fi module, Bluetooth module and peripherals, as shown in Figure 3.5. The CPU is still operational and changes its frequency automatically. The frequency depends on the CPU load and the peripherals used. When Wi-Fi is enabled, the chip changes between Active and Modem sleep modes, to reduce power consumption.

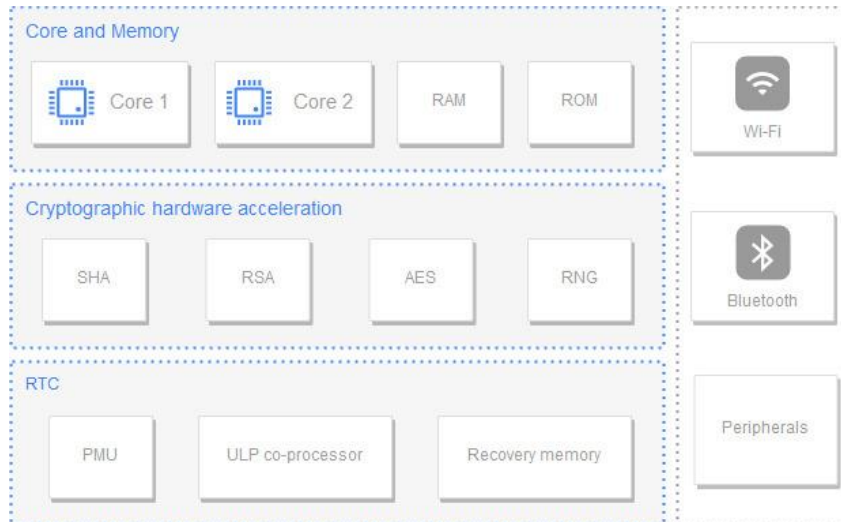


Figure 3.5. Active features of ESP-32 during Modem and Light Sleep mode

Light sleep mode has a similar behaviour to the Modem sleep mode. The only difference is that the digital peripherals, most of the RAM, and CPUs are clock-gated, thus reducing supply voltage. During this mode, the RTC memory and RTC peripherals, as well as the Ultra-Low Power (ULP) co-processor are kept active. When in this mode, the power consumption is approximately 0.8 mA, which is less than the modem sleep mode (as shown in Table 3.3).

Table 3.3. ESP-32 power consumption during Modem and Light sleep modes

Power Mode	Mode	Power Consumption
Modem Sleep	CPU is powered on	240 MHz: 30 mA ~ 68 mA
		160 MHz: 27 mA ~ 44mA
		80 MHz: 20 mA ~ 31 mA
Light Sleep	-	0.8 mA

3.2.1.1.3. Deep Sleep Mode

In this mode, the CPU, the Bluetooth and Wi-Fi modules, most of the RAM and all the digital peripherals are powered off. Only the RTC memory and RTC peripherals (including ULP co-processor) are powered on. Because the RTC memory remains powered on, all its contents are preserved during this sleep mode.

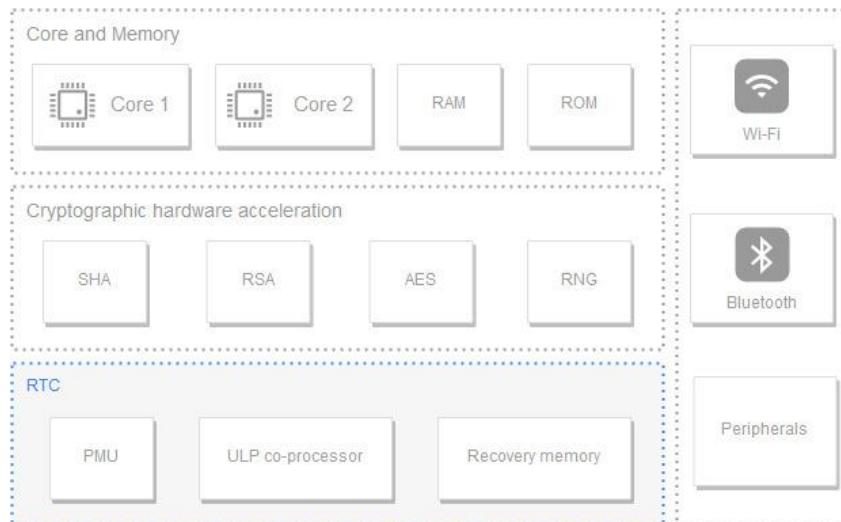


Figure 3.6. Active features of ESP-32 during Deep Sleep mode

Since the main memory of the chip is disabled, everything stored in that memory is wiped out and can no longer be accessed after the chip restarts. So, any data that needs to be used over reboot must be stored in the RTC memory. This mode allows the awakening of the CPU by an external event, timer, or both.

This is the sleep mode that will be used in this project and its implementation will be described in section 4.1.2.5. The reduction of power consumption levels will significantly make the batteries of each node last longer. Table 3.4 shows the ESP-32 power consumption in deep sleep mode.

Table 3.4. ESP-32 power consumption during Deep sleep modes

Power Mode	Mode	Power Consumption
Deep Sleep	ULP co-processor powered on	150 μ A
	ULP sensor-monitored pattern	100 μ A @ 1% duty
	RTC timer + RTC memory	10 μ A

When the system works in the ULP sensor-monitored pattern, the ULP co-processor works alongside with the ULP sensor and the ADC works with a duty cycle of 1 %.

3.2.1.1.4. Hibernation Mode

This is the less power consuming mode when compared to the previous ones. Everything is disabled, except the RTC timer and some RTC GPIOs, which are responsible for waking up the chip from the hibernation mode. In this mode, the chip only consumes about 5 μ A.

3.2.2. Node 1 – Thermal Conditions Measuring Node

Node 1 monitors various parameters of the indoor environment, having a special focus on indoor thermal quality, that besides affecting and individual's quality of life, is also a trigger for respiratory distress to people with respiratory impairments. In addition to this parameters monitoring, the presence or absence of lighting in the indoor environment is also monitored as a complement to increase levels of lighting quality, which is also a parameter present in the Indoor Environmental Quality (IEQ) index. An additional factor to consider that contributes in a relevant way to everyone's quality of life is a good environmental noise quality. The monitoring of noise levels will also be done to alert the user if they exceed the limits of human hearing tolerance or possibly cause a certain level of discomfort.

Regarding the elements mentioned above, Node 1 is formed by a temperature and relative humidity sensor, a light intensity sensor (Light Dependent Resistor (LDR)) and an electret microphone amplifier.

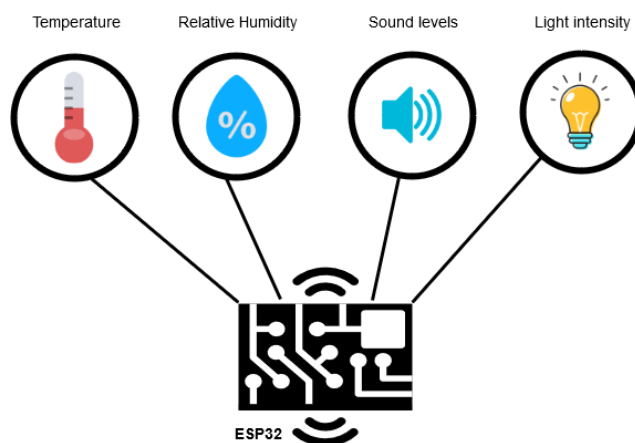


Figure 3.7. Environmental parameters measured by Node 1

For the temperature and relative humidity measurements, the Si7021 solid state sensor from Silicon Labs was used. It performs analog-to-digital conversions, signal processing, data calibration and it has an I²C communication interface. It has low power consumption and performs relative humidity measurements with $\pm 3\%$ accuracy and a measurement range of 0-80% RH, and temperature measurements accuracy of $\pm 0.4^{\circ}\text{C}$ for a 10°C to 85°C measurement range [48]. Due to its high accuracy and low power consumption, this sensor was the chosen temperature and relative humidity sensor to integrate Node 1.



Figure 3.8. Temperature and Relative humidity sensor - Si7021

To measure indoor's light intensity, a Light Dependent Resistor (LDR), like the exemplar of Figure 3.9, is used. This sensor is based on the principle of photo conductivity: an optical and electrical phenomenon in which a material increases its electrical conductivity when it absorbs electromagnetic radiation, such as visible light and infra-red light. When the incident light exceeds a certain frequency, the photons absorbed by the sensor's semiconductor material excite the electrons, which makes them jump from the valence band to the conduction band. The result of this process is the increase of free electrons in the material, which will then conduct electricity and therefore lower its resistance [49]. The sensor's resistance can go up to $1\text{ M}\Omega$ when kept in the dark and will drop significantly when exposed to light, even down to a few ohms, as shown in Figure 3.10.

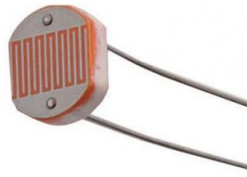


Figure 3.9. Light Dependent Resistor (LDR) exemplar

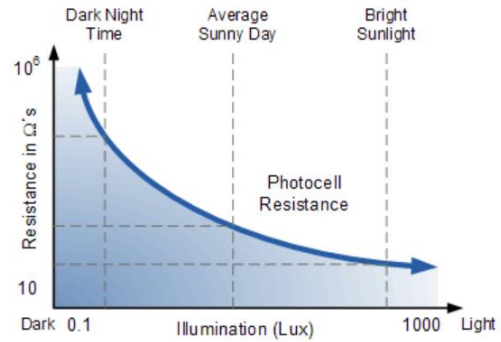


Figure 3.10. Photocell resistance dependency with the incident illumination

An acoustic-to-electric transducer that converts sound into an electric signal is needed to monitor the acoustic environment. For that purpose, an electret microphone based on the MAX9814 amplifier was used. This model from Adafruit is a high-quality microphone amplifier with automatic gain control (AGC) and low-noise microphone bias, which helps avoiding distortion of the amplifier when sound levels change randomly. Moreover, thanks to the AGC, far away sounds will be amplified. It provides an operating frequency from 20 Hz to 20 kHz, which is the frequency range of human hearing, and an automatic gain of 40dB, 50dB or 60dB [50][51].



Figure 3.11. Electret Microphone Amplifier - MAX9814

Therefore, and according to the referred elements above, the proposed circuit that integrates all these sensors with the ESP32, thus creating Node 1, is presented in Figure 3.12.

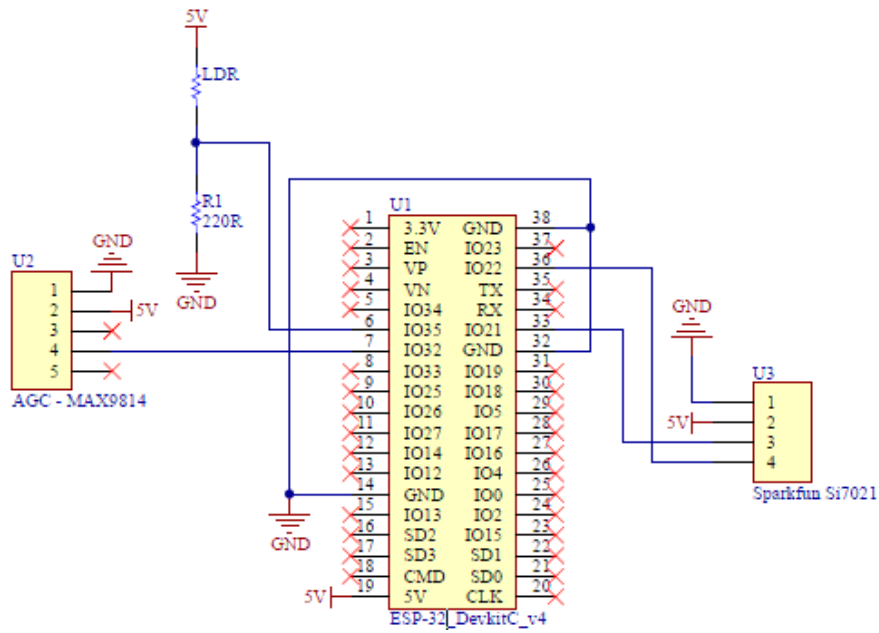


Figure 3.12. Schematic circuit of Node 1

Firstly, a prototype was created in which a simple breadboard was used to connect all components, as shown in Figure 3.13.

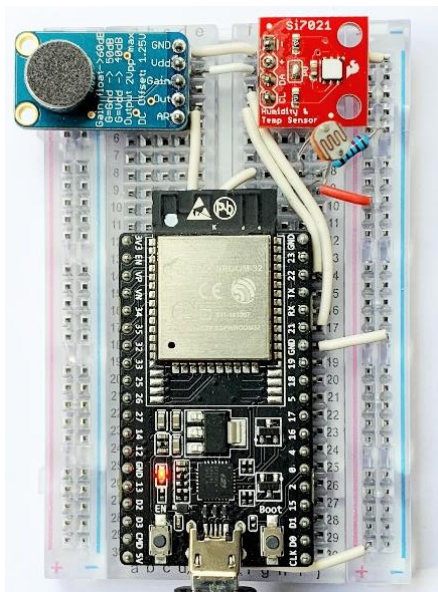


Figure 3.13. First prototype of Node 1

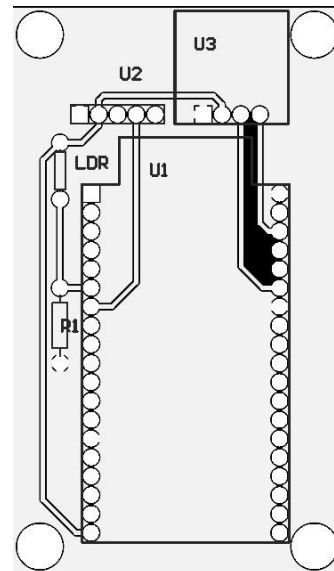


Figure 3.14. PCB schematic of Node 1

The final implementation of Node 1 can be seen in the next figure.

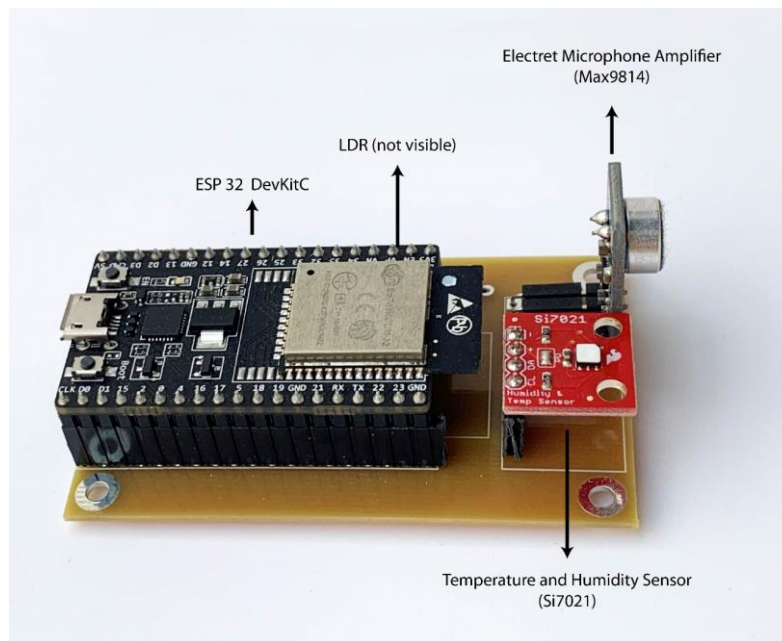


Figure 3.15. Node 1

3.2.3. Node 2 – Gas Sensing Node

In order to perform indoor air quality monitoring by measuring indoor gas concentrations, Node 2 includes a set of reliable gas sensors. Each sensor detects various kinds of gases and belong to the MQ series. An exemplar of this sensor can be seen in Figure 3.16. The gases under monitoring comprise those considered relevant to the triggering of asthma crisis and COPD exacerbation. Such gases include NO_x, CO and Smoke [2], and therefore, the MQ-135, MQ-4, and MQ-9 sensors are used. The types of sensors associated with each type of gas they detect are presented in Table 3.5.

These gas sensors include a heating element and an electrochemical sensing unit expressed by a SnO₂ semiconductor. These sensors have a heater because the sensor's sensitive surface, which in this case consists of a metal oxide, will only let the gases and particles penetrate if they achieve a certain temperature level. For that reason, the sensors




are mainly used in closed environments, so that the heating filament's temperature keeps more constant [52].



Figure 3.16. Exemplar of a MQ series Gas Sensor

This surface has a low electrical conductivity when exposed to clean air, so whenever the sensing element detects gases and particles in the air, its electrical conductivity increases. This means the sensor's voltage values depend on the quantity of gas found in the air in which the sensor is located.

Table 3.5. Types of Gas detected by each sensor

Sensor Type	Types of Gas
<p>MQ-135</p> 	<p>Air quality sensor with low selectivity (Ammonia (NH₃), Nitrogen Oxides (NO_x), Alcohol, Benzene, Smoke and Carbon Dioxide (CO₂))</p>
<p>MQ-4</p> 	<p>Natural gas and Methane gas</p>
<p>MQ-9</p> 	<p>Carbon Monoxide (CO), Methane and Liquified Petroleum Gas (LPG)</p>

The corresponding sensor unit's circuit is presented in the next figure. The sensor requires two voltage inputs: one for the circuit (V_c) and another for the heater (presented by H). The heater voltage is necessary to maintain the sensing element at a specific temperature. The circuit voltage is used to allow the measurement of voltage (V_{out}) across a load resistor (R_L) connected in series with the sensor. For the sensors in question, a common power supply is used for both circuit voltage and heater voltage. With this measuring circuit, the changes in conductivity are converted into output signals, which are directly proportional to the concentration of gas.

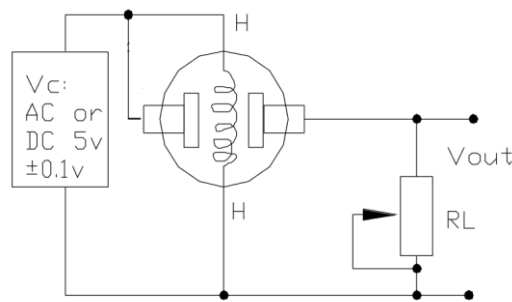


Figure 3.17. Gas sensing unit circuit (V_c – circuit voltage, H – heater, V_{out} – gas sensor output, R_L – load resistance)

The proposed circuit that integrates all the three gas sensor units with the ESP32, thus creating Node 2, is presented in Figure 3.18.

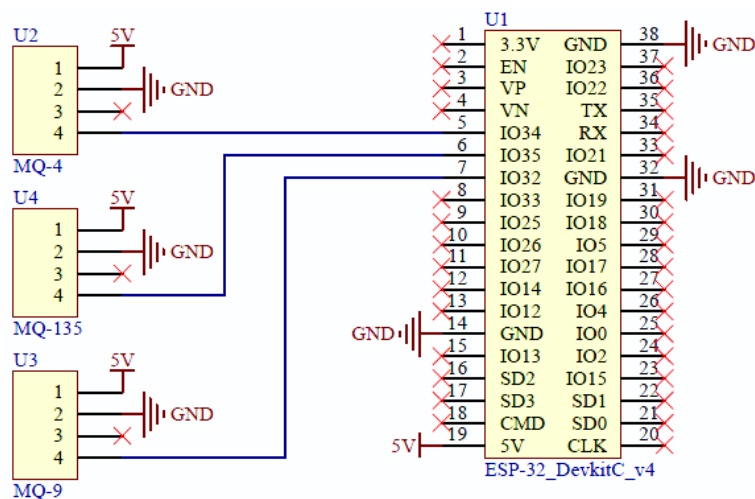


Figure 3.18. Node 2 circuit schematic

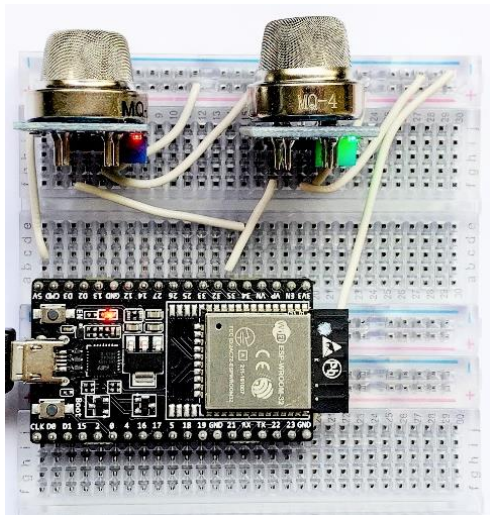


Figure 3.19. First prototype of Node 2

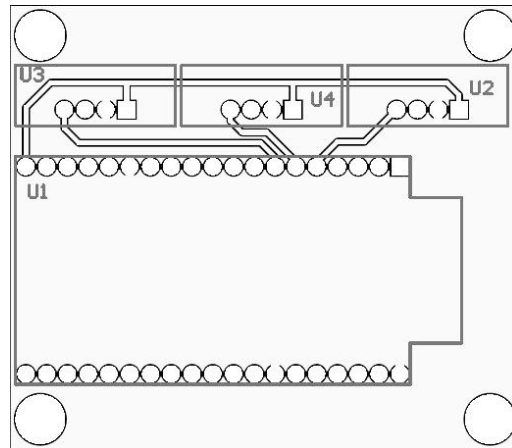


Figure 3.20. PCB schematic of Node 2

Its first prototype is shown in Figure 3.19, and its PCB schematic is in Figure 3.20.

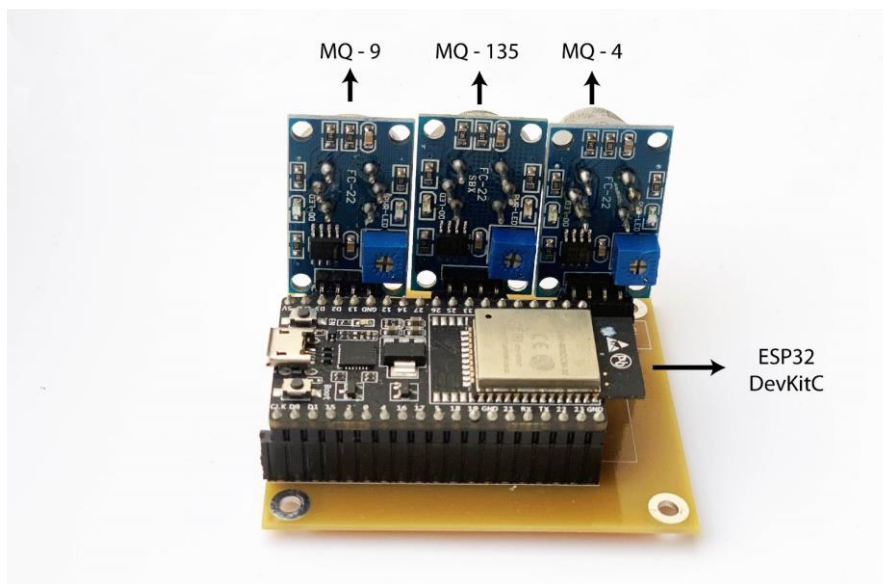


Figure 3.21. Node 2

As mentioned before, due to the sensor's low selectivity, each sensor reacts to more than one type of gas, which means they will have higher resistive variations to one or two types of gas included in the sensor's gas detection range. The sensitivity of the sensor to each of the detected gases is given in the sensor datasheet (available in Appendix C). However, it is not possible to know which specific gas the sensor detected and what were their respective concentration levels. Sensors need calibration, as described in the next sub-section.

3.2.3.1. Gas sensors calibration

The gas sensors output signal is expressed by voltage levels instead of gas concentration (in parts per million - ppm). For that reason, their voltage output must be normalized and calibrated. To perform this calibration, the sensors were tested in a calibration box, model SR-3 from Figaro Engineering. The calibration box is made of acrylic resin and it has 235W x 180D x 210H mm of size, and an effective inner capacity of 5,400 ml. Different volumes of gas can be injected in the chamber with a syringe through a designated hole (see Fig.3.22). The injected gas is mixed with air by a built-in fan to achieve a uniform gas concentration throughout the chamber. Several calibration tests were carried out. For the particular case of Ethanol, to find out a correlation between the gas concentration and the injected volume of gas in the chamber, different volumes of Ethanol (C_2H_6O) were injected. Tests were only made with this substance because it is easier to obtain and safer to use than the other types of gas. Since the MQ-135 is highly reactive to Ethanol, the calibration methods will be based on this sensor behaviour.

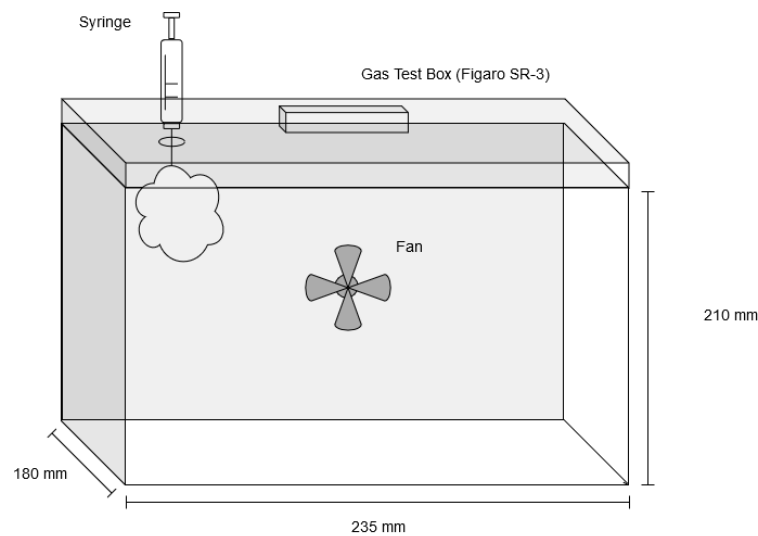


Figure 3.22. Figaro gas test chamber

After the gas sensor voltage output is acquired, a digital value from 0 to 4,095 is obtained at the ESP-32 ADC output. The digital value conversion to gas concentration levels is based on the gas sensors calibration curves available in their respective datasheets (Appendix C).

The Figaro gas calibration system provides a product information sheet [53] that includes some information about the injected volume of gas (ml) in the box and its correlation with gas concentration units in ppm (Table 3.6).

Table 3.6. Gas concentration in ppm and its associated volume of gas

Gas Concentration (ppm)	Volume of Pure Gas (ml)
50	0,27
100	0,54
200	1,08
400	2,16
600	3,24
800	4,32
1000	5,4

The following formula [53] can be used to calculate the volume (ml) of pure gas required to achieve a certain gas concentration (ppm) in the test chamber:

$$ppm = \frac{\text{Volume of Gas (ml)}}{0.0054} \quad (1)$$

A volume of 0,54 ml of Ethanol, equivalent to 100 ppm, was injected in the gas chamber to test the MQ-135 sensor's reaction. An average of the values obtained in the ADC during a certain period and after stabilization was calculated. The average value of the sensor's output was approximately 555,8 on the ADC.

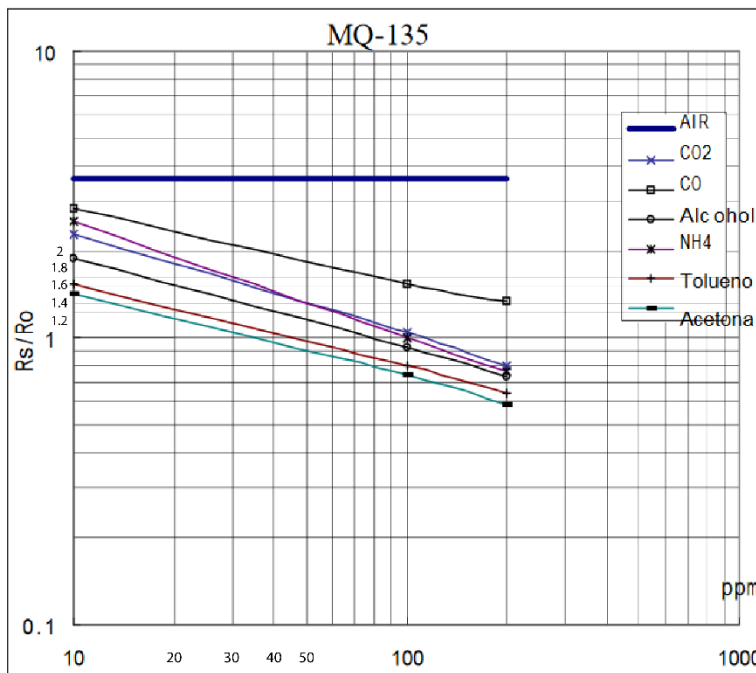
The ADC values were converted to voltage levels by using the following expression:

$$V_{out} = \frac{ADC}{4095} \times V_c \quad (2)$$

where ADC is the output value of the sensor and V_c is the gas sensing unit circuit voltage.

To perform the next steps of the sensor's calibration, the sensitivity calibration curve available in each sensor's datasheets [54][55][56] was used. Taking the MQ-135 sensitivity characteristic curve as an example (Figure 3.23), a formula based on the correlation between R_s/R_o and PPM needs to be deduced.

Table 3.7. Sensitivity characteristic of MQ-135 for Alcohol



R_s/R_o	ppm
1.9	10
1.6	20
1.45	30
1.3	40
1.2	50
0.9	100
0.75	200

Figure 3.23. Sensitivity characteristics of the MQ-135 for CO₂, CO, Alcohol, NH₄, Toluene and Acetone

For that purpose, a y-axis and x-axis graph was created by picking the data points from the sensitivity characteristic of the sensor in the presence of Ethanol (Table 3.7).

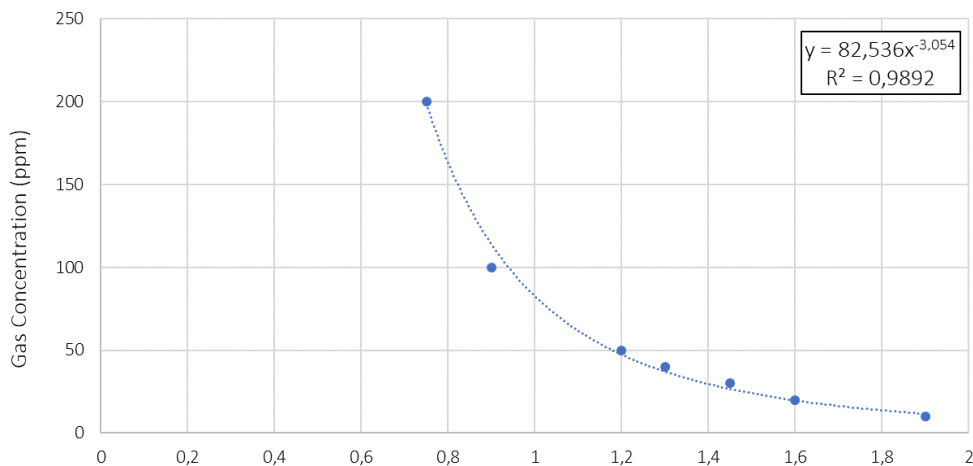


Figure 3.24. Sensitivity characteristics of the MQ-135 gas sensor in the presence of Alcohol

By adding a power trendline to the resulting graph (see Figure 3.24), the following formula was obtained:

$$ppm = 82.536 \times \left(\frac{R_s}{R_o}\right)^{-3.054} \quad (3)$$

where R_s presents the sensor resistance at various concentrations of gases and R_o the MQ-135 sensor resistance at 100 ppm of NH_3 in clean air or 50 ppm of alcohol in clean air.

The value of R_s can be obtained by the following expression:

$$R_s = R_L \times \left(\frac{V_c}{V_{out}} - 1\right) \quad (4)$$

where R_L is the load resistance. A R_L of 20 k Ω , as specified in the sensor's datasheet was considered, alongside with a V_c value of 5V.

The other gas sensors, MQ-4 and MQ-9, were calibrated using their sensitivity characteristic curves. Figure 3.25 and 3.26 shows the sensor's characteristics to different concentrations of gas substances, respectively.

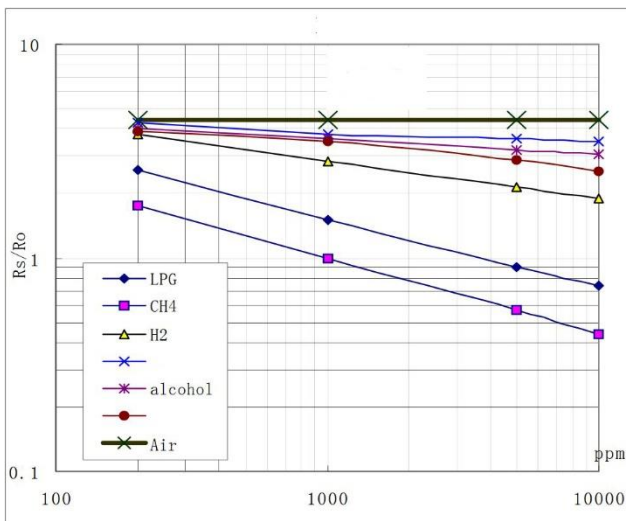


Figure 3.25. Sensitivity characteristics of the MQ-4 for LPG, CH₄, H₂, CO, Alcohol and Smoke

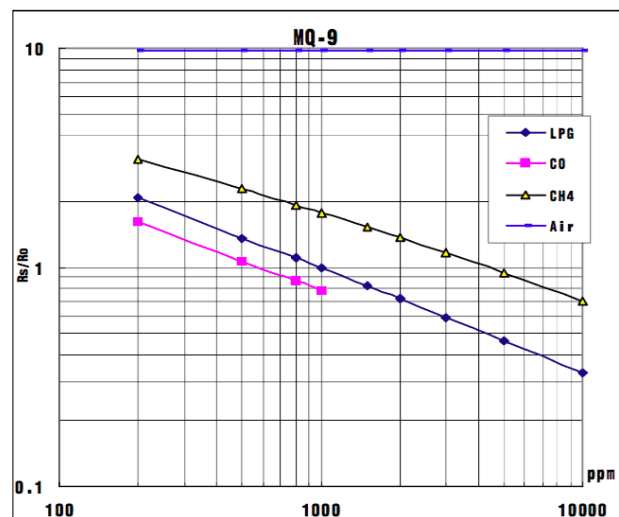


Figure 3.26. Sensitivity characteristics of the MQ-9 for LPG, CO and CH₄

Similarly, several data points were picked from the sensitivity characteristic curve of the MQ-4 and MQ-9 sensors in the presence of CH₄ and LPG, respectively.

Table 3.8. Sensitivity characteristic of MQ-4 for CH₄

Rs/R0	ppm
1,8	200
1	1000
0,58	5000
0,45	10000

Table 3.9. Sensitivity characteristic of MQ-9 for LPG

Rs/R0	ppm
2	200
1,5	500
1,2	800
1	1000
0,8	1500
0,7	2000
0,6	3000
0,48	5000
0,34	10000

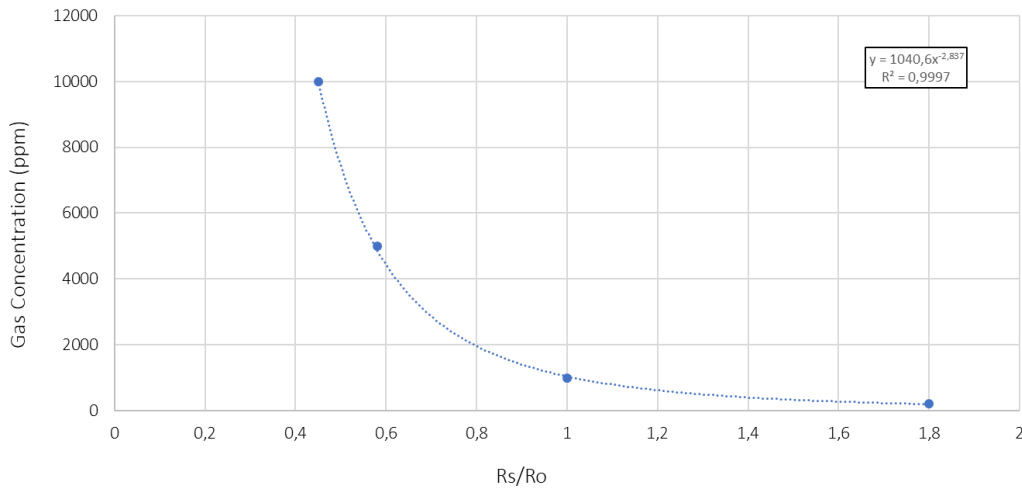


Figure 3.27. Sensitivity characteristic of the MQ-4 gas sensor in the presence of CH₄

An estimation of the Rs/R0 correlation with the gas concentration (ppm) is given by the power trendline's equation. In the MQ-4's case:

$$ppm = 1040.6 \times \left(\frac{Rs}{Ro}\right)^{-2.837} \quad (5)$$

where Rs presents the sensor resistance at various concentrations of gases and Ro the MQ-4 sensor resistance at 1000 ppm of CH₄ in the clean air.

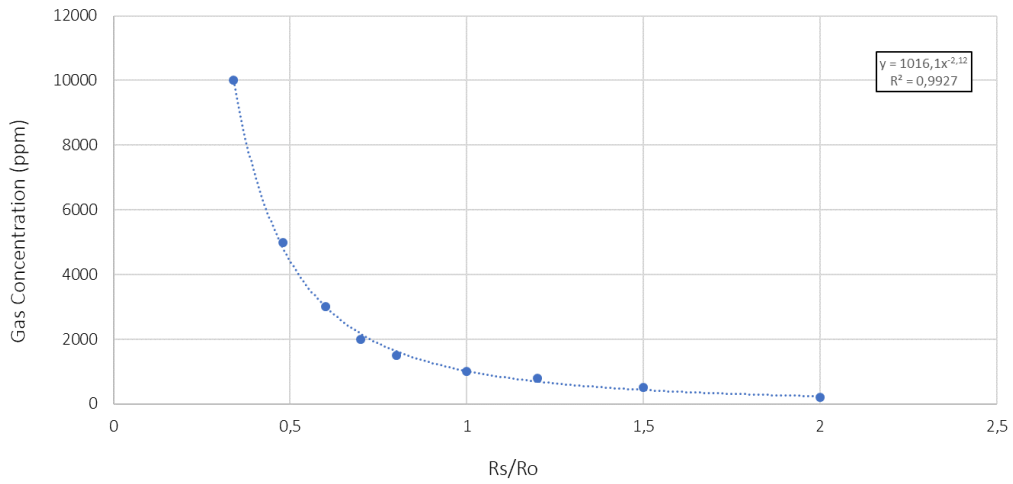


Figure 3.28. Sensitivity characteristic of the MQ-9 gas sensor in the presence of LPG

For the MQ-4, the power trendline results in the following equation:

$$ppm = 1016.1 \times \left(\frac{R_s}{R_o}\right)^{-2.12} \quad (6)$$

where R_s presents the sensor resistance at various concentrations of gases and R_o the MQ-9 sensor resistance at 1000 ppm of PPG in the clean air.

3.2.4. Node 3 – Particulate Matter Measuring Node

The airborne particulate matter (PM) has a great impact on human health, especially in individuals with respiratory impairment. Concentrations of PM are associated with hospital visits due to respiratory diseases, and this correlation has been addressed by several epidemiological studies worldwide [57]. Since 2006 that PM_{2.5} serves as an indicator of pollution caused by particulates, according to the World Health Organization Air Quality Guidelines (WHO AQG) [58].

To measure PM concentrations, an additional WSN measurement node (Node 3) was considered. It includes a Shinyei PPD42NS particle counter that detects particles with 1 μm or less in diameter. Its operation mode is based on the light-scattering principle, by determining the size of small particles in suspension. The sensor has a light chamber with a light emitting diode and a photo-diode detector. Once the particles present in the air get inside the chamber, near-forward scattering properties of those particles are measured [59]. The resistor/heating element on the bottom of the light chamber helps moving the air from the bottom inlet to the top outlet of the chamber. The sensor's output signal consists of Low Pulse Occupancy (LPO) measurements (the amount of time that the digital signal is held low, due to the presence of particles in the chamber), which are proportional to the particles count concentration.

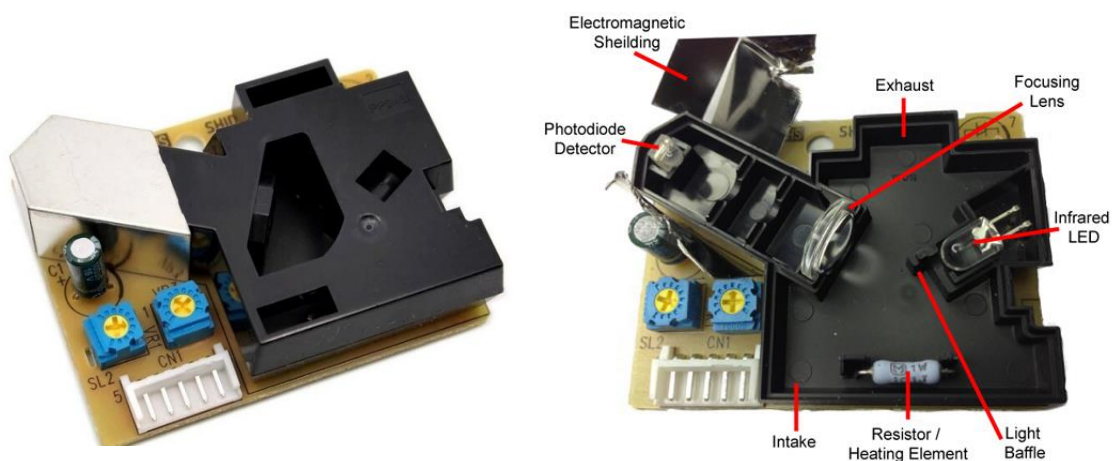


Figure 3.29. Shinyei PPD42NS and its inner components

To better understand how the Shinyei PPD42NS works internally, the author in [60] de-constructed the sensor, placed a red LED at the position of the photodiode and sprayed artificial smoke into the detection area. In Figure 3.30 it is possible to see the focal point of the lens. That focus point is where the photodiode will detect the light-scattered particles by the Infrared LED.

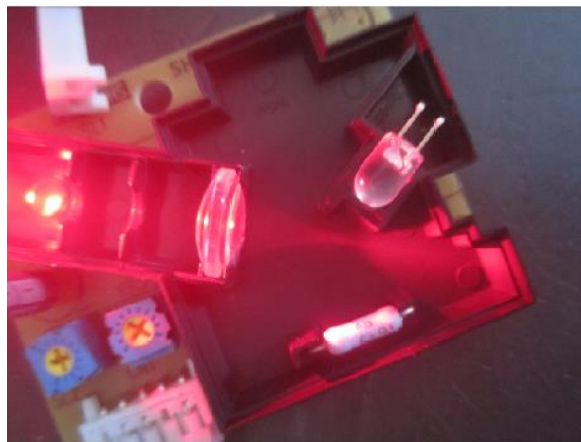


Figure 3.30. De-contruction of the Shinyei PPD42NS. Source: [60]

The signal pin from the Shinyei PPD42 is connected to GPIO 32 pin of the ESP32 and its supply voltage is 5V. The sensor's calibration is based on the sensor's output characteristics in the presence of smoke, which results are available in the sensor's information sheet. The calibration steps will be further described in section 4.1.2.3.

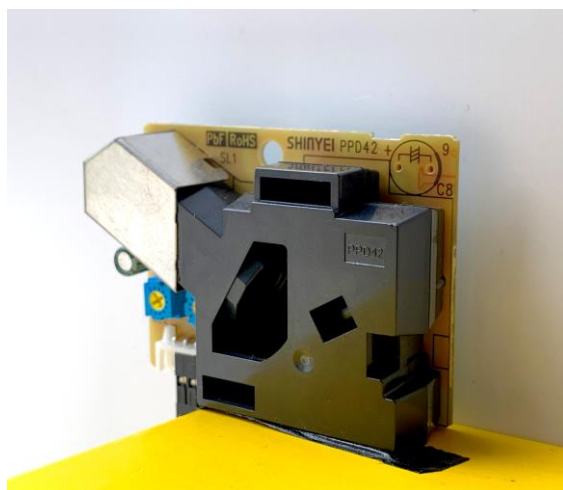


Figure 3.31. Node 3, with a Shinyei PPD42NS particle counter

Node 3 is presented in the previous figure. The sensor was placed in a vertical position as recommended by the sensor's manufacturer, in order to achieve the desired airflow.

3.2.5. Node 4

Node 4, presented in figure 3.34, includes a Si7021 smart sensor characterized by temperature and relative humidity measurement capabilities. It provides, alongside with Node 1, information about the spatial distribution of temperature and humidity. The following figure presents the Node's circuit schematic and its PCB schematic is shown in Figure 3.33.

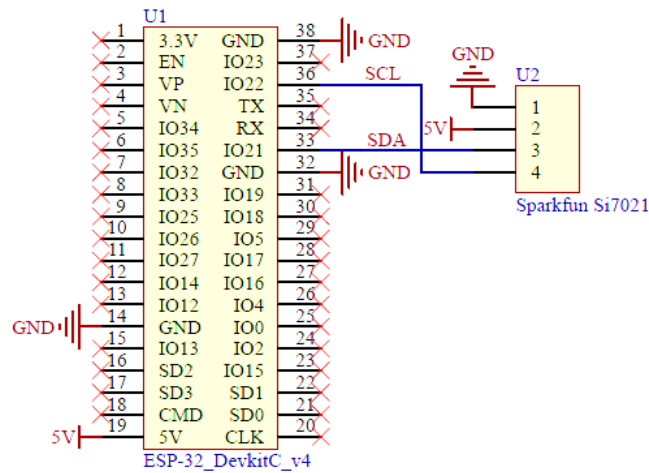


Figure 3.32. Node 4 circuit schematic

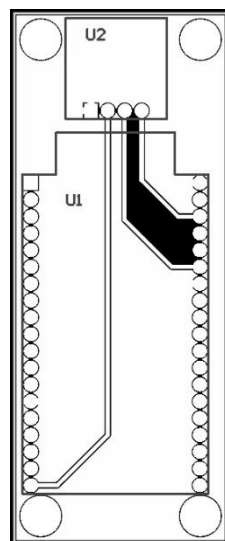


Figure 3.33. PCB schematic of Node 4

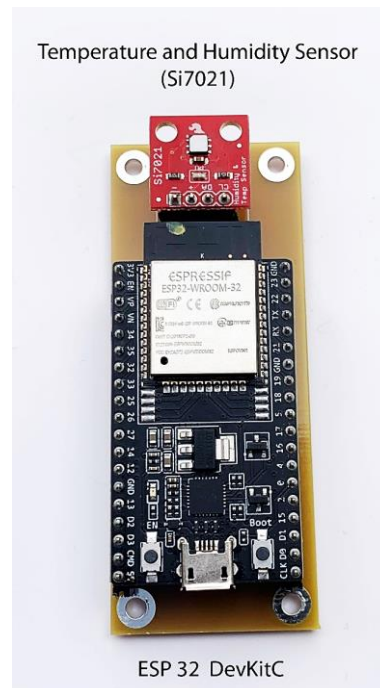


Figure 3.34. Node 4

3.2.6. Node 5 – Cardiac Activity Monitoring Node

The monitoring of physiological parameters in non-invasive ways is a crucial step to assure the user's comfort while important vital signs are obtained. As mentioned before, Ballistocardiography is a technique that measures those physiological signs. One of the sensors used in this monitoring system is an EMFi sensor (EMFIT L-3030), as shown in Figure 3.35. It consists of a plastic film that converts mechanical energy to an electrical signal. It is a flexible and thin polypropylene film with electrically conductive layers. When pressure is applied on the sensor, a charge is generated on its electrically conductive surface, that can be measured as a voltage signal with a charge amplifier.



Figure 3.35. EMFIT sensor of the L-series

To perform the BCG with this sensor, the implemented circuit uses a TLC2274 quadruple low-noise rail-to-rail operational amplifier and a parallel combination of $R_Q=10\text{ M}\Omega$ and $C_Q= 39\text{ pF}$ (see Figure 3.36). The operational amplifier exhibits high input impedance and low noise.

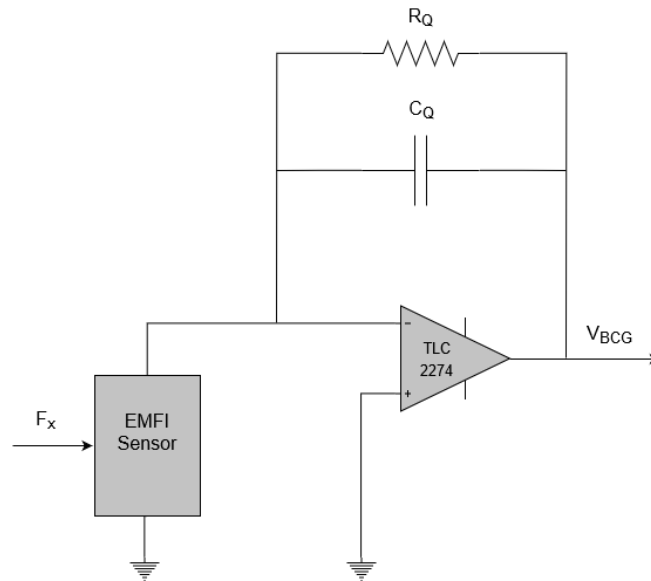


Figure 3.36. BCG charge amplifier scheme

Two acquisition system setups were considered to obtain BCG measurements:

- First setup includes a 24 bit, 4-Channel voltage input module NI USB-9239. All the input analog signals are conditioned, amplified and then converted by 24-bit Delta-Sigma ADC. To obtain low levels of noise on the BCG digital signal, digital filter algorithms were also implemented by programming this measurement device with compatible software (e.g. LabVIEW).
- In the second setup, the heartbeat signals were acquired with the ESP-32, with its embedded 12-bit ADC.

A pulse sensor was also considered as part of cardiac activity monitoring node to get heart-rate data, mainly bits-per-minute (BPM) and inter-beat intervals (IBI).

This sensor uses the Photoplethysmography (PPG) principle to obtain pulse data: The LED from the sensor, which can be seen in Figure 3.37, emits light into the user's fingertip and the ambient light sensor, placed right below the LED, reads the amount of light that is reflected.



Figure 3.37. Pulse sensor for PPG

The following figure depicts the proposed placement of the sensors on a chair. The EMFi sensor is embedded on the seat, while the pulse sensor is on the chair armrest.



Figure 3.38. Physiological parameters measurement system with BCG and PPG sensing units embedded on a chair

3.3. Actuator Nodes

Several actuator nodes were added to the system in order to give the user visual alert mechanisms for critical indoor air conditions, to change indoor lighting and enhance visual perception, to help changing the user's emotional state and to improve the environment's air quality and thermal conditions. The importance of each actuation and how is it going to be implemented will be described in the next sub-sections. The block diagram of the system based on three actuator nodes is shown in Figure 3.39.

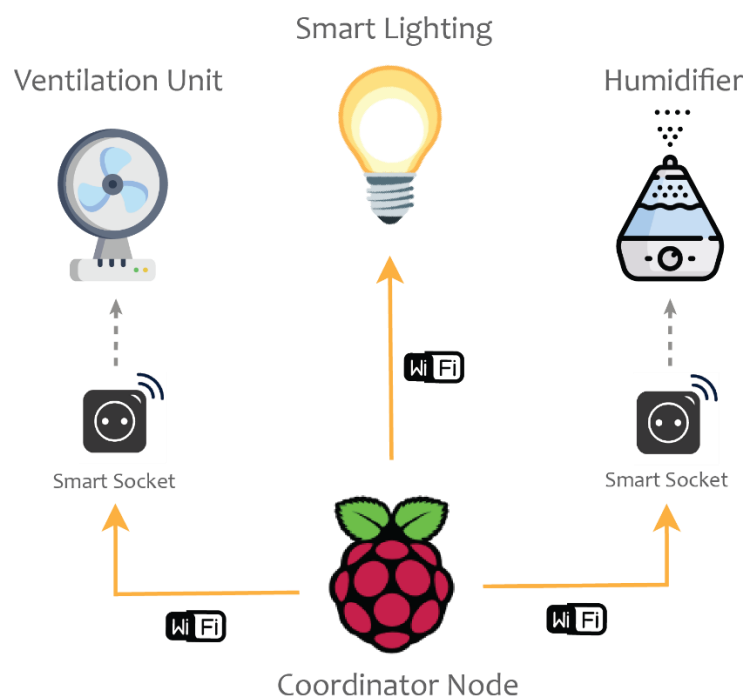


Figure 3.39. Scheme of interaction between the coordinator node and the actuator nodes

3.3.1. Smart Lighting

Light has a variety of significantly positive biological effects. It affects sleep and wake cycles, body temperature, hunger, human physiology and behaviour [61]. It improves well-being, productivity, alertness and relaxation by stimulating the bodies' natural circadian rhythms. When natural light does not reach the indoor environment, smart lighting systems are the best option to help balance such rhythms and thus improve quality of life. These systems can mimic natural light's colour transitions, from the energizing

blue wavelengths of early morning to the calmer and softer amber hues at night. There are several solutions on the market regarding these smart lights. Some require a dedicated hub in order to function, others don't; some even use Bluetooth to connect the smartphone to the light bulbs, but most use Wi-Fi; some systems work with smart home systems such as Amazon Echo, Google Home and Apple HomeKit; and so on.

Many companies have already been following this new trend, with Philips Hue being one of the first to offer customizable lighting [62]. It has a vast family of products and it is considered one of the best smart lighting options on the market. However, better and budget-friendly options are also available, such as Xiaomi Yeelight [63]. In terms of technology and connectivity, the Philips Hue requires a dedicated hub – the Philips Hue Bridge - in order to function and connect via Zigbee technology. The hub also needs to be connected to a router via an ethernet cable. This extra expense and additional hardware are two of this product's disadvantages. On the other hand, the Xiaomi Yeelight light bulbs present Wi-Fi connectivity and connect directly to a 2.4GHz 802.11 b/g/n compatible router. It's a simpler solution and easier to implement as no bridges or hubs are required. Both have very similar levels of brightness, color temperature ranges and around 16 million color choices.

A comparison between the two options is presented in Table 3.10.

Table 3.10. Comparison between Philips Hue and Xiaomi Yeelight

	Philips Hue Gen 3	Xiaomi Yeelight
Lumens	806 Lm	800 Lm
Color Temperature	2000 - 6500 K	1700 – 6500 K
Color Range	16 million colors	16 million colors
Dimming	Yes	Yes
Communication Protocol	Bluetooth and ZigBee	Wi-Fi 2.4Ghz 802.11 b/g/n
Requires a Hub/Bridge	Yes	No
Security	N/A	WPA/WPA2
Rated Power	9.5 W	9 W
Open API Supported	Yes	Yes

Both smart lights have open APIs, which means they can solely be controlled by the coordinator node without the need for a smartphone app. This will be more detailed in section 4.2.

After considering the two options, the Yeelight LED Light Bulb from Xiaomi was the chosen smart bulb to implement smart lighting into our system. Additionally, and considering the same family of products and operating mode, a Yeelight Lightstrip (Color) is also used to extend the smart lighting system. Figure 3.40 and 3.41 present the two models.



Figure 3.40. Xiaomi's Yeelight LED Light Bulb

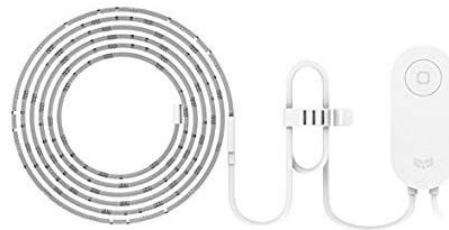


Figure 3.41. Xiaomi's Yeelight Lightstrip (Color)

3.3.2. Indoor thermal conditions

Two actuator nodes were added to help improve indoor thermal conditions and air quality, thus preventing respiratory distress and discomfort feelings related to the surrounding thermal environment. A humidifier was chosen to increase humidity (moisture) levels and keep them within safe threshold values, as well as a single-room ventilation unit to displace indoor pollutants, increase thermal comfort and dehumidify the environment.

Contrary to the smart lighting bulb, the humidifier and ventilation units do not have wireless connectivity and cannot be remotely controlled unless they have external hardware. For that purpose, a smart socket/plug is used to remotely turn these units ON or OFF. A TP-LINK Wi-Fi Smart Plug, model HS100, was considered the best choice, as it connects to a wireless network without requiring any hub and offers integration with other products and systems. In this way, the coordinator node can control the humidifier and ventilation units' power state by a set of commands sent via Wi-Fi.

The interaction between the coordinator node and these smart sockets will be described with more detail in the software section.

3.4. Coordinator Node / Gateway

A Raspberry Pi 3 Model B+ [64] was used as a smart gateway between the final user and the sensing nodes. It performs data analysis, actuators control and data transmission to an online database. This mini-computer is characterized by a 64-bit quad core processor running at 1.4 GHz and 1GB LPDDR2 SDRAM. Regarding its connectivity, this single-board computer provides dual-band 2.4 GHz and 5 GHz IEEE 802.11 b/g/n/ac wireless LAN, Bluetooth 4.2, BLE, four USB 2.0 ports and Gigabit Ethernet over USB 2.0. Its operating system is the Raspbian, a Debian-based computer OS from the Unix-like family, and it runs on its microSD card.

Recently, a more powerful Raspberry PC board was released – the Raspberry Pi 4 [65]. It has better CPU, faster memory, two USB 3.0 ports and 4K monitor support. However, it doesn't have a full-size HDMI port like the previous version.

Since this system doesn't require any graphical abilities and better processing power, the Raspberry Pi 3 B+ was selected as a gateway. Its software configuration will be further described in the software section.



Figure 3.42. Smart gateway - Raspberry Pi 3 B+

Chapter 4

System Software

In addition to all the hardware and physical connections that make the system operational, software is one of the essential components that defines the behavior and characteristics of the system. Thinking on providing a good user experience and the option of scalability of the entire system, the next section describes the node's embedded software, as well as the smart gateway and web application's software.

4.1. Embedded software

Each sensor node behaves very similarly, as shown in Figure 4.1. All node software is implemented on the ESP32 microcontroller with the Arduino IDE using a C compiler. The code can be directly uploaded by the micro-USB port or, if the board is not easily accessible, over-the-air (OTA). OTA programming uses an OTA Web Updater that creates a web server and allows the code to be uploaded to an ESP32 by using a browser. Additional code for OTA needs to be added in every microcontroller's sketch. In this project, the software is uploaded to the ESP32 by using its integrated serial USB converter.

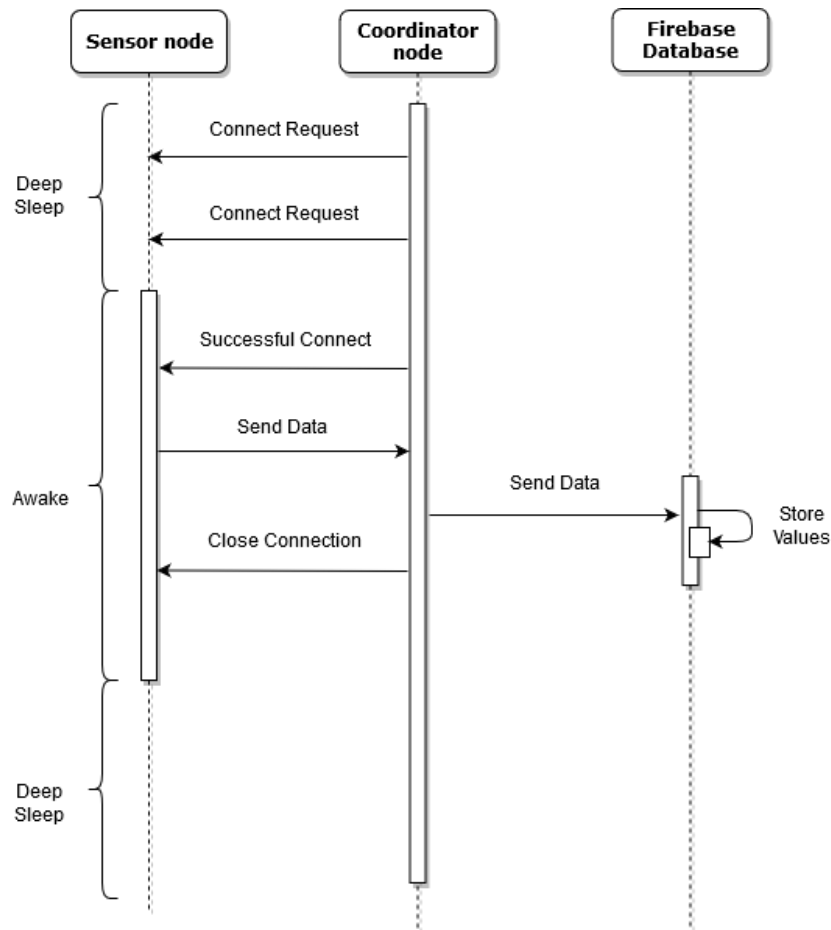


Figure 4.1. Interaction flow between the Sensor node and Coordinator node

As demonstrated in Figure 4.1, each sensor node follows the same number of tasks in order to interact with the coordinator node. The coordinator itself also has the same behavior with the four sensor nodes when it comes to establishing a connection and receive data.

Each sensor node enters in deepsleep mode for 3 minutes to reduce power consumption and extend battery life. When the ESP32 is on deepsleep mode, every connection request addressed to it is ignored, since all radio communication modules are powered down. The coordinator will keep sending connection requests till it successfully connects via Bluetooth to the sensor node. When the connection is successfully established, the coordinator node waits for a data transmission from the node containing data from each sensor. After receiving it, the values are sent to an online database, as it's going to be described in the following section. The connection is then closed between the coordinator node and the sensor node. After being active during approximately 10 seconds, the sensor node enters deep sleep mode once more.

4.1.1. Sensor nodes data transmission

Every sensor node performs data transmission to the coordinator node by using the Bluetooth protocol. To enable this feature, a set of commands were considered in the ESP32's software.

The Bluetooth Serial ESP32 library is used for that purpose. This library is based on the principle of sending data to an emulated serial connection that operates over Bluetooth.

```
1 #include "BluetoothSerial.h"
2
3 BluetoothSerial SerialBT;
4
5 void callback(esp_spp_cb_event_t event, esp_spp_cb_param_t *param){
6     if(event == ESP_SPP_SRV_OPEN_EVT){
7         Serial.println("Client is connected");
8     }
9 }
```

Figure 4.2. Callback function to detect new client connection events

As presented in Figure 4.2, the **BluetoothSerial.h** library needs to be included in each of the microcontroller's code in order to use its functionalities and allow the establishment of serial connections over Bluetooth. An object of this class is then added to initialize the Bluetooth interface. Whenever the sensor node wakes up, the Bluetooth is initialized, and it only performs data transmission whenever an event occurs. In this case, this event consists of a client connection from the coordinator node. For this to happen, a callback function to handle Serial Port Profile (SPP) events needs to be implemented. This function needs to follow a signature specified by the **esp_spp_cb_t** type [66], which in this case receives as first parameter a variable of type **esp_spp_cb_event_t** that indicates the type of SPP event that has occurred. Since the objective is to send data only when a client connection is received, the choice of which SPP events are going to be handled needs to be specified.

From the many available SPP callback function events [67], the required SPP event for this case has the signature of **ESP_SPP_SRV_OPEN_EVT**, which occurs whenever a SPP Client connection opens.

To register this callback, a **register_callback** method is called on the **BluetoothSerial** object, that receives as input the previously mentioned callback function.

The Bluetooth interface needs to be initialized in the **setup()** function, by calling the **begin** method on the **BluetoothSerial** object. The name we wish to assign to the ESP32 is

provided as a parameter for this method. In this case, each sensor node has its own name, which eases the coordinator node's discovery procedure.

4.1.2. Sensor data reading and processing

Most readings from the sensors are collected from a specified analog pin of the ESP32. As already mentioned, the ESP32 board contains a 12-bit analog to digital converter. Therefore, it will map input voltages between 0 and the operating voltage (3.3V to 5V) into integer values between 0 and 4,095.

4.1.2.1. Node 1 and Node 4 - Thermal Conditions Measuring Nodes

The Si7021 sensor that integrates Node 1 and Node 4 is an I2C sensor, and its SCL pin needs to be connected to the clock SCL pin of the ESP32 and the SDA pin to the respective I2C data pin. To read this sensor data, a dedicated library, Adafruit Si7021 Library, is used [68]. There are no pins to set on the code since the I2C bus is being used. To get the temperature and relative humidity readings from the sensor, an object from the class `Adafruit_Si7021` had to be created, followed by its initialization. Once initialized, the temperature was obtained in °C with `readTemperature()` function, and the relative humidity with `readHumidity()` function.

Relatively to the electret microphone amplifier present in Node 1, its output signal is a varying voltage. As shown in Figure 4.3, to convert those voltage levels into sound levels, multiple measurements of the signal were taken to find the minimum (`signalMin`) and maximum (`signalMax`) levels of that signal, or the also called peak to peak amplitude (`peakToPeak`). A sample window of 50 milliseconds was enough to measure sound levels of frequencies as low as 20 Hz, which is the lower limit of the human hearing. After getting the minimum and maximum samples, the difference between both is calculated and then converted into volts.


```

126 unsigned long startMillis= millis();
127 unsigned int peakToPeak = 0;
128 unsigned int signalMax = 0;
129 unsigned int signalMin = 4095;
130
131 while (millis() - startMillis < sampleWindow){
132     sound = analogRead(pin_sound);
133     if (sound < 4095)
134         if (sound > signalMax){
135             signalMax = sound;
136         }
137     else if (sound < signalMin){
138         signalMin = sound;
139     }
140 }
141 }
142 peakToPeak = signalMax - signalMin;
143 double volts = (peakToPeak * 5.0) / 4095;
144 Serial.print("\tSound: ");
145 if(volts >= 0.0 && volts < 5.0){
146     Serial.print(volts);
147 }else{
148     Serial.print("0");
149     volts = 0;
150 }

```

Figure 4.3. Sound sensor signal conversion

As for the LDR, the read analog value is directly sent to the coordinator node without needing any analysis.

4.1.2.2. Node 2 - Gas Sensing Node

The values obtained from the gas sensors in node 2, which are also acquired by the ESP32's analog to digital converter (ADC), require the calibration as was mentioned in section 3.2.3.1. Based on those calibration methods, the value from the ADC is converted to a voltage level in first place. The Rs value for each sensor is calculated by using the sensor's resistive value at various concentrations of gases as demonstrated in equation 4. The concentration of gas in parts per million (ppm) is given by following equation 3.

The estimation of gas concentration levels from each sensor is performed with the following equations, as shown in Figure 4.4.

```

35 //MQ-135
36 float vout = val_mql35/4095*5;
37 rs_mql35 = 20 * ((5/vout_mql35)-1);
38 ppm_mql35 = 82.536 * (pow(rs_mql35/ro_mql35,-3.054));
39
40 //MQ-4
41 float vout_mq4 = val_mq4/4095*5;
42 rs_mq4 = 20 * ((5/vout_mq4)-1);
43 ppm_mq4 = 1040.6 * (pow(rs_mq4/ro_mq4,-2.837));
44
45 //MQ-9
46 float vout_mq9 = val_mq9/4095*5;
47 rs_mq9 = 20 * ((5/vout_mq9)-1);
48 ppm_mq9 = 1016.1 * (pow(rs_mq9/ro_mq4,-2.12));

```

Figure 4.4. Conversion of gas sensor's readings into gas concentration levels

4.1.2.3. Node 3 – Particulate Matter Measuring Node

The Shinyei PPD42NS particle sensor present in Node 3 estimates the particles count concentration based on the duration of time that the digital signal from the ESP32's pin is held low, as demonstrated in Figure 4.5. The samples are taken for 30 seconds, as recommended by the sensor's manufacturers [69].

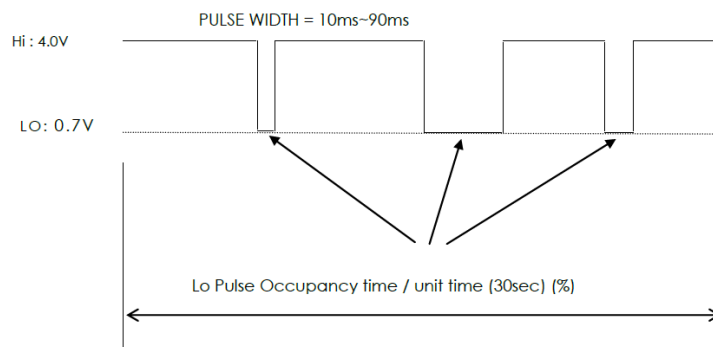


Figure 4.5. Lo Pulse Occupancy time example. Source [63]

To find a correlation between the LoPulse Occupancy Time (LoP) and the concentration of particles in the air, data points from the sensor's characteristic curve in the presence of cigarette smoke, shown in Figure 4.6, were fit into an X and Y graph.

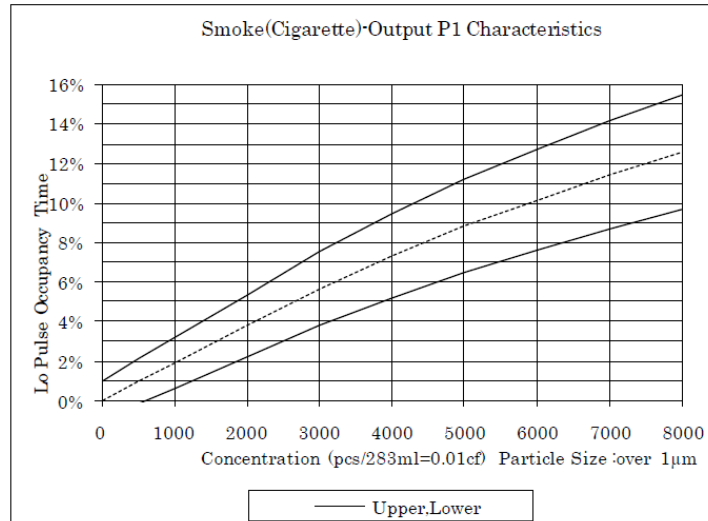


Figure 4.6. PPD42NS characteristic graph. Source [63]

By adding a cubic polynomial trendline to the obtained curve, the following equation is achieved:

$$C [pcs/0.01cf] = 1.1LoP^3 - 3.8LoP^2 - 520LoP + 0.62 \quad (7)$$

where C is the concentration of particles and variable LoP represents the Lo Pulse Occupancy Time ratio.

It is then possible to estimate the concentration of particles per 0.01 cubic feet (cf) (equivalent to pcs/283 ml) by getting the low pulse duration from the sensor (line 64 from Figure 4.7) and the ratio during a 30000 milliseconds sample time.

```

64 duration = pulseIn(pin, LOW);
65 lowpulseoccupancy = lowpulseoccupancy+duration;
66
67 if ((millis()-starttime) > sampletime_ms && count < N)
68 {
69     ratio = lowpulseoccupancy/(sampletime_ms*10.0);
70     concentration = 1.1 * pow(ratio,3) - 3.8 * pow(ratio,2) + 520*ratio + 0.62;
71     Serial.print(lowpulseoccupancy);
72     Serial.print(",");
73     Serial.print(ratio);
74     Serial.print(",");
75     Serial.println(concentration);
76     lowpulseoccupancy = 0;
77     starttime = millis();
78 }

```

Figure 4.7. PPD42NS estimation of the particle's concentration per 0.01cf

4.1.2.4. Node 5 – Cardiac Activity Monitoring Node

To test the proper function of the EMFi sensor and to acquire the BCG signal, the first setup includes a 24-bit C Series analog input module (e.g. NI USB-9239). The measurement device was programmed to acquire data by using the LabVIEW graphical programming environment.

In the second setup an acquisition system based on the ESP32 microcontroller was used to acquire the BCG signal. The voltage signals generated by the sensor and measured by the microcontroller's ADC were analyzed with the Serial Plotter from Arduino IDE.

Relatively to the pulse oximetry sensor, a heartbeat can be easily detected by displaying the acquired signal at the Arduino Serial Plotter. A heartbeat occurrence is detected by the visualization of a peak of amplitude at the ADC. By following the PPG method, a heart rate estimation can be given by calculating the interval per beats (IBI) parameter, which refers to the time interval between individual heart beats.

The ESP32 reads the analog signal from the pulse sensor, and when the signal goes higher than a threshold value, a heartbeat is considered. Because the ADCs readings go up to 4095, the obtained reading was divided by four, so the threshold values can be any number between 0-1024. This does not affect the readings and it was only made to get lower amplitudes. A threshold value of 550 was considered ideal to calculate the interbeat interval (IBI) and the heart rate in beats per minute (BPM).

The values in BPM were calculated by considering the time interval between the first pulse and the second pulse. As previously mentioned, the pulse is detected when values from the ADC are higher than the established threshold value. In order to convert IBI into heart rate (HR), the following equation was used [70]:

$$HR = \frac{60\,000}{IBI} \quad (8)$$

The heart rate measured by the sensor is sent to the coordinator node over Bluetooth, whenever a pulse is noticed.

The readings and results of the multiple tests performed with the EMFi sensor and pulse sensor will be described in section 5.1.

4.1.2.5. Deep sleep mode implementation on the ESP-32

The node's autonomy can be greatly improved by implementing power saving strategies on the microcontroller. As previously mentioned, the ESP32 chip has different available power saving modes, in which deep sleep mode is considered the best suitable for this project. To enable this power saving mode on the ESP-32's chip, it was first necessary to configure its wake-up sources. There are several sources that can be used and even combined – in this case, the chip will wake up when any of the sources is triggered. The different wake up sources can be the configuration of a timer, a GPIO pin or the ULP co-processor. If no wakeup sources are configured, the chip will be in deep sleep mode indefinitely, until an external reset is applied.

For this case, a timer has been configured as the wake up source. The RTC controller has a built-in timer that can be used to wake up the chip at predefined amounts of time, therefore to enable this wake up source, a certain amount of time must be specified in the following function: `esp_sleep_enable_timer_wakeup(time_in_microseconds)`

The period in microseconds is defined by these two variables (`uS_To_S_FACTOR` and `TIME_TO_SLEEP`), which will be then used in the previous function:

```
#define uS_TO_S_FACTOR 1000000 /* Conversion factor for micro seconds to seconds */
#define TIME_TO_SLEEP 180 /* Time ESP32 will go to sleep (in seconds) */

...

esp_sleep_enable_timer_wakeup(TIME_TO_SLEEP * uS_TO_S_FACTOR);
```

The ESP-32 microcontroller will remain in deep sleep mode for 3 minutes, since collected data of indoor environmental conditions do not vary much in shorter time intervals. In order to save data on the RTC memories, `RTC_DATA_ATTR` must be added before the variables we want to keep. The following example is used to test this functionality, by saving the number of times the ESP32 has woken up from deep sleep:

```
RTC_DATA_ATTR int bootCount = 0;

...

//Increment boot number and print it every reboot
++bootCount;
Serial.println("Boot number: " + String(bootCount));
```

Once wakeup sources are configured and all the important data is set to be stored in the RTC memories, the application can finally enter sleep mode by calling the following function: `esp_deep_sleep_start()`

While implementing the deep sleep mode, the `loop()` function is never used. All the code, except for the variables, must be written inside the `setup()` function.

The following figure shows the printed messages of the ESP-32 on the Arduino IDE serial monitor each time it wakes up.

```
rst:0x5 (DEEPSLEEP_RESET),boot:0x13 (SPI_FAST_FLASH_BOOT) 1
configspi: 0, SPIWP:0xee
clk_drv:0x00,q_drv:0x00,d_drv:0x00,cs0_drv:0x00,hd_drv:0x00,wp_drv:0x00
mode:DIO, clock div:1
load:0x3fff0018,len:4
load:0x3fff001c,len:1100
load:0x40078000,len:9232
load:0x40080400,len:6400
entry 0x400806a8
Boot number: 3 2
Wakeup caused by timer
Setup ESP32 to sleep for every 180 Seconds
Si7021 test!
Found model Si7021 Rev(2) Serial #7843374C15B5FFFF

Humidity: 49.25 Temperature: 25.65
Going to sleep now 3
ets Jun 8 2016 00:22:57

rst:0x5 (DEEPSLEEP_RESET),boot:0x13 (SPI_FAST_FLASH_BOOT) 1
configspi: 0, SPIWP:0xee
clk_drv:0x00,q_drv:0x00,d_drv:0x00,cs0_drv:0x00,hd_drv:0x00,wp_drv:0x00
mode:DIO, clock div:1
load:0x3fff0018,len:4
load:0x3fff001c,len:1100
load:0x40078000,len:9232
load:0x40080400,len:6400
entry 0x400806a8
Boot number: 4 2
Wakeup caused by timer
Setup ESP32 to sleep for every 180 Seconds
Si7021 test!
Found model Si7021 Rev(2) Serial #7843374C15B5FFFF

Humidity: 49.36 Temperature: 25.71
Going to sleep now 3
```

Figure 4.8. ESP-32 printed messages while deep sleep mode is configured

In the message marked by number one, the chip prints which type of sleep mode was configured. In this case, it describes the reason for the reset (`deepsleep_reset`). Message number two displays how many times the chip has rebooted after leaving sleep mode and presents the wake up reason. In number 3, after performing some tasks, the chip enters deep sleep mode again.

4.2. Smart gateway

The smart gateway or coordinator node is represented in the present system by a Raspberry Pi 3 B+ computation platform. The software for the smart gateway was developed in Python. The gateway performs sensors data analysis and processing, actuators control and data transmission to an online database.

A simplified sequence diagram, presented in Figure 4.9, depicts the gateway's interaction with the different sensor nodes.

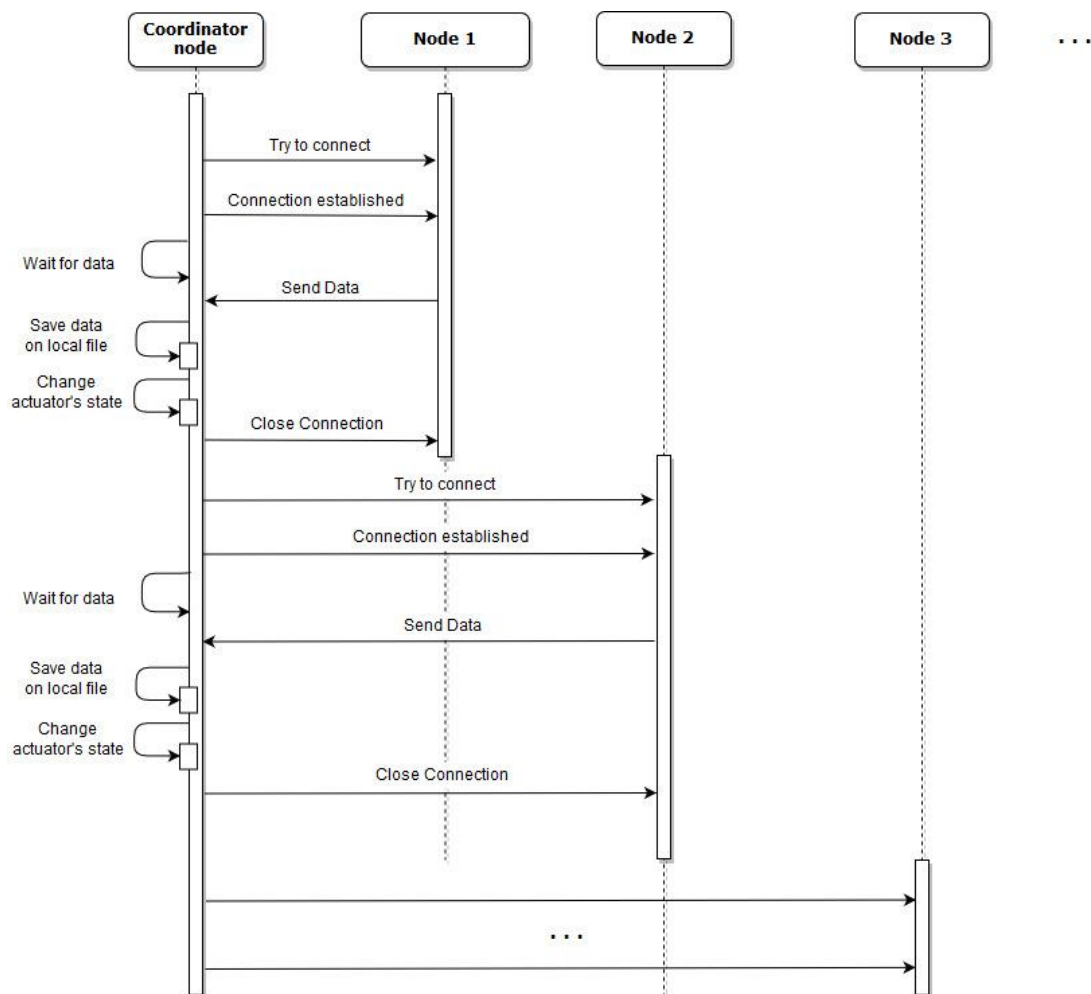


Figure 4.9. Interaction flow between the Coordinator node and Sensor nodes

The coordinator node is connected with the sensor nodes through Bluetooth, as stated above. The Python Bluetooth library named PyBluez is used to enable Bluetooth programming. Bluetooth programming in Python is based on socket programming, and connections are established and terminated with the sensor nodes by using an RFCOMM socket. An RFCOMM service is a connection-oriented protocol, similar to TCP. An

RFCOMM socket was created by passing RFCOMM as an argument to the Bluetooth socket constructor.

Since the coordinator node only starts receiving data after establishing a connection with a sensor node, the **connect (bt_addr, port)** method is used after creating the socket. It receives the Bluetooth device address we wish to connect to, and a port number. To receive the sensors data, a **recv(1024)** method allowing a maximum of 1024 characters received at a time, is called.

By following the sequence diagram on Figure 4.9, the coordinator tries, in first place, to connect with sensor node 1. If the node is active and it successfully connects with it, the coordinator will wait for a data transmission from the sensor node. Otherwise, if the connection is not successful, it will move on to the next sensor nodes. Once it receives the sensory data, it will save it on a LibreOffice calc spreadsheet to prevent any lost data events if internet connection is disabled. Based on the information received from the sensors, the coordinator analyses those values and compares it with pre-defined thresholds. Thresholds for temperature and relative humidity are configured by the user on the Web Application and can be personalized to its needs, given that different people may react to different types of triggering factors or have different thermal comfort level requirements. As for the gas concentration and particulate matter threshold levels, those are kept in a fixed safe value. If the data from the sensors exceed the thresholds, the coordinator node changes the actuators state, as further described. After all events are handled, the coordinator closes the connection with the sensor node and moves on to the next nodes.

4.2.1. Actuators control

The smart gateway controls all actuator nodes in order to provide an adaptive environment. Regarding the smart lighting system, this actuator node is controlled through Wi-Fi and it is considered the main alert mechanism to prevent respiratory distress (asthma crisis and COPD) by executing warning signals: if relative humidity or temperature values exceed an imposed threshold value, a command is sent via Wi-Fi to the Yeelight Light Bulb. This command orders the smart bulb to perform a color transition cycle between two tonalities of red, thus performing a warning signal. The same behavior is also applied for gas and particulate matter sensors readings.

Besides providing visual alerts for critical air conditions, the lights will also mimic natural light's colour transitions to improve the user's well-being, productivity, alertness and relaxation feelings.

Yeelight smart LED products support remote control over WiFi and allow 3rd party control [71]. A small Python Yeelight library was used to control the smart lights from the coordinator node. The Yeelight WiFi LED is controlled by the manufacturer's cloud service. Whenever a command is sent from the coordinator node, it will first reach the cloud server and then forwarded to the device. However, it also provides LAN control – if the coordinator node and the smart bulb are in the same local network, the control command is sent directly to the device via LAN instead of going through the cloud service.

To establish a connection with the smart bulb, its IP address on the local network needs to be specified. Yeelight uses a single TCP connection for all commands that are sent to the smart bulb.

In order to adapt both light levels and colour throughout the day, multiple commands are sent to the smart bulb specifying the colour temperature we want to set. Each command adjusts its colour temperature according to the time of the day, considering the colour temperature range of the smart bulb and the schedule presented in Fig. 4.10.

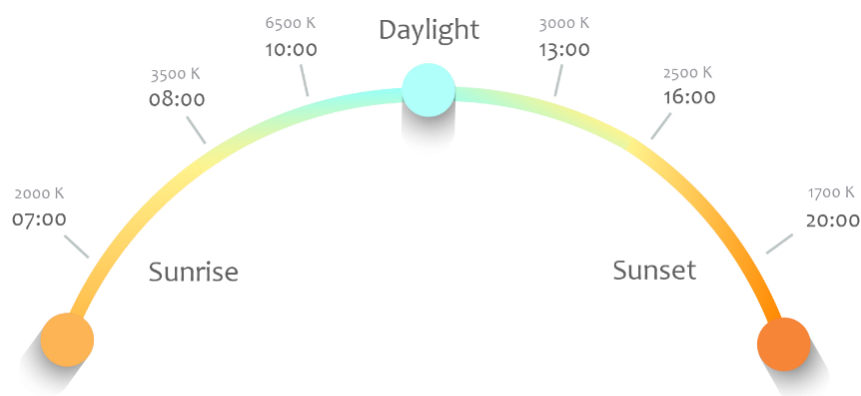


Figure 4.10. Smart light's color temperature variance throughout the day

The algorithm that follows Figure 4.11 schedule and changes the light's color temperature according to the time of the day has the following sequence, presented in the next figure:

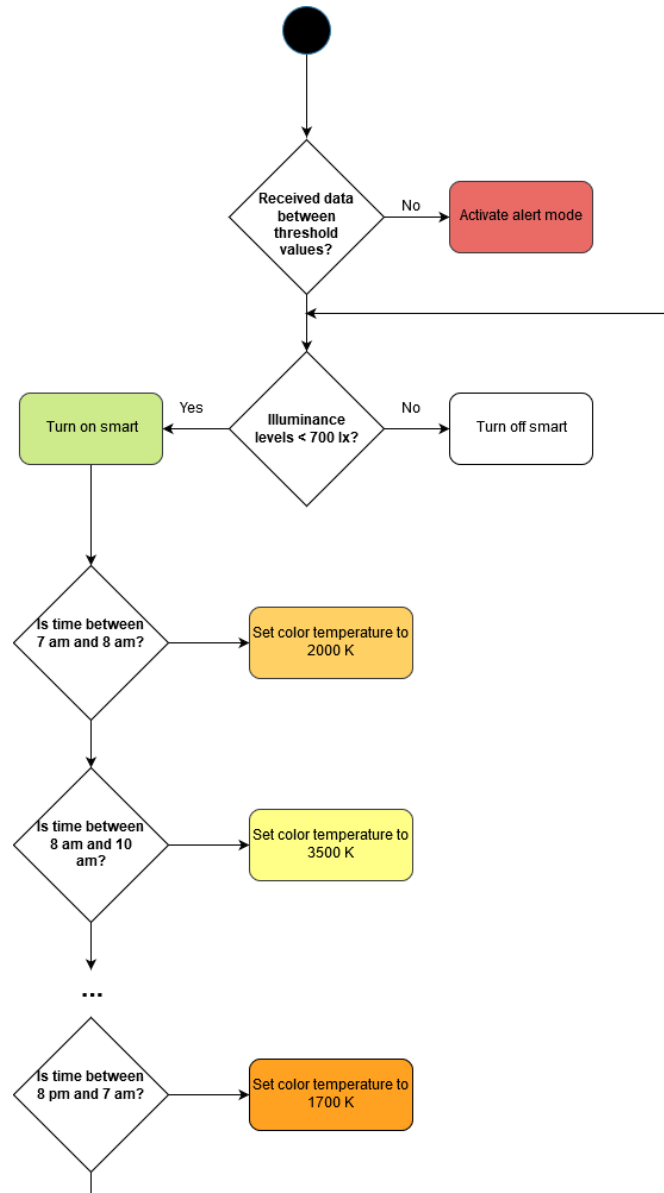


Figure 4.11. Acuator's control logic performed by the Coordinator node

In first place, the coordinator analyses if air quality-related data collected from the sensors is between safe threshold values. If it is not, the alert mode is activated on the smart bulb. A command specifying the tonalities of red, its brightness levels and the

duration of those transitions are sent from the Raspberry to the light bulb. The warning systems are set to last for 10 seconds whenever it receives critical air quality data.

After performing the warning signal, the lights adopt once more their colour temperature according to the time of the day, and so on. If the thresholds are between safe values, the alert mode is not triggered.

The same principle is applied to another smart light object that acquires different tonalities of blue whenever the pulse rate measured by the biomedical node is above a certain threshold, expressed in bpm (e.g. 110 bpm).

Smart lights only turn on to perform warning signals or whenever the indoors light intensity measured by the LDR sensor is below 700 lux. Otherwise, they remain off for power saving purposes.

Relatively to the humidifier and ventilation unit, their power state is also induced by the temperature and humidity threshold values. If relative humidity is below the minimum value (dry environment), the coordinator node sends a command to the humidifier's smart plug that will change its power state. The same logic is used with the ventilation unit, for when the temperature readings exceed the maximum values. Just like smart lighting, the smart plug can be remotely controlled over Wi-Fi. To control the smart plug state, its IP address must be known and therefore specified in the Python's script. The smart plug is turned on and off by calling appropriate methods on the smart plug's object. These methods are called according to the indoor thermal conditions, as previously mentioned. The actuators will remain turned on until new values acquired from the sensor nodes are between the threshold interval. In that case, a command that changes the smart plug's switch is sent.

4.3. Data Storage

An online database is used to store data from the sensor nodes, allowing it to be further analyzed on the web application and from anywhere in the world.

Firestore Database [45] was considered the best option and was therefore used for this purpose. It is a NoSQL cloud database which consists of a nonrelational database with flexible data models, optimized for applications that require large volume of data and low latency. The NoSQL databases provide flexibility, scalability, high-performance, functionality and ease of development.

In Firestore Database, data is stored as JSON and is synchronized in real-time with every connected client. Whenever data changes, every device connected to the database receives the updated data.

Unlike SQL databases, there are no tables nor records. The database can be seen as a cloud hosted JSON tree. Whenever new data is added to the JSON tree, it becomes a new node in the existing structure and with an associated key. Those keys can be provided by the user or can be automatically generated. In Figure 4.12 is an example of how data is structured on the database. Each sensor node (Node 1, Node 2, etc.) is a child of the “Sensor Nodes” node. This structure makes the task of retrieving data much easier and clearer.

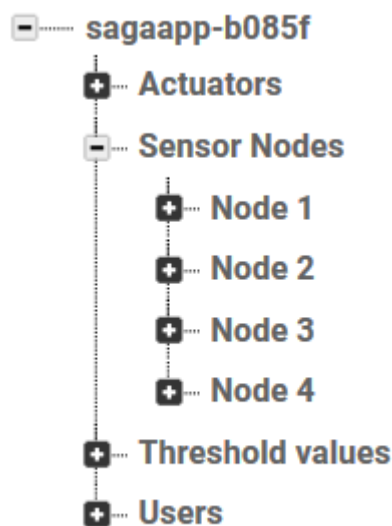


Figure 4.12. Database structure

Firestore allows secure access to its database directly from client-side code. A Python interface to the Firestore's REST API is used to send the sensory data from the coordinator to the database. HTTP requests are sent to the Firestore to save the data.

The MQTT protocol was also considered as an alternative to the HTTP, but it proved to be unsuitable for this system for several reasons: its advantages regarding lower power consumption over the HTTP protocol did not apply to this system since it is the coordinator node that sends the HTTP requests (because the coordinator node is plugged in, it does not require energy saving strategies); since Firestore Realtime Database is being used, the MQTT protocol is not suitable, as this database has almost the same role as an MQTT broker; finally, the sensor nodes send data via Bluetooth to the coordinator node, which demonstrates that this protocol would not apply either.

Similarly to other REST APIs, and considering the HTTP protocol, there are many methods used to save data on the database:

- **PATCH** method is used to update a key of a defined path. It can be used to post new data with a specific key provided by the user.
- **PUT** method is used to write or replace data on a defined path.
- **POST** request method is used to add new data on a specific path on the database. It generates a unique key for every POST request.
- **DELETE** method is used to remove data from a specified path reference.

The used method to send the sensors data to the firestore is the **PATCH** method. A key can be provided by the user, which will make the task of generating charts on the web application and retrieving data much more easier. Sensor node 1 has the following structure on the database:

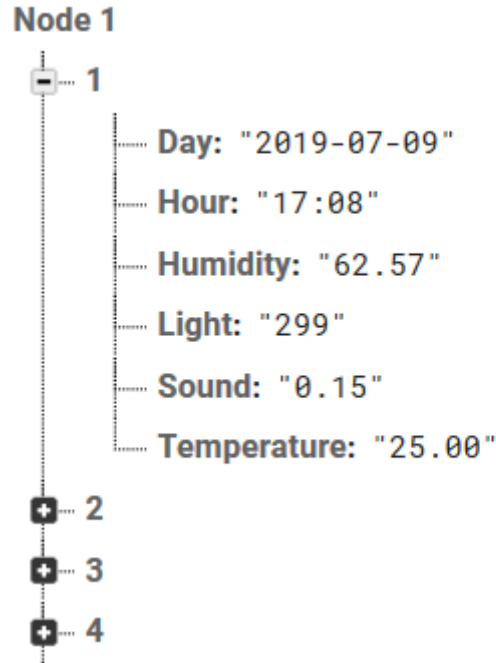


Figure 4.13. Database structure for Node 1

It includes the day in which the sensory data was obtained, the respective time and the relative humidity, temperature, sound and light levels. Other nodes will include their respective sensor values.

For future data analysis, every sensor node stores a timestamp with HH:MM and the date in yyyy-mm-dd in which the sensor reading was obtained.

To fetch data from the database, which happens whenever a new obtained value from the sensors needs to be compared with the threshold values, a GET request method is sent. It includes the path where the values are stored and some extra key-value pairs that specifies the parameter we want to obtain in particular.

Firestore also provides authentication services and methods that can be used in applications. Firebase Authentication will be used to authenticate the user on the developed web application, and its usage will be further described in the web app section.

4.4. Web application

As for the web application, it provides full remote control over the system and real-time monitoring of the environment. It is also designed to warn the user if indoor air conditions are critical by displaying on-screen notifications. It offers many other functionalities as well which are going to be described. The web application works on multiple platforms and it is compatible with the most common operating systems, enabling it to be used by anyone through its personal computer, laptop, tablet or smartphone. It is built using HTML 5, JavaScript, CSS and uses Bootstrap 4, jQuery and FusionCharts frameworks. Bootstrap framework enables responsive web design (RWD) in the web application, making the web page render on a variety of devices with different screen or window sizes.

Its interaction with the user and online database can be seen in Figure 4.14.

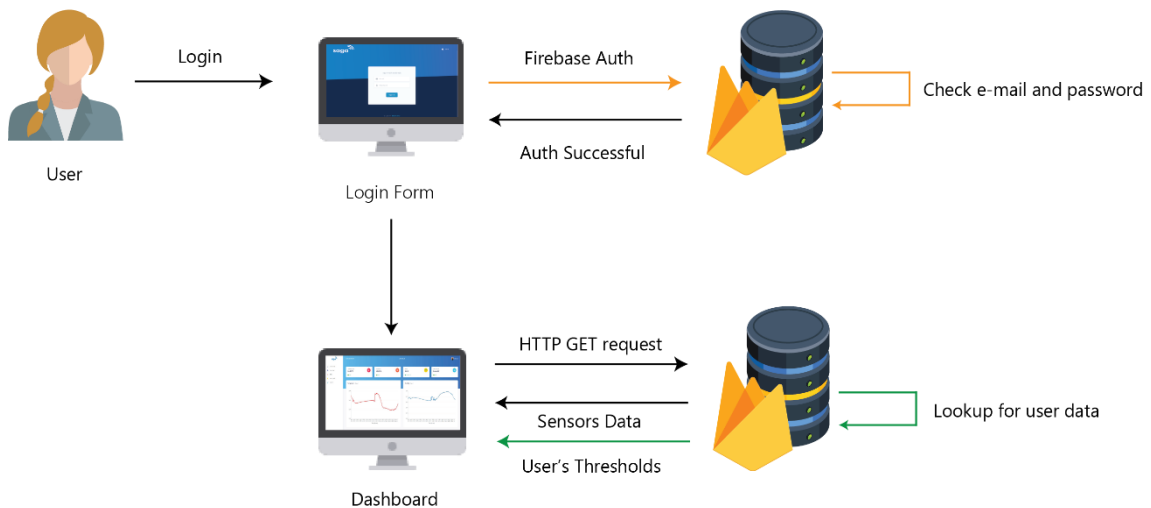


Figure 4.14. Flow of interaction between the Web application and the database

The application starts with a login page that requires an email and password authentication, as seen in Fig. 4.15.

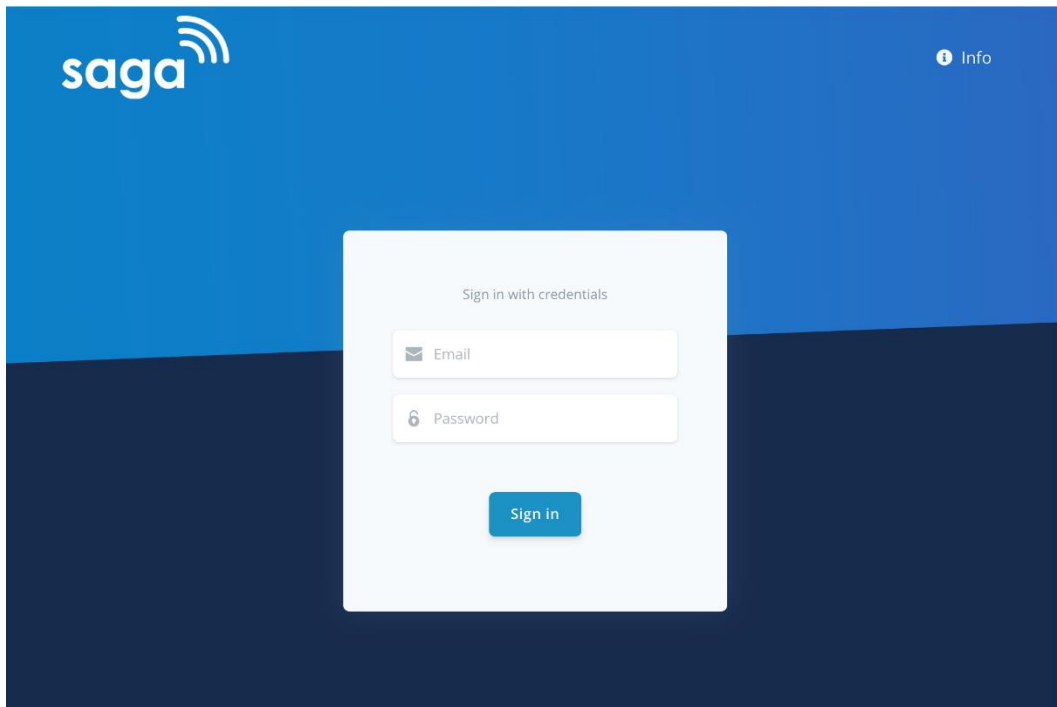


Figure 4.15. Login form of the web application

Firebase SDK Authentication methods are used for that purpose. This authentication will provide a personalized experience to the user and guarantee that only registered users have access to the web application.

Firebase authentication provides email and password authentication, phone number authentication, anonymous authentication with temporary accounts and also allows users to sign in with Google, Facebook and other accounts. For this system, the email and password authentication method was chosen. The Firebase Authentication SDK provides methods to create and manage users who sign in with an email and password. Different steps were followed in order to enable this feature. First, Firebase needed to be added to the web app's JavaScript project.

After the email and password login method is specified in the Firebase console, new users were added in the console's Users section. New users can only be added in this console as no user registration method is implemented in the web application, for safety purposes.

The JavaScript method to sign in a user with and email and password on the web application is demonstrated in the next figure.


```

<script type="text/javascript">
  /**
   * Handles the sign in button press.
   */
  function toggleSignIn() {
    if (firebase.auth().currentUser) {
      firebase.auth().signOut();
    } else {
      var email = document.getElementById('email').value;
      var password = document.getElementById('password').value;
      if (email.length < 4) {
        alert('Please enter an email address.');
```

Figure 4.16. JavaScript method to authenticate a user on the web application

The method first detects if the user is already authenticated or not. If not, it requires the filling of the email and password fields. If those elements are inside the minimum requirements in terms of word length, they are passed as arguments in the **signInWithEmailAndPassword** Firebase method.

Figure 4.17 illustrates with more detail the authentication flow performed by the user and Firebase services in order to sign in users.

Firestore signs in the user with the email and password credentials provided in the form. It sends back either an error object or a `userData` object. If the login is successful, the authentication token is saved to the browser's local storage, so it persists when the page refreshes. After confirming a successful authentication, the user gets redirected to another page as it is going to be described.

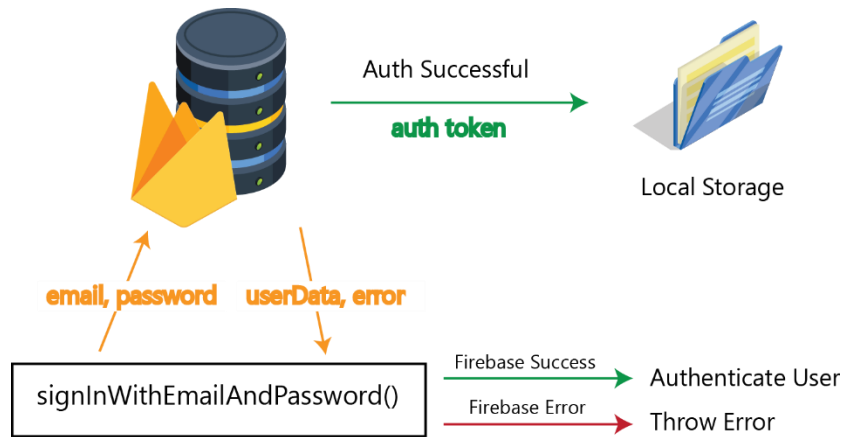


Figure 4.17. Authentication process of Firebase Authentication SDK

Firestore SDK also offers the ability to specify if a signed in user remains logged in indefinitely until he manually signs out, refreshes the browser’s window/tab or closes the page. From the three supported types of Auth state persistence, the SESSION state was implemented. It indicates that the authentication state will only persist in the current session or tab, meaning that it will be cleared when the user closes the window or tab.

In the sign in method there are common errors that need to be handled, such as when the inserted password does not match the corresponding email or does not exist. In that case, an alert message appears stating “Wrong Password”.



Figure 4.18. Dashboard of the web application with temperature, relative humidity, light color temperature and air quality estimation in real-time

After the user is successfully logged in, several pages are available. The first page appearing right after logging in is a dashboard displaying relevant information about indoor air conditions (as seen in Figure 4.18).

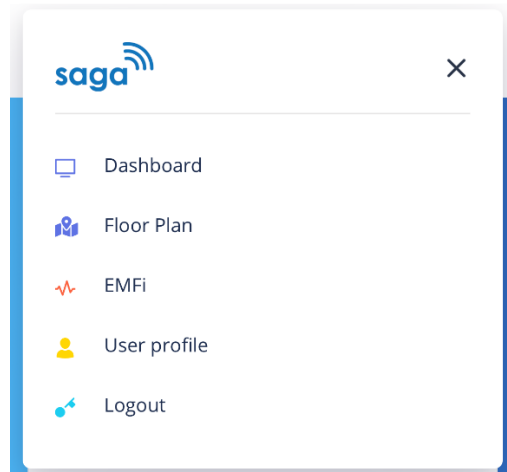


Figure 4.19. Available pages on the web application

Other pages currently available on the web app include the “Floor Plan”, “EMFi” and a “User Profile” page, as seen in Figure 4.19, and which will be discussed next. If the user wishes to log out, it can either choose the “Logout” option, or close the tab/browser.

As demonstrated in Figure 4.14, the data displayed on the web application is retrieved from the Firebase Realtime database by using HTTP GET requests. The method specifies the path where the values are stored and some extra key-value pairs with the parameter we want to get.

The values displayed on the dashboard include temperature, relative humidity, the current light’s temperature on the smart bulb, an air quality estimation based on the particulate matter concentrations and the gas concentration values in ppm. In order to develop an alert mechanism and inform the user about the different asthma and COPD attack triggering factors state, a small text revealing the safety status associated with each variable is presented below each reading: If temperature and humidity values exceed the threshold values assigned to these two parameters (which by default are set between 15 °C-30 °C for temperature and 40% – 60% for relative humidity [5]), a red "Not Safe" message with an exclamation icon is displayed. If the values are within that range, a green “Safe” message takes place. For the light’s indicator, its power state and the current color temperature of the smart bulb are displayed.

Real time data charts for each sensor reading are also available. Beyond the temperature and relative humidity charts that can be seen in Figure 4.20, the web app also displays charts for gas concentration levels, particulate matter, light intensity and sound levels. Additionally, for better data analysis, each chart displays key data on the hover of the mouse. As being shown in Figure 4.18, the temperature and time is displayed at the mouse cursor point if the user goes through a chart section.

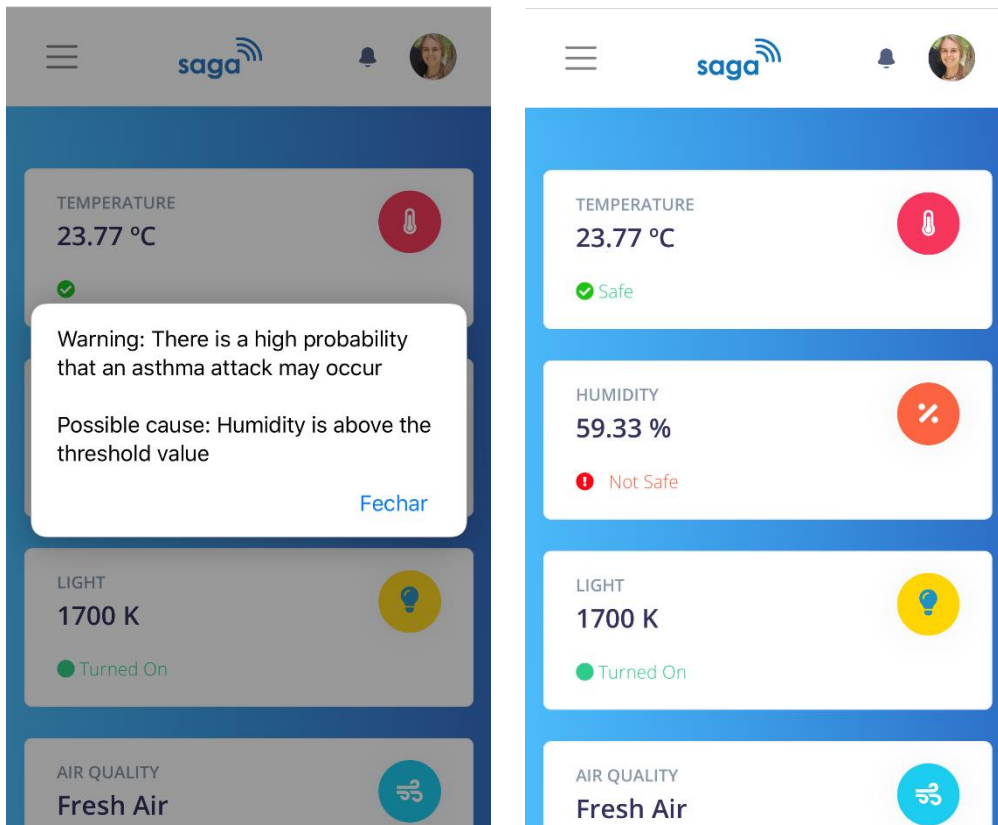


Figure 4.20. Dashboard and notification message viewed on the smartphone

The web application also triggers an alert message as seen in Figure 4.20, followed by an explanation of its possible cause. The message can only be dismissed if the user presses the “Close” button. If the readings are still out of the specified thresholds after 3 minutes, the same alert mechanism is triggered.

The app adapts its layout to the viewing environment, which means the content can be viewed on different devices with different sizes, such as the display of a desktop computer, tablet and smartphone. Figure 4.20 shows the web application viewed on a smartphone, with the exact same elements as the desktop version.

An additional page with the room’s floor plan is also available. For better analysis, it shows the nodes placement and distribution in a room or house. The user can visualize

the data collected by each sensor node by moving the mouse cursor point on top of the circle that belongs to a given node, as seen in Figure 4.21.

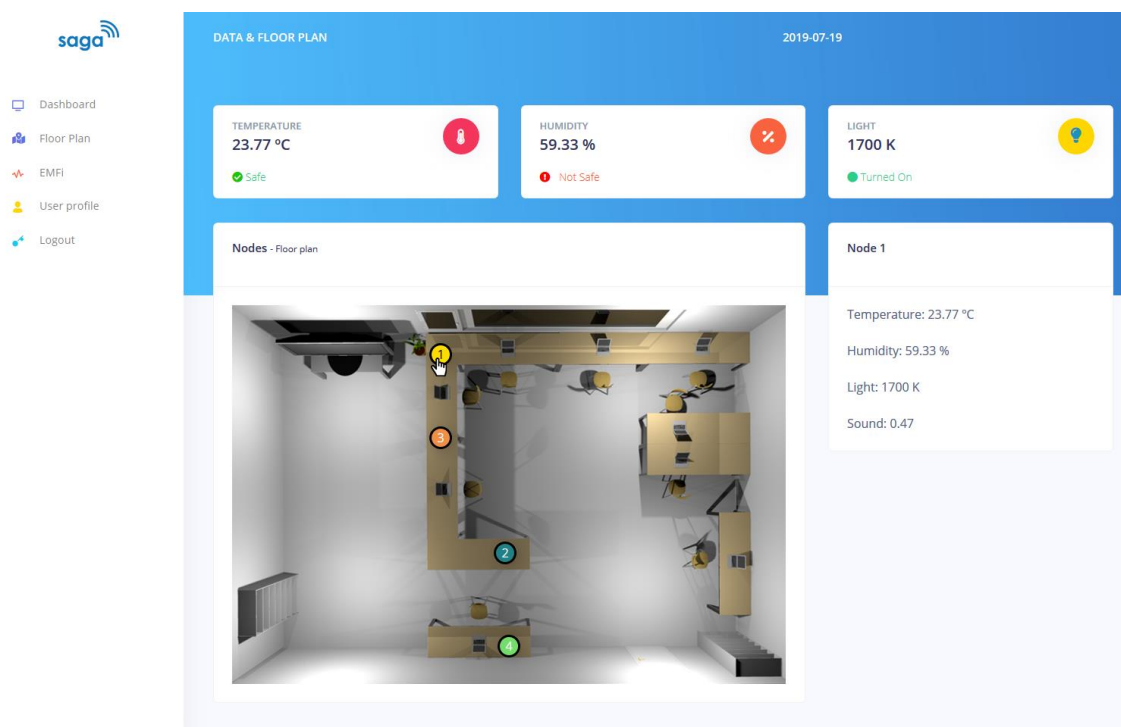


Figure 4.21. Sensor nodes location and their respective data displayed on the web application

As mentioned before, it is given the possibility for the user to change the threshold values used to signalize a likelihood of an asthma attack. To do so, the user needs to access his “User Profile” page where all the configurable values are displayed, as shown in Figure 4.22, on the next page.

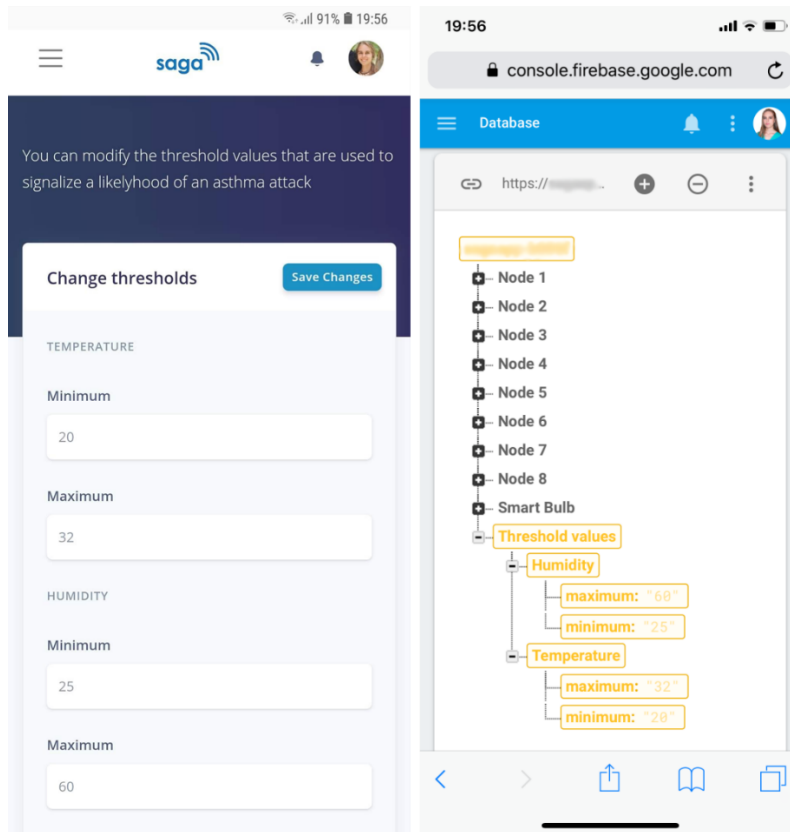


Figure 4.22. User Profile page with the change of thresholds and their update on the database

In this example, the temperature's maximum and minimum value, as well as humidity's were changed. After clicking the "Save Changes" button, the new values are immediately updated in the database. The coordinator node fetches these new values and compares them with the collected values from the sensors. If they are out of those threshold intervals, the alarm system will be both triggered by the smart lighting and the web application.

Physiological parameters such as heart rate, measured by the biomedical node, are also provided by the web application. After obtaining the BPM and IBI parameters from the biomedical node, the coordinator node sends two sets of data to the firebase: one is the current pulse rate and current IBI, and the other is an average of all pulse rates measured for one minute along with a timestamp.

The web page for heart rate measurements is shown in the next figure.

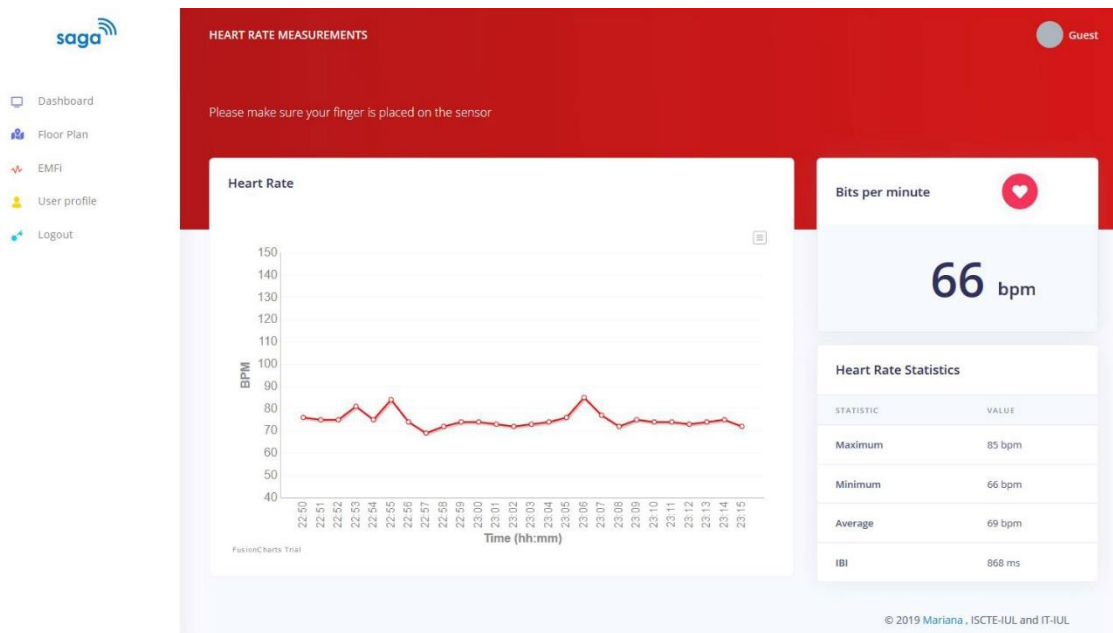


Figure 4.23. Heart Rate Measurements page with data collected from the biomedical node

The user can visualize its current heart rate in real time. The bits per minute (bpm) parameter is updated whenever a new heart rate measurement, in bpm, is sent to the database.

The maximum, minimum and average heart rate, as well as the current interbeat interval are also displayed in real-time on the “Heart Rate Statistics” table.

A chart with all the historical heart rate data gives the user a better analysis over his heart rate variability. All data samples recorded for one minute are averaged and then displayed on the chart.

The user can also export the chart data into three formats: export as a .png, .pdf and .xls.

Chapter 5

Results

This chapter presents the various experimental results obtained when using the system. These results include various data collected by the sensor nodes, its analysis, the web application performance and usage, the effectiveness of the alert mechanism and the different actuator's behavior.

5.1. Data analysis of the sensor nodes

The system was tested in the laboratory occupied by 10 people throughout the day. The sensor nodes were placed near the user's workplace and away from direct sunlight so that the readings performed by the temperature, humidity and gas sensors were not influenced. The microcontrollers of Node 1 - 4 were programmed to send data every 3 minutes to the coordinator node.

A practical approach regarding the indoor's spatial distribution of temperature and relative humidity levels was considered. Therefore, Node 1 and Node 4 were placed at different locations of the room. The node's placement can be seen in Figure 5.1.

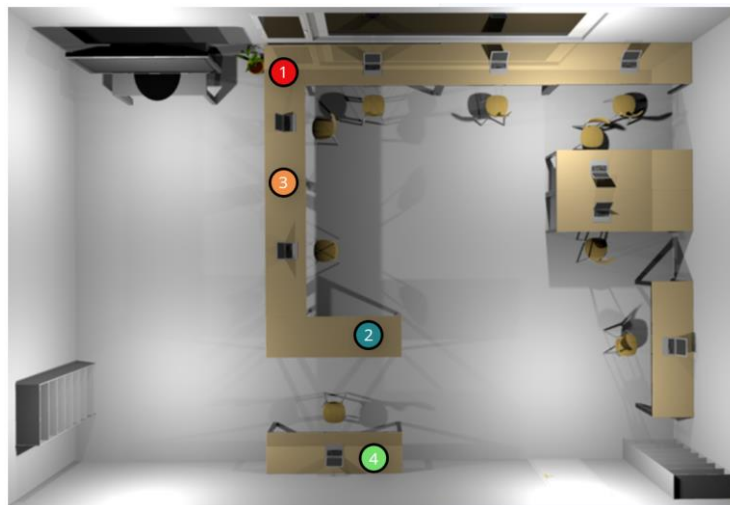
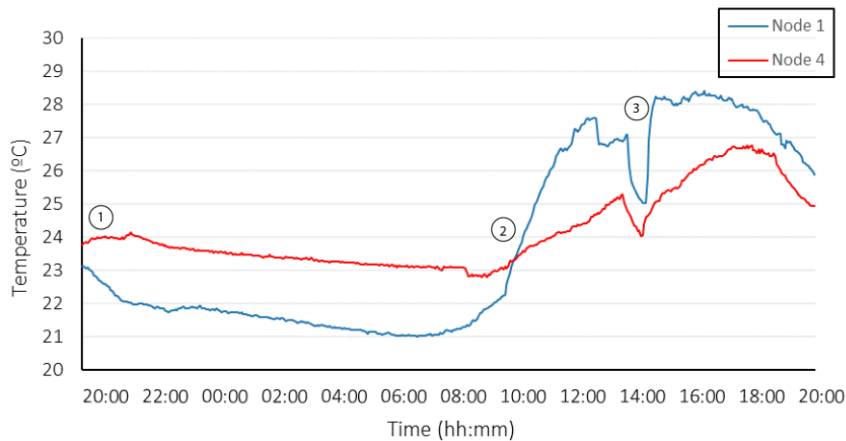


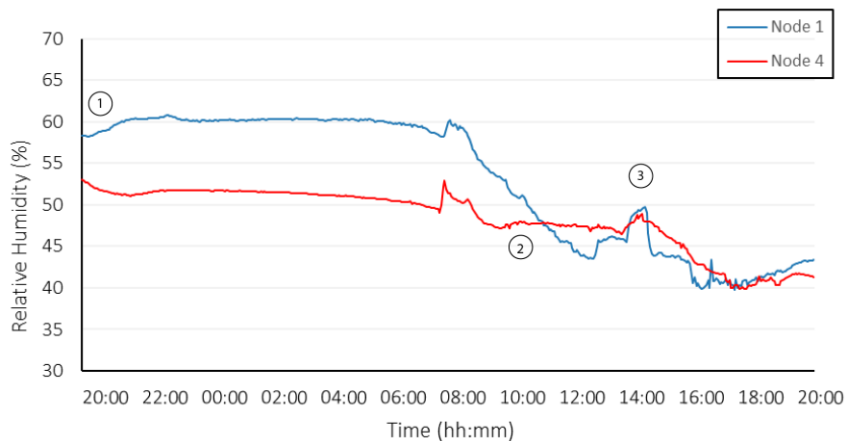
Figure 5.1. Spatial distribution of the sensor nodes

Figure 5.2 presents temperature and relative humidity measurements performed by Node 1 and Node 2 during 24h, where:

- Stage ① corresponds to the moment when the room is empty. Higher relative humidity levels are measured by the node close to the window (Node 1) during the night (20h - 8h).
- At stage ②, the room starts to be occupied and the window's shutter is opened, which results in the rapid growth of temperature levels inside the room.
- At stage ③, windows were opened and, considering that outdoors temperature rounded the 30°C, the indoor's temperature levels increased even more. Relative humidity, as expected, presented low levels during the day and started to increase at around 18h00.



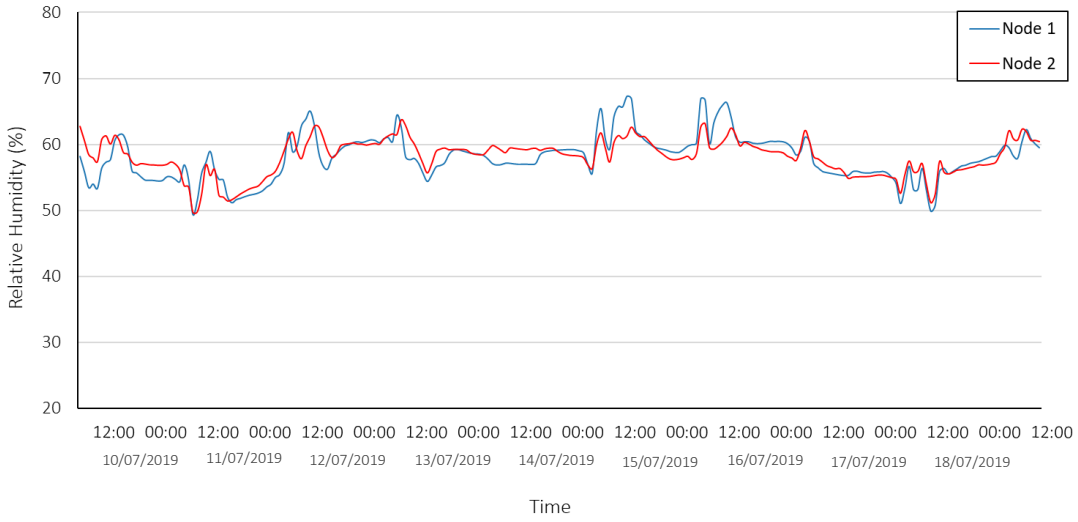
a)



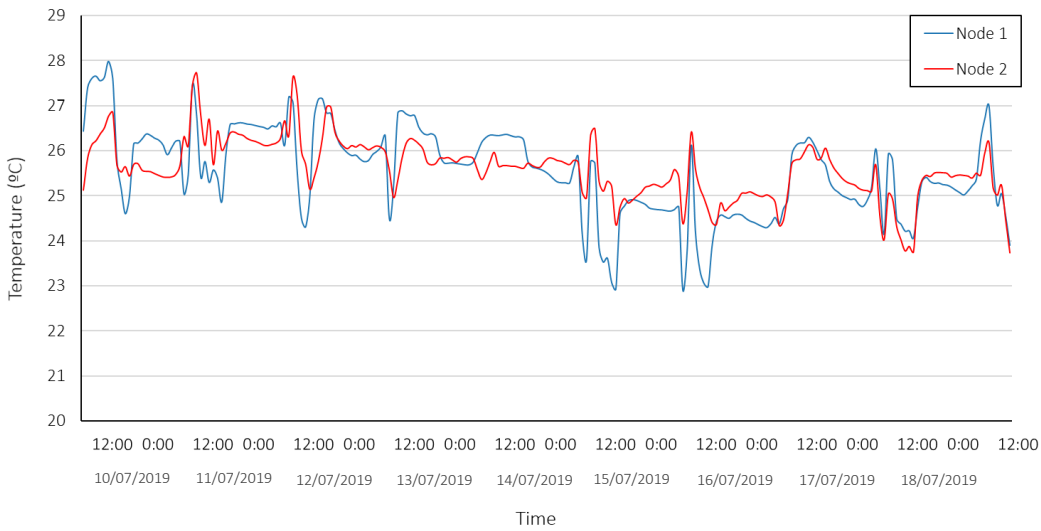
b)

Figure 5.2. Distributed temperature a) and relative humidity b) measurements during 24h.

The next figure shows temperature and relative humidity data collected for 1 week. The two sensors present very similar readings, which means that temperature and relative humidity do not vary much in this indoor environment. Humidity levels are slightly higher near the window, as expected.



a)



b)

Figure 5.3. Distributed temperature a) and relative humidity b) measurements for 1 week.

In order to test the gas sensor's calibration, the MQ-135 sensor was placed inside a gas sensor test chamber.

By following Table 3.3 and equation 1:

- A gas volume of 0,27 ml corresponds to 50 ppm.
- A gas volume of 0.54 ml corresponds to 100 ppm.

Therefore, a volume of 0.27 ml and 0.54 ml of Ethanol was injected in the chamber to verify that these values of gas concentration are obtained.

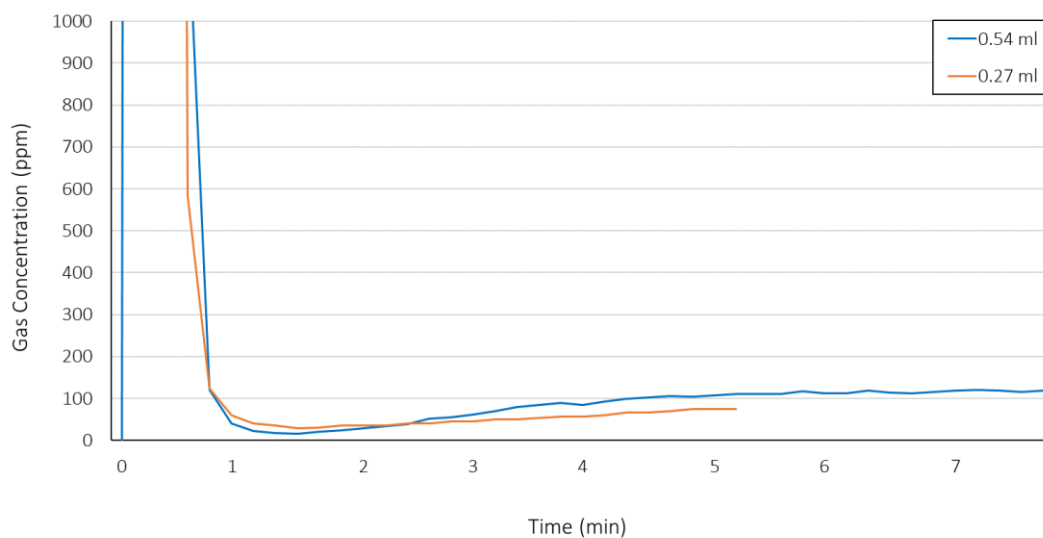


Figure 5.4. Gas Concentration variation in PPM for different volumes of injected Ethanol (MQ-135 gas sensor)

The readings are presented in parts per million (PPM) and the tests lasted 8 minutes and 5 minutes (the amount of time the sensor took to achieve a steady-state condition) for a 0.54 ml volume and a 0.27 ml volume, respectively.

As shown in Figure 5.4, the gas concentration level stabilizes at 100 ppm for 0.54 ml after 4 min, which is the time this substance takes to effectively reach the sensor's surface. For 0.27 ml of ethanol, the concentration levels stabilize at 50 ppm right after the first minute.

Regarding the particulate matter measurements, the particles sensor was placed in a vertical position, in order to achieve the desired airflow expected by the designers. The samples were taken every 30s, as recommended by the manufacturers, and then averaged after 3 minutes.

The particle's concentration is calculated by using a cubic polynomial derived from the characteristic graph that correlates the LPO time with the concentration of particles per 0.01 cubic feet (pcs/283ml).

To test the sensor performance, two tests were made in two different indoor environments: a living room and a laboratory occupied by 10 people throughout the day.

In the first case, samples were obtained for 14 hours continuously, as shown in Figure 5.5. Average values demonstrate an indoor environment with very low pollution levels, when compared with Table 5.1. The growth of particulate matter concentration levels at 11h is due to the opening of a window, which brought a greater quantity of air particles from outdoors to indoors. Lower values after 12h also indicate that the room was not being occupied at that period of time. A slight increase of particles at 15h is related with the presence of people in the room and some air flow through the house.

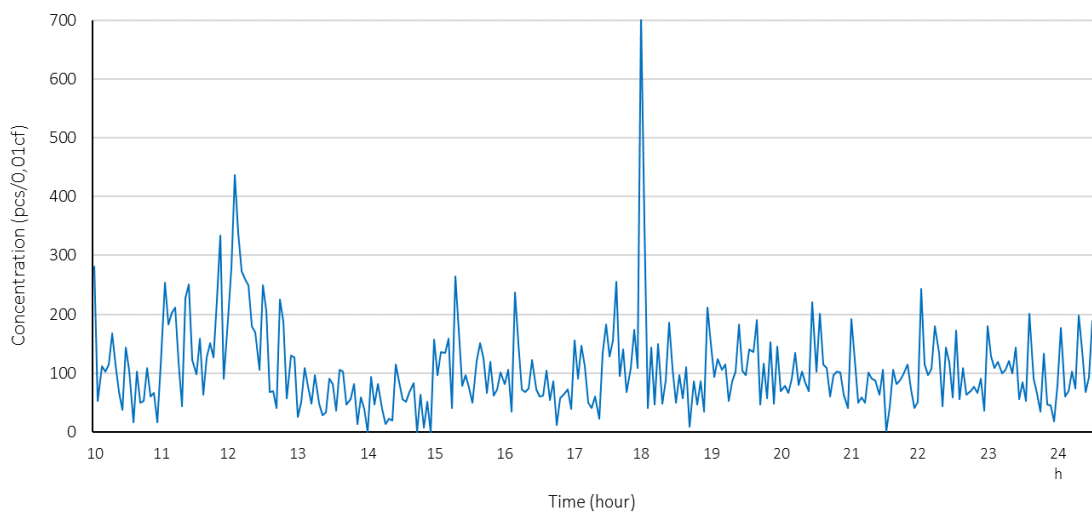


Figure 5.5. Particulate Matter (pcs/0.01 cf) over time for the first testing scenario

In the second case, in which the sensor is located at the laboratory, higher concentrations of particles are measured from 13h to 18h, which corresponds to the period of time where the laboratory is fully occupied. The windows were also opened during that time, which resulted in the entrance of a great number of airborne particles from the exterior. This environment is located relatively close to an airport, where airplanes constantly fly over the building and liberate a great variety of air pollutants that can be extremely harmful to human health. Moreover, it is also located near an avenue with constant vehicle traffic, which further increases the likelihood of particles entering in the indoor environment.

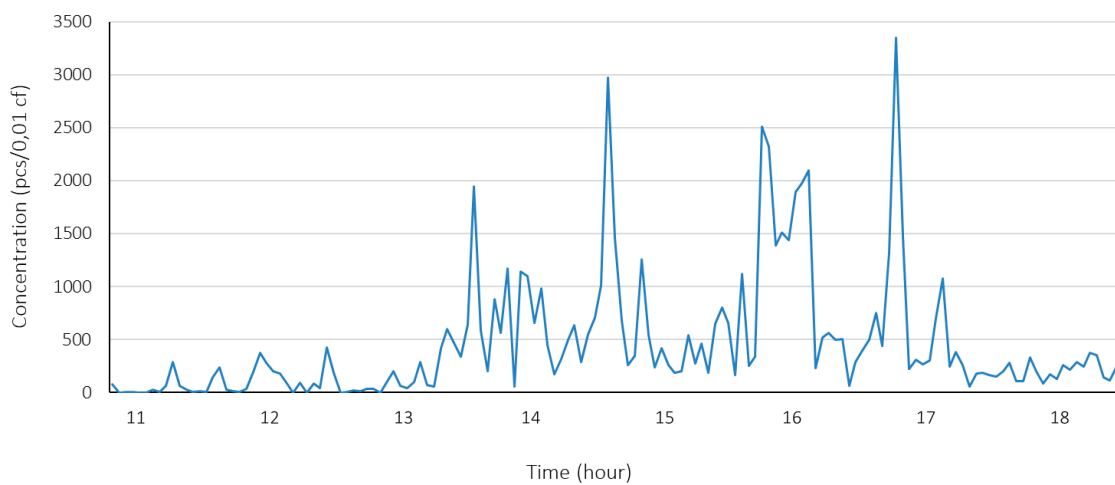


Figure 5.6. Particulate Matter (pcs/0.01 cf) over time for the second testing scenario

The following table gives an estimation of the correlation between pollution levels and particle matter concentration levels.

Table 5.1. PM Concentration levels and the associated levels of air pollution

Pollution levels	PM concentrations (pcs/0.01 cf)
Low	300 - 600
Medium	600 - 900
High	900 - 1500
Very High	> 1500

As mentioned before, two experiments were made to test the proper function of the EMFi sensor and collect BCG signal samples. The hardware was first tested with a 24-bit C Series analog input module (e.g. NI USB-9239) with analog and digital filtering capabilities.

The LabVIEW graphical programming environment was used to acquire data and control this measurement device. To reduce levels of noise of the ballistocardiograph signal, additional filtering was required. Therefore, an IIR Elliptic digital low-pass filter (LPF) characterized by $f_c = 20$ Hz and $N = 6$ (N-filter order) was implemented. The BCG signals obtained by the EMFi sensor placed in the seat of a chair were acquired at a 500 Hz/s sampling rate, and can be seen in Figure 5.7 and Figure 5.8.

Figure 5.7 presents a single sample, showing a well-defined J peak, from the IJK complex. This peak can be used to determine a heartbeat occurrence and estimate the heart rate.

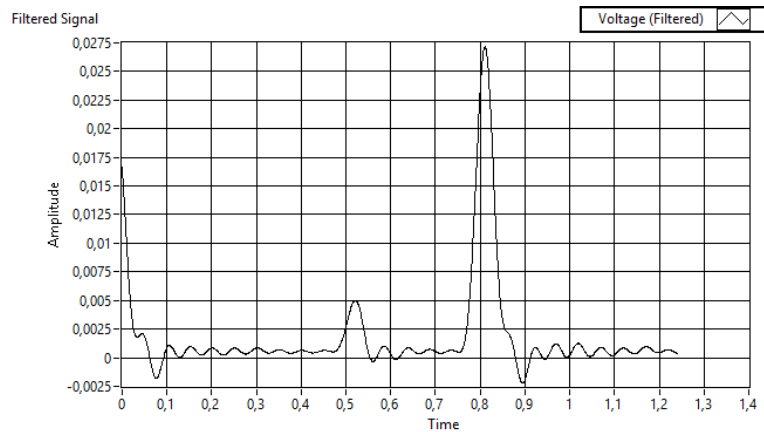


Figure 5.7. Sample of a BCG wave collected from the EMFi sensor embedded on a chair

Figure 5.8 reports multiple samples of an accurate BCG signal from a subject seating on the chair. Heartbeats are easily noticed with the expression of J peaks.

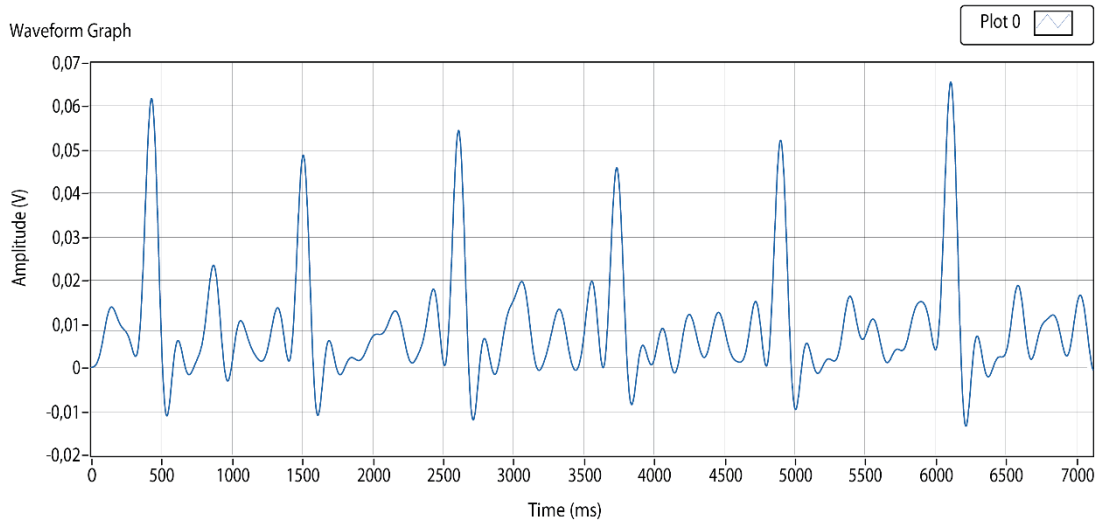


Figure 5.8. BCG waves collected from the EMFi sensor embedded on a chair

Considering the ESP32 microcontroller as the signal acquisition device, some BCG samples were recorded in order to test its performance. Arduino IDE and its Serial Plotter were used to analyze the output signals. The EMFi signals acquired by the ESP32 can be visualized in Figure 5.9 with the Arduino Serial Plotter, at a baud rate of 115200.

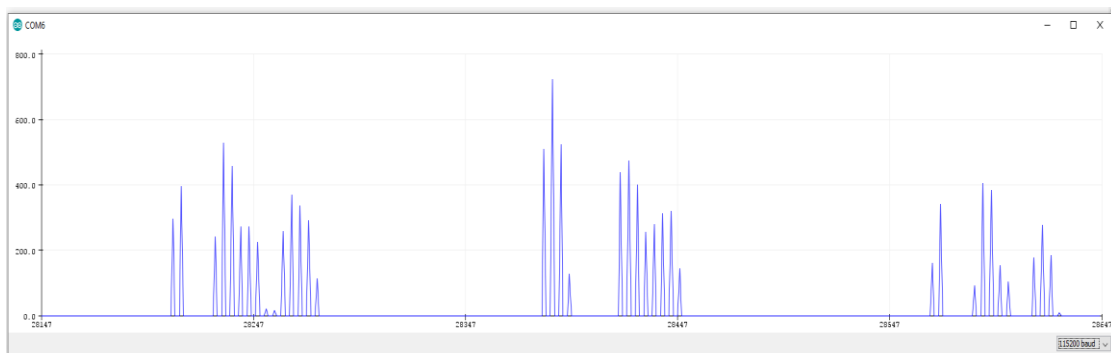


Figure 5.9. EMFi sensor signals acquired by the ESP32 microcontroller

In fact, it is possible to detect a heartbeat occurrence by analyzing the signal variances between 0 and a positive value. In this case, the time between two beats can also be used to determine the heart rate, much like the PPG method. However, it is quite difficult to obtain such clear signals. Even with a charge amplifying circuit, those signals are very hard to detect, and the user must be sat still at a very specific position on the chair, which is somehow unnatural.

For that reason, and considering the ESP32 as the node’s microcontroller, PPG methods were thought as a heartbeat measuring alternative.

Figure 5.10 demonstrates a pulse waveform visualized on the Arduino Serial Plotter. A clean signal is obtained by only using an analogRead() method, since the pulse sensor’s amplification and noise cancellation circuitry improves the pulse readings.

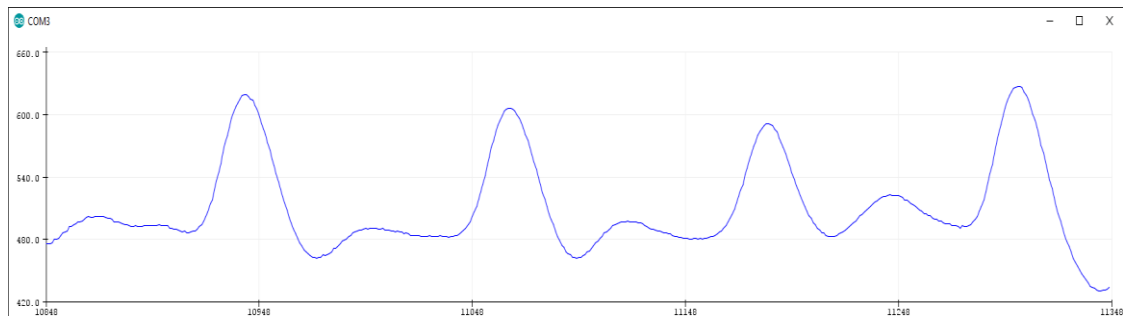


Figure 5.10. PPG waves collected from the pulse sensor

Regarding the continuous monitoring of these physiological parameters the web application exhibits a dedicated page with the user’s pulse rate in bits per minute, updated in real-time, a table with interbeats interval, maximum, minimum and average bpm parameters, and a graph with HR historical data.

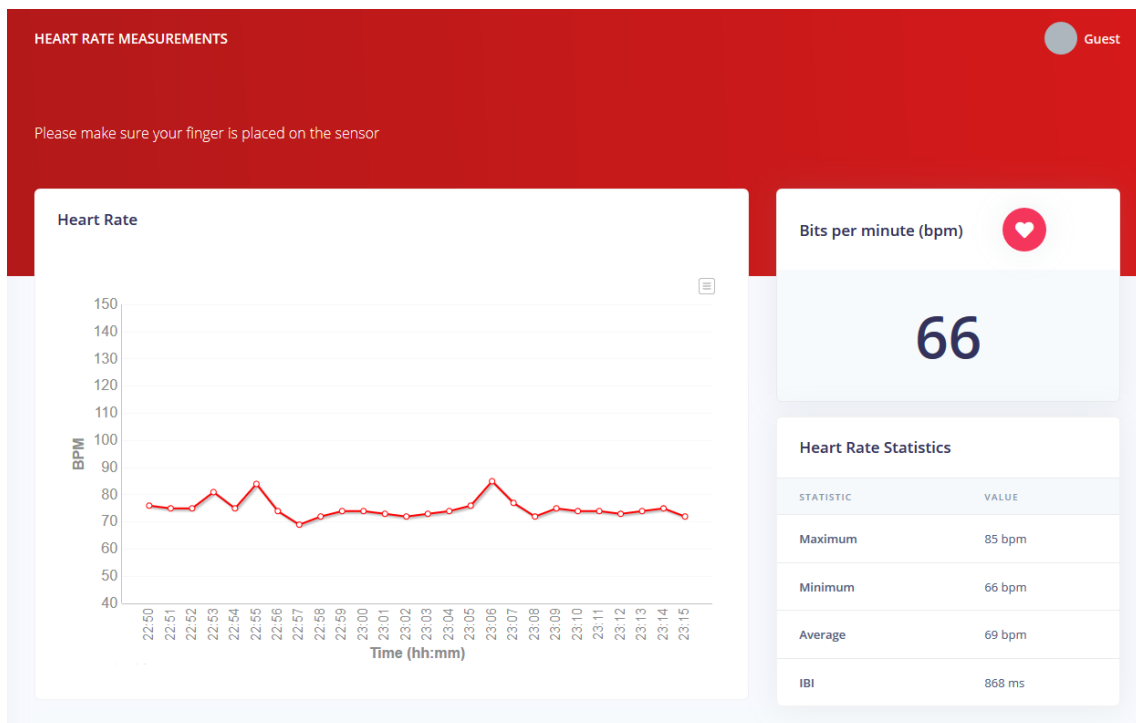


Figure 5.11. Screenshot of the “Heart Rate Measurements” webpage

After obtaining the BPM and IBI parameters from the biomedical node, the coordinator node sends two chunks of data to the database: one is the current pulse rate and current IBI, and the other is an average of all pulse rates measured for one minute, alongside a timestamp, which are then displayed on the web application. To test the effectiveness of the system, some experimental results were obtained.

Two tests were performed with two different subjects, both resting on a chair. Figure 5.12 presents the historical heart rate for subject n°1. Considering that the normal resting heart rate is between 60 and 100 beats per minute (bpm), the subjects' average bpm is kept between this interval (see Figure 5.13). Therefore, the smart light's color remained unchanged for most of the time. It is important to take into consideration that the resting heart rate can vary in response to different changes, such as body temperature, emotional triggers, and body position.



Figure 5.12. Recorded heart rate data of subject n°1 for 20 minutes while resting on a chair

Heart Rate Statistics	
STATISTIC	VALUE
Maximum	100 bpm
Minimum	83 bpm
Average	90 bpm
IBI	334 ms

Figure 5.13. Real-time heart rate statistics of subject n°1

Figure 5.14 shows heart rate data relative to subject n° 2. The average bpm is relatively lower than subject n°1. Certain peaks of bpm present in the graph may be related with a higher pulse rate when making small movements or changing body position. Figure 5.15 shows the maximum, minimum and average bpm, as well as the subject's interbeat at a certain time.

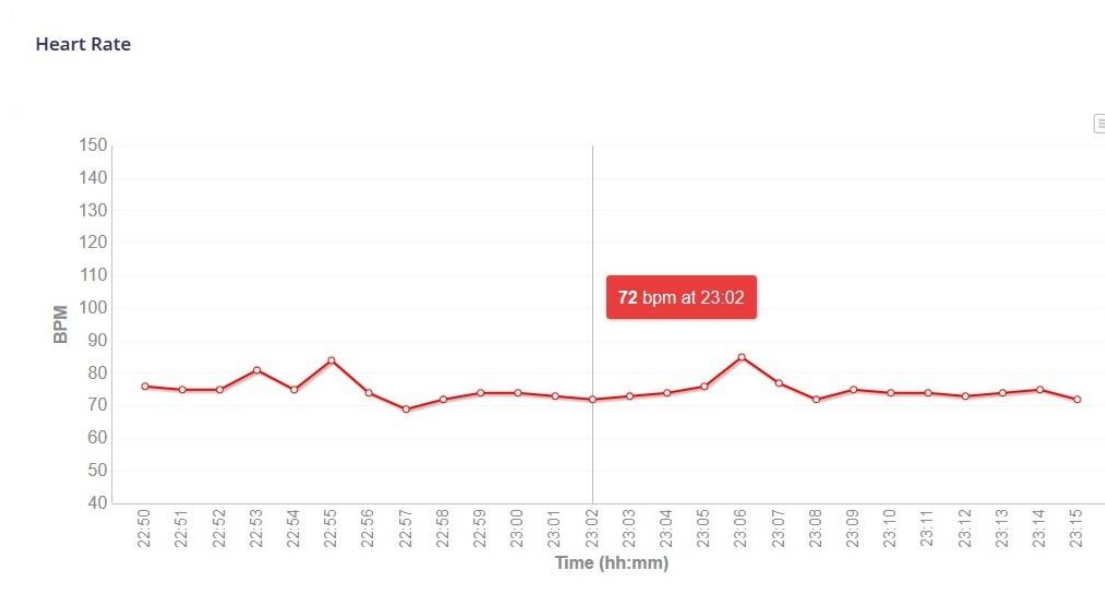


Figure 5.14. Recorded heart rate data of subject n°2 for 25 minutes

Heart Rate Statistics	
STATISTIC	VALUE
Maximum	85 bpm
Minimum	66 bpm
Average	69 bpm
IBI	868 ms

Figure 5.15. Real-time heart rate statistics of subject n°2

5.2. Power consumption

Energy consumption of the sensor nodes 1 to 4 was also monitored. Each node was powered up by a 10400 mAh power-bank. To reduce power consumption and extend these node's battery life, deep sleep modes were implemented on the ESP-32. The biomedical node (Node 5), however, is the only node that does not use these power saving strategies, since it must be constantly collecting physiological data. The measurements were made on each node by a digital multimeter and their current consumption graphs are presented in the next sub-section.

5.2.1. Node 1

Each Bluetooth connection and data transmission are characterized by a sudden increase of the node's energy consumption. Node 1 presents an approximate value of only 4 mAh when on sleep mode, and 114 mAh when sending data over Bluetooth.

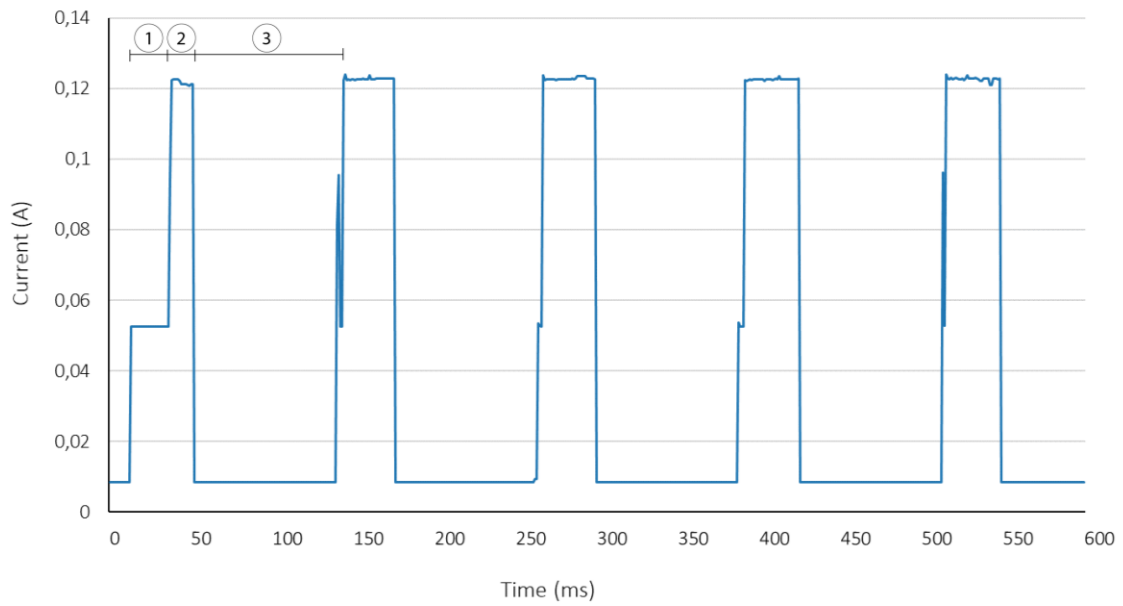


Figure 5.16. Current consumption of of Node 1 while: (1) Waiting for connection, (2) Transmitting data, (3) Deep Sleep mode



(1)



(2)



(3)

Figure 5.17. Current values of Node 1 while: (1) Waiting for connection, (2) Transmitting data, (3) Deep Sleep mode

5.2.2. Node 2

Node 2, composed by three gas sensors with high energy consumption levels, presents values around 364 mAh when on deep sleep mode, 403 mAh when waiting for a Bluetooth connection and around 466 mAh when transmitting to the coordinator node. This gives the node an autonomy of approximately 20 hours.

Even on deep sleep mode the node consumes a great amount of energy. Point 4 on the next figure shows a current variation when a gas substance, in this case Ethanol, reaches the gas sensor surface.

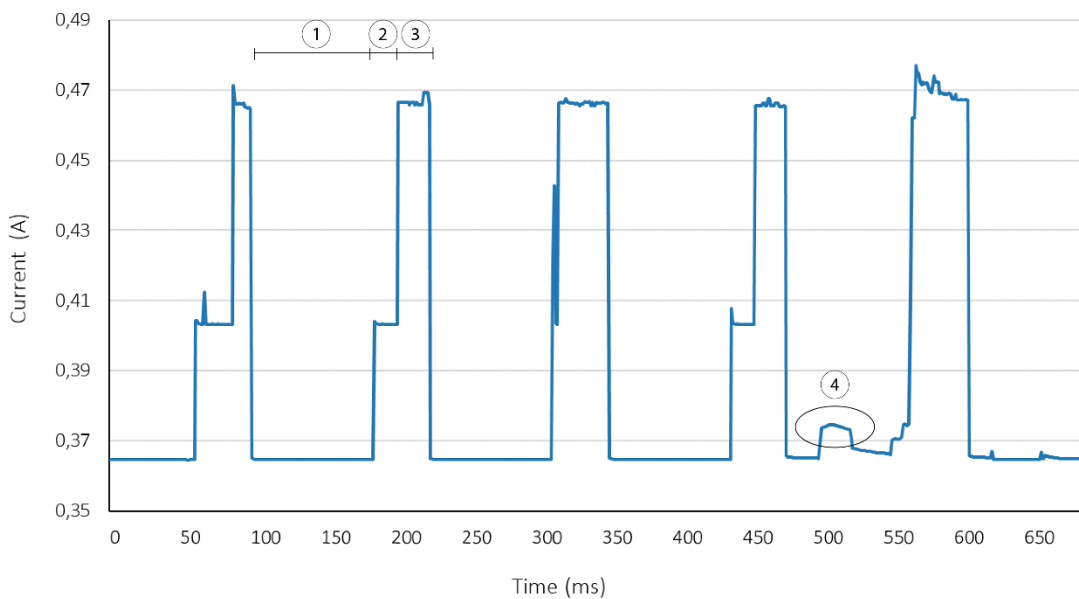


Figure 5.18. Current consumption of Node 2 while: (1) on Deep Sleep Mode, (2) Waiting for connection, (3) Transmitting data, (4) Current variations when in presence of Ethanol



(1)



(2)



(3)

Figure 5.19. Current values of Node 2 while: (1) on Deep Sleep Mode, (2) Waiting for connection, (3) Transmitting data

5.2.3. Node 3

Node 3, with a particulate matter sensor presents values around 144 mAh when on deep sleep mode and around 210 mAh when transmitting to the coordinator node.

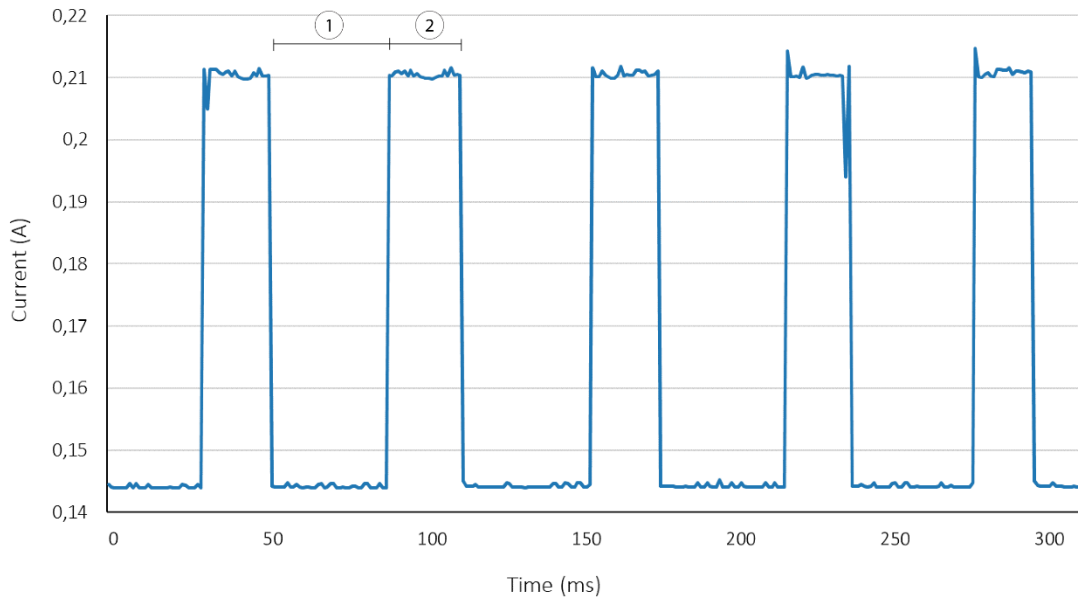


Figure 5.20. Current consumption of Node 3 while: (1) on Deep Sleep Mode, (2) Transmitting data



(1)



(2)

Figure 5.21. Current values of Node 3 while: (1) on Deep Sleep Mode, (2) Transmitting data

5.2.4. Node 4

Node 4, only composed by a Si7021 temperature and relative humidity sensor presents values around 4 mAh when on deep sleep mode, 44 mAh when waiting for a Bluetooth connection and around 109 mAh when transmitting to the coordinator node.

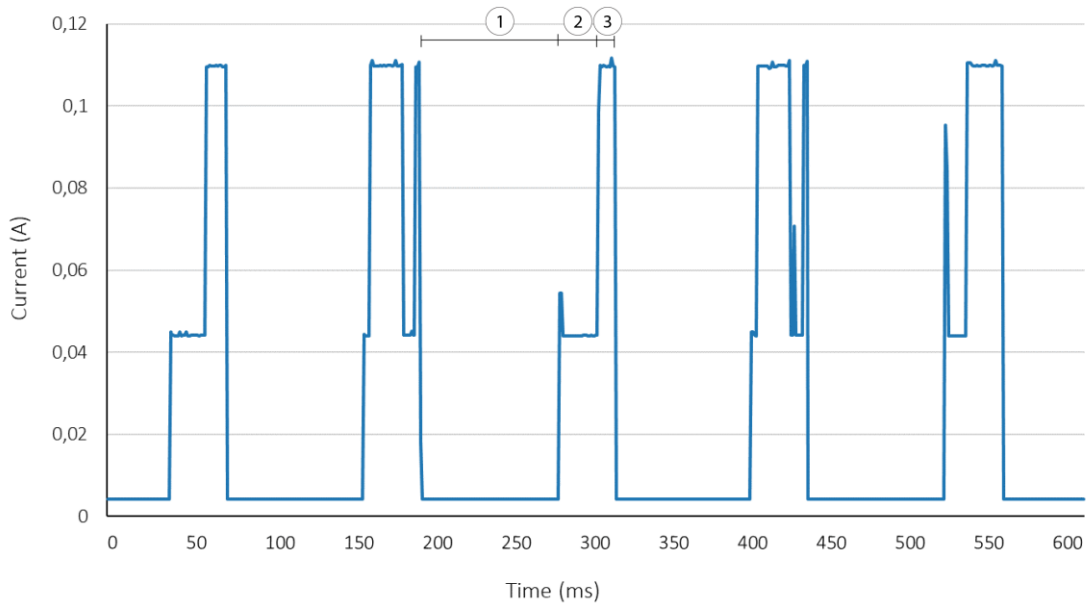


Figure 5.22. Current consumption of Node 4 while: (1) on Deep Sleep Mode, (2) Waiting for connection, (3) Transmitting data



(1)



(2)



(3)

Figure 5.23. Current values of Node 4 while: (1) on Deep Sleep Mode, (2) Waiting for connection, (3) Transmitting data

Chapter 6

Conclusions and Future Work

6.1. Conclusions

In this research work, an adaptive environment based on a wireless sensor network system was developed. This system was designed to help provide maximum comfort and healthcare assessment. Such objectives were achieved by monitoring indoor environmental quality, physiological parameters and by implementing some actuation systems.

Taking a special focus on the monitoring of indoor air quality and the prevention of respiratory distress, a smart system that performs real-time monitoring and actuates as part of a primary-prevention strategy was considered. The presented system was based on a WSN and performed indoor air quality monitoring, consisting on multiple sensor nodes with temperature, relative humidity, gas and particulate matter sensors, and on several actuator nodes. To help enhance indoor air quality and indoor thermal comfort levels, different approaches were considered: the first approach was the increasing of the room's ventilation rate to displace indoor pollutants, by using a smart ventilation unit; the second approach was the use of a humidifier to increase humidity levels, an extremely important factor when thinking about asthma distress prevention. As a primary prevention strategy, the system implemented different alert mechanisms to warn the user for the presence of respiratory distress triggers and poor air conditions.

As one of the sub-domains of the Indoor Environmental Quality indicator, Indoor Lighting Quality was also considered. A smart lighting system to adapt indoor lighting throughout the day by changing light temperature color and light intensity was implemented and tested. Additionally, this lighting system was also used to perform visual warning signals, easily noticed by the user.

Regarding the measurement of physiological parameters, especially cardiac activity, ballistocardiography and photoplethysmography methods were used.

Ballistocardiography signals were not accurate when using an ESP32 microcontroller. Therefore, photoplethysmography was considered the most reliable method for this case. Finally, a unique web application was developed to provide data analysis, give the user manual control over the smart lighting system and other actuators, allow the user to modify the threshold values related to asthma, and to implement an additional alert mechanism. The web application was developed to work in different platforms and to be compatible with the most common operating systems, so it could be used by a smartphone, tablet or personal computer.

The efficiency, ease of use, versatility and scalability of the developed system was ensured through its implementation on a daily used indoor environment, thereby achieving all the initial objectives proposed for this dissertation.

6.2. Future Work

The developed system and its functionalities are already complete and implemented. However, additional work can be done in order to further improve the system's efficiency.

Future work includes the expansion of the wireless sensor network for a full-house coverage by adding more sensor nodes and actuators, taking advantage of the WSN's scalability.

Data fusion can also be performed to acquire more consistent and accurate information for future analysis.

Regarding the node's connectivity to the coordinator node, a lower energy wireless protocol, such as Bluetooth 4.0/Bluetooth Low Energy, can be implemented, thus replacing classic Bluetooth.

Energy harvesting methods, such as mechanical energy harvesting, are also an option to improve the sensor node's autonomy.

References

- [1] M. A. Mujeebu, "Introductory Chapter: Indoor Environmental Quality," *Indoor Environmental Quality*, IntechOpen, 2019.
- [2] Ozlem Kar Kurt, Jingjing Zhang, and Kent E. Pinkerton, "Pulmonary Health Effects of Air Pollution", *Current opinion in pulmonary medicine*, vol 22(2), pp.138-143, 2016.
- [3] "Indoor Air Quality," EPA, 16-Jul-2018. [Online]. Available: <https://www.epa.gov/report-environment/indoor-air-quality> [Accessed: 11-Mar-2019].
- [4] Galán, I., et al. "Short-Term Effects of Air Pollution on Daily Asthma Emergency Room Admissions." *European Respiratory Journal*, vol. 22, no. 5, 2003, pp. 802–808.
- [5] A. V. Arundel, E.M. Sterling, J. H. Biggin and T.D Sterling, "Indirect health effects of relative humidity in indoor environments", *Environmental health perspectives*, vol. 65, pp.351-61, 1986.
- [6] E. C. Pinheiro, O. A. Postolache and P. S. Girão, "Automatic wavelet detrending benefits to the analysis of cardiac signals acquired in a moving wheelchair," *2010 Annual International Conference of the IEEE Engineering in Medicine and Biology*, Buenos Aires, 2010, pp. 602-605.
- [7] O. A. Postolache, P. M. B. S. Girão, J. Mendes, E. C. Pinheiro and G. Postolache, "Physiological Parameters Measurement Based on Wheelchair Embedded Sensors and Advanced Signal Processing," in *IEEE Transactions on Instrumentation and Measurement*, vol. 59, no. 10, pp. 2564-2574, Oct. 2010.
- [8] E. J. Pino, C. Larsen, J. Chavez and P. Aqueveque, "Non-invasive BCG monitoring for non-traditional settings," *2016 38th Annual International Conference of the IEEE Engineering in Medicine and Biology Society (EMBC)*, Orlando, FL, 2016, pp. 4776-4779.
- [9] O. Postolache, P. S. Girão, E. Pinheiro, and G. Postolache, "Unobtrusive and Non-invasive Sensing Solutions for On-Line Physiological Parameters Monitoring," *Wearable and Autonomous Biomedical Devices and Systems for Smart Environment Lecture Notes in Electrical Engineering*, pp. 277–314, 2010.
- [10] J. Alametsä, A. Väri, M. Koivuluoma and L. Barna, "The Potential of EMFi Sensors in Heart Activity Monitoring", *2nd Open ECG Workshop*, Berlin, Germany, April 2004.
- [11] E. J. Pino, J. A. P. Chávez and P. Aqueveque, "BCG algorithm for unobtrusive heart rate monitoring," *2017 IEEE Healthcare Innovations and Point of Care Technologies (HI-POCT)*, Bethesda, MD, 2017, pp. 180-183.

- [12] S. Gilaberte, J. Gómez-Clapers, R. Casanella and R. Pallas-Areny, "Heart and respiratory rate detection on a bathroom scale based on the ballistocardiogram and the continuous wavelet transform," *2010 Annual International Conference of the IEEE Engineering in Medicine and Biology*, Buenos Aires, 2010, pp. 2557-2560.
- [13] O. Postolache, P. S. Girao, J. Mendes and G. Postolache, "Unobstrusive heart rate and respiratory rate monitor embedded on a wheelchair," *2009 IEEE International Workshop on Medical Measurements and Applications*, Cetraro, 2009, pp. 83-88.
- [14] M. Paajanen, J. Lekkala, and H. Välimäki, "Electromechanical modelling and properties of the electret film EMFi," *IEEE Trans. Dielectr. Electr. Insul.*, vol. 8, no. 4, pp. 629–636, Aug. 2001.
- [15] D. Y. C. Leung, "Outdoor-indoor air pollution in urban environment: challenges and opportunity," *Frontiers in Environmental Science*, vol. 2, 2015.
- [16] S. Baldacci et al. "Allergy and asthma: Effects of the exposure to particulate matter and biological allergens", *Respiratory Medicine*, vol. 109, no. 9, pp. 1089-1104, 2015.
- [17] Stephanie Watson, "Humidity and Asthma: Effects of Humidity on Asthma & How to Prevent It," *Healthline*, 05-Apr-2018. [Online]. Available: <https://www.healthline.com/health/humidity-and-asthma> [Accessed: 11-Mar-2019].
- [18] H. Qureshi, A. Sharafkhaneh, and N. A. Hanania, "Chronic obstructive pulmonary disease exacerbations: latest evidence and clinical implications," *Therapeutic Advances in Chronic Disease*, vol. 5, no. 5, pp. 212–227, 2014.
- [19] V. Vajão, "O poder da luz", *Tecno Hospital*, no.85, 2018.
- [20] M. Fernandes, "Importância da iluminação na humanização de ambientes hospitalares", *Tecno Hospital*, no.85, 2018.
- [21] A. C. Daré, "Iluminação & saúde", *Tecno Hospital*, no.85, 2018.
- [22] "What is Circadian Rhythm?" National Sleep Foundation. [Online]. Available: <https://www.sleepfoundation.org/articles/what-circadian-rhythm>. [Accessed: 29-Jun-2019].
- [23] A. Muzet, "Environmental noise, sleep and health", *Sleep Medicine Reviews*, vol. 11, no. 2, pp. 135 – 142, 2007.
- [24] D. Halperin, "Environmental noise and sleep disturbances: A threat to health?", *Sleep Science*, vol. 7, no. 4, pp. 209 –212, 2014.
- [25] J. Kranjec, S. Beguš, G. Geršak, M. Šinkovec, J. Drnovšek, and D. Hudoklin, "Design and Clinical Evaluation of a Non-Contact Heart Rate Variability Measuring Device," *Sensors*, vol. 17, no. 11, p. 2637, 2017.
- [26] O. Postolache, P. S. Girão, G. Postolache and J. Gabriel, "Cardio-respiratory and daily activity monitor based on FMCW Doppler radar embedded in a wheelchair," *2011 Annual International Conference of the IEEE Engineering in Medicine and Biology Society*, Boston, MA, 2011, pp. 1917-1920.

- [27] D. Castaneda, A. Esparza, M. Ghamari, C. Soltanpur, and H. Nazeran, "A review on wearable photoplethysmography sensors and their potential future applications in health care," *International Journal of Biosensors & Bioelectronics*, vol. 4, no. 4, 2018.
- [28] M. Elgendi, R. Fletcher, Y. Liang, N. Howard, N. H. Lovell, D. Abbott, K. Lim, and R. Ward, "The use of photoplethysmography for assessing hypertension" , *npj Digital Medicine*, vol. 2, no. 1, 2019.
- [29] "Market Pulse Report, Internet of Things (IoT)", *GrowthEnabler*, 2019.
- [30] "IoT: number of connected devices worldwide 2012-2025," *Statista*, 2019.
- [31] Rajiv, A. Jain, and A. Jain, "What are the major components of Internet of Things," RF Page, 10-Jan-2018. [Online]. Available: <https://www.rfpage.com/what-are-the-major-components-of-internet-of-things/>. [Accessed: 12-Jan-2019].
- [32] "What is IoT gateway? - Definition from WhatIs.com," *WhatIs.com*. [Online]. Available: <https://whatis.techtarget.com/definition/IoT-gateway>. [Accessed: 12-Jan-2019].
- [33] "World of Electronics" , *World of Technology & Science*. [Online]. Available: <https://wots.nl/world-of-electronics>. [Accessed: 13-Sep-2019].
- [34] P. Rawat, K. D. Singh, H. Chaouchi, and J. M. Bonnin, "Wireless sensor networks: a survey on recent developments and potential synergies," *The Journal of Supercomputing*, vol. 68, no. 1, pp. 1–48, 2013.
- [35] I. F. Akyildiz, Weilian Su, Y. Sankarasubramaniam and E. Cayirci, "A survey on sensor networks," *IEEE Communications Magazine*, vol. 40, no. 8, pp. 102-114, Aug. 2002.
- [36] Parul Bakaraniya , Sheetal Mehta, "Features of WSN and various routing techniques for WSN: a survey," *International Journal of Research in Engineering and Technology*, vol. 1, issue 3, pp: 349-354, Nov-2012.
- [37] D. Sharma, S. Verma, and K. Sharma, "Network Topologies in Wireless Sensor Networks: A Review," *International Journal of electronics & communication technology*, vol. 4, no. 3, Jun. 2013.
- [38] S. Darroudi, C. Gomez, "Bluetooth Low Energy Mesh Networks: A Survey", *Sensors*, vol. 17, Jun. 2017.
- [39] M. J. Mcgrath and C. N. Scanail, "Sensor Network Topologies and Design Considerations," *Sensor Technologies*, pp. 79–95, 2013.
- [40] J. Lee, Y. Su and C. Shen, "A Comparative Study of Wireless Protocols: Bluetooth, UWB, ZigBee, and Wi-Fi," *IECON 2007 - 33rd Annual Conference of the IEEE Industrial Electronics Society*, Taipei, 2007, pp. 46-51.
- [41] E. Ferro and F. Potorti, "Bluetooth and Wi-Fi wireless protocols: a survey and a comparison," in *IEEE Wireless Communications*, vol. 12, no. 1, pp. 12-26, Feb. 2005.

- [42] J. Tosi, F. Taffoni, M. Santacatterina, R. Sannino, and D. Formica, "Performance Evaluation of Bluetooth Low Energy: A Systematic Review," *Sensors*, vol. 17, no. 12, p. 2898, 2017.
- [43] S. Banerji, R. Chowdhury, "On IEEE 802.11: Wireless LAN Technology" *International Journal of Mobile Network Communications & Telematics*, vol. 3, issue 4, Aug. 2013.
- [44] K. Mekki, E. Bajic, F. Chaxel, and F. Meyer, "A comparative study of LPWAN technologies for large-scale IoT deployment", *ICT Express*, vol. 5, no. 1, pp. 1–7, 2019.
- [45] "Firebase Realtime Database", Google [Online]. Available: <https://firebase.google.com/docs/database>.
- [46] "I2S," Arduino. [Online]. Available: <https://www.arduino.cc/en/Reference/I2S>. [Accessed: 14-Jun-2019].
- [47] Expressif Systems, "ESP 32 Series", Version 3.0 Datasheet, 2019
- [48] "Si7021 Datasheet." *Silicon Laboratories*, 2016. Available:<https://www.silabs.com/documents/public/datasheets/Si7021-A20.pdf>, 2019
- [49] "Photo resistor - Light Dependent Resistor (LDR) » Resistor Guide," RSS. [Online]. Available: <http://www.resistorguide.com/photoresistor/>. [Accessed: 15-Jun-2019].
- [50] "Adafruit AGC Electret Microphone Amplifier - MAX9814," *Adafruit Learning System*. [Online]. Available: <https://learn.adafruit.com/adafruit-agc-electret-microphone-amplifier-max9814/overview>. [Accessed: 15-Jun-2019].
- [51] "MAX9814 - Microphone Amplifier with AGC and Low-Noise Microphone Bias", *Maxim Integrated*, Rev.3.
- [52] "Presenting MQ sensors: low-cost gas and pollution detectors," *Open Electronics*. [Online]. Available: <https://www.open-electronics.org/presenting-mq-sensors-low-cost-gas-and-pollution-detectors/>. [Accessed: 16-Mar-2019].
- [53] Figaro, "SR-3 – Bench Top Test Chamber", *Product Information*.
- [54] "Technical Data MQ-135 Gas Sensor", *Hanwei Eletronics*. Available: https://www.electronicoscaldas.com/datasheet/MQ-135_Hanwei.pdf
- [55] "MQ-4 Semiconductor Sensor for Natural Gas", *Hanwei Eletronics*. Available: <https://www.pololu.com/file/0J311/MQ4.pdf>
- [56] "Semiconductor Sensor for CO/Combustible Gas", *Hanwei Eletronics*. Available: <http://www.haoyuelectronics.com/Attachment/MQ-9/MQ9.pdf>
- [57] J. Z. Wu, D. D. Ge, L. F. Zhou, L. Y. Hou, Y. Zhou, and Q. Y. Li, "Effects of particulate matter on allergic respiratory diseases," *Chronic Diseases and Translational Medicine*, vol. 4, no. 2, pp. 95–102, 2018.
- [58] WHO, "Who's global air-quality guidelines", *The Lancet*, Volume 368, Issue 9544, pp. 1302, 2006


- [59] E. Austin, I. Novosselov, E. Seto, and M. G. Yost, “Laboratory Evaluation of the Shinyei PPD42NS Low-Cost Particulate Matter Sensor,” *Plos One*, vol. 10, no. 9, Sep. 2015.
- [60] T. Allen, “De-construction of the Shinyei PPD42NS dust sensor.”, *EME Systems*, v.2, 2013.
- [61] “The Benefits of Smart Lighting and Smart Bulbs,” *Now from Nationwide* ®, 18-Dec-2017. [Online]. Available: <https://blog.nationwide.com/smart-light-bulbs/>. [Accessed: 29-Jun-2019].
- [62] “The official site of Philips Hue | Meethue.com,” *Philips Hue*. [Online]. Available: <https://www2.meethue.com/en-us>. [Accessed: 30-Jun-2019].
- [63] Yeelight, “LED Bulb (Color)” *Yeelight*. [Online]. Available: https://www.yeelight.com/en_US/product/wifi-led-c. [Accessed: 30-Jun-2019].
- [64] “Buy a Raspberry Pi 3 Model B – Raspberry Pi,” *Raspberry Pi Foundation*. [Online]. Available: <https://www.raspberrypi.org/products/raspberry-pi-3-model-b-plus/>. [Accessed: 08-Jul-2019].
- [65] “Buy a Raspberry Pi 4 Model B – Raspberry Pi,” *Raspberry Pi Foundation*. [Online]. Available: <https://www.raspberrypi.org/products/raspberry-pi-4-model-b/>. [Accessed: 08-Jul-2019].
- [66] Espressif, “espressif/arduino-esp32,” *GitHub*. [Online]. Available: <https://github.com/espressif/arduino-esp32> [Accessed: 18-Jul-2019].
- [67] Espressif, “SPP API,” *ESP-IDF Programming Guide*. [Online]. Available: https://docs.espressif.com/projects/esp-idf/en/latest/api-reference/bluetooth/esp_spp.html. [Accessed: 18-Jul-2019].
- [68] Adafruit, “adafruit/Adafruit_Si7021,” *GitHub*, 04-Apr-2019. [Online]. Available: https://github.com/adafruit/Adafruit_Si7021. [Accessed: 19-Jul-2019].
- [69] Shinyei Corporation of America, “Specification sheet of PPD42NS”, 19-Sep-2016.
- [70] D. Chabot, M. Bayer, and A. D. Roos, “Instantaneous heart rates and other techniques introducing errors in the calculation of heart rate,” *Canadian Journal of Zoology*, vol. 69, no. 4, pp. 1117–1120, 1991.
- [71] Yeelight, “Yeelight WiFi Light Inter-Operation Specification”, 2015.

Appendix A

Published Papers

The 1st article, entitled “**Wireless Sensor Network for Indoor Air Quality Monitoring**”, was accepted and presented at the 11th Conference on Telecommunications (ConfTele 2019), in June 26-28, 2019.

The conference was held at Sede da Ordem dos Engenheiros, Lisbon, and it was organized by the Telecommunications Specialization (Colégio de Engenharia Eletrotécnica) of Ordem dos Engenheiros (OE) and Instituto de Telecomunicações (IT).



11th CONFERENCE ON TELECOMMUNICATIONS
June 26th, 27th and 28th, 2019
Sede da Ordem dos Engenheiros, Lisboa
PORTUGAL

SCOPE
The 11th Conference on Telecommunications, **ConfTele 2019**, organized by the Telecommunications Specialization (Colégio de Engenharia Eletrotécnica) of Ordem dos Engenheiros and Instituto de Telecomunicações, will be held in the Headquarters of Ordem dos Engenheiros, Lisbon, Portugal, on June 26, 27 and 28, 2019. The theme of this year's conference is "Telecommunications Technologies Pursuing New Ways of Living and Travelling". The 11th ConfTele will bring together academia, operators, service providers, manufacturers and standardization bodies to explore activities, trends and future challenges towards ICT globalization for health, vehicular and resource optimization issues in existing and future telecommunication technologies.

FORMAT
The Conference includes plenary sessions with invited keynote speakers and talks, parallel thematic sessions (including regular oral and poster presentations), interactive sessions on the discussion of previously published papers, tutorials and exhibition. The exhibition will display recent developments in the area of telecommunications (prototypes, services, applications and trials). The technical activities will be held in English or Portuguese.

THE TECHNICAL PROGRAMME COMMITTEE INVITES THE SUBMISSION OF HIGH QUALITY, UNPUBLISHED TECHNICAL PAPERS IN (BUT NOT LIMITED TO) THE FOLLOWING LIST OF TOPICS:
Antennas, Microwaves and Radiowave Propagation | Artificial Intelligence and Machine Learning | Cloud Computing | Data Science | E-learning | Electronics for Telecommunications | Electronics and Power Systems for Telecommunications | Indoor and Outdoor Localization | Information Security, Jamming and Interference Techniques | Materials and Devices | Mobile and Wireless Communications | Mobile Computing | Multimedia Computing, Technologies and Applications | Networking | Optical Communications Systems | Photonics, Plasmonics, Electromagnetic Metamaterials | Quantum Effects in Information and Transmission | Sensors, Instrumentation, IoT and Applications | Serious Games, Entertainment Computing and Applications | Interactive Computing and Graphics | Services and Applications | Signal Processing | Vehicular Communications and Drones

SUBMISSION OF PAPERS
All contributions must be electronically submitted as 3/4-page full papers in PDF format according to the template provided at the Conference website. Please refer to the website for further submission ([easychair link](#)) details. At least one of the authors of accepted papers is required to be registered by June 5, 2019.

Technical Program Committee Abel Gomes, Adolfo Cartaxo, Américo Correia, Ana Aguiar, Ana Charas, Ana Fred, Armando Rocha, Arnaldo Oliveira, António Grilo, Atílio Gameiro, Carlos Fernandes, Custódio Peixeiro, Carlos Martinho, Catarina Brites, Daniel Corujo, Edmundo Monteiro, Fernando Martins, Frutuoso Silva, Henrique Gomes, Hugo Proença, João Canas Ferreira, João Vilela, Jorge Morgado, José Alberto	Fonseca, José Machado da Silva, José Vieira, Lúcia Bilro, Luís Bernardo, Luís Alexandre, Marco Gomes, Miguel Coimbra, Mário Figueiredo, Mário Freire, Maria do Carmo Medeiros, Nuno Garcia, Nuno Horta, Nuno Pombo, Paulo Monteiro, Pedro M. Ramos, Rafael Caldeirinha, Rogério Nogueira, Rui Campos, Rui Dinis, Sérgio Crisóstomo, Sérgio Faria, Sílvia Mariano, Telmo R. Fernandes and Vítor Silva	Organizing Committee Carlos Sá da Costa, Carlos Salema, Fernando J. Velez, Francisco Cercas, Ivo Sousa, Marcelino Pousa, Octavian Postolache, Paula Queluz, Pedro Sebastião, Rodolfo Oliveira and Teresa Salema
--	--	---

Special Sessions and Tutorials
Please, send email to conftele2019@e-projects.ubi.pt

DEADLINES
Reception of full-papers/Abstracts: April 29, 2019
Authors notification: May 15, 2019
Registration: June 5, 2019
ADDITIONAL INFORMATION AT
<http://www.conftele2019.ordemengenheiros.pt/>

Deadline for Interactive Sessions: May 20, 2019
Interactive Sessions Request Approval Notification: May 30, 2019
Conference secretariat: Secretariado dos Colégios da Ordem dos Engenheiros, Av. António Augusto de Aguiar, 3D, Lisboa

Wireless Sensor Network for Indoor Air Quality Monitoring

Mariana Jacob Rodrigues
Instituto de Telecomunicações, IT-IUL
ISCTE-IUL
Lisbon, Portugal
Mariana_Jacob@iscte-iul.pt

Octavian Postolache
Instituto de Telecomunicações, IT-IUL
ISCTE-IUL
Lisbon, Portugal
opostolache@lx.it.pt

Francisco Cercas
Instituto de Telecomunicações, IT-IUL
ISCTE-IUL
Lisbon, Portugal
francisco.cercas@lx.it.pt

Abstract— In this paper an indoor air quality monitoring system based on a wireless sensor network (WSN) is presented, within the Internet of Things (IoT) concept, to help preventing asthma crisis. The system not only monitors indoor environmental conditions, to prevent the triggering of an asthma crisis, but it also provides comfort-related conditions and information for people with obstructive pulmonary diseases, highlighting critical air quality conditions. The monitoring system consists of multiple sensing nodes designed to acquire temperature, humidity and the concentration levels of relevant gases. The data is wirelessly sent by each node to a coordinator node and then to an online database. A Web-based application was developed to provide data analysis, system control and alert mechanisms. Information mechanisms and environment conditions, such as a coded ambient lighting system, are also designed to generate a simple and efficient visual alert mechanism.

Keywords— wireless sensor network (WSN), internet of things (IoT), indoor air quality, respiratory impairment, web application, smart lighting

I. INTRODUCTION

Air pollution is one of the greatest environmental risks for human health and it can lead to a variety of health problems related to respiratory diseases. Chronic obstructive pulmonary diseases (COPD) and Asthma are among the most common respiratory illnesses, and they can be prevented by monitoring certain air quality parameters. These parameters are generally air pollutants that are widely present in urban areas, such as particulate matter (PM), ozone (O₃), sulphur dioxide (SO₂), nitrogen oxides (NO_x) and carbon monoxide (CO) [1]. According to the study in [2] several pollutants present in the air are associated with asthma-related hospital emergencies, from which PM₁₀, NO₂ and O₃ are the major contributors that potentially aggravate this respiratory illness.

In addition to these air pollutants, humidity can also trigger asthma exacerbations. A relative humidity between 40%-60% is ideal for indoor environments, as it minimizes most adverse health effects [3]. Values above 60% will turn the air harder to breath – besides narrowing and tighten the airways, humidity also makes the air stagnant and traps the pollutants and allergens, which can help trigger asthma attacks [4].

COPD exacerbations, for instance, are often triggered by viral or bacterial respiratory infections (70-80%), where the remaining 20-30% are related with exposure to environmental pollution [5], such as tobacco smoke and biomass-burning smoke.

The monitoring of these parameters and the implementation of an alert mechanism is crucial to help preventing respiratory

distress. The main objective of this work is to present an indoor air quality monitoring system that measures all critical causes able to trigger asthma crisis, such as the levels of pollutants present in the air, as well as the temperature and humidity levels in real-time. A smart lighting system will also be implemented to alert the user when the air-quality parameters exceed an imposed threshold value. This lighting system works both as an ambience optimizer and as an efficient alert system, according to the colour and frequency of the radiated light. In order to provide data analysis, system control and alert mechanisms, a dedicated web application called “Saga” was developed.

This paper is organized as follows: Section II presents the literature review, followed by Section III to describe the hardware and software of the system. Section IV presents and discusses the results obtained and Section V summarises the main conclusions and presents a perspective for future work.

II. RELATED WORK

Adopting a primary-prevention strategy for potential asthma attacks and COPD, authors in [6] developed a distributed smart sensing network for indoor air quality assessment based on semiconductor heated sensors and on three-electrode electrochemical sensors. A hybrid solution based on polynomial and artificial networks modelling was used for data processing purposes. A smartphone application was also developed to prevent asthma and COPD attacks through warnings, based on previously stored threshold values.

Salamone et al. [7] reported the design and implementation of a smart object that controlled the overall air quality using an air exchange system, as well as a lighting system, to optimize energy consumption and improve the user's comfort. Concentrations of CO₂ and luminosity levels were measured for that purpose. The final version of this smart object was built by following a “do-it-yourself” (DIY) approach.

Xinrong Li and Sherin Abraham [8] presented a wireless sensor network that used micro gas sensors, Xbee modules and an Arduino. The proposed system could simultaneously obtain 6 air quality-related parameters at different locations. A least-square estimation-based method was used for the sensor's data calibration.

Jung-Yoon Kim, Sang-Moon Shin and Chao Chu [9] created a system that monitors the concentration levels of six types of gas - ozone (O₃), carbon monoxide (CO), nitrogen oxides (NO₂), sulphur dioxide (SO₂), volatile organic compound (VOC) and carbon dioxide (CO₂) and particulate

matter (PM) – in real-time basis, providing overall air quality alerts.

Nikolas Vidakis et al. created Recodify [10], an embedded monitoring system that measures environmental parameters such as temperature, humidity, luminance and sound, as well as carbon monoxide, ozone levels and current consumption in real-time. A web application was also developed to support continuous monitoring, data visualization and node management, with an alert mechanism to notify users when measured values are out of a specific range.

The referred works are centred on the monitoring of air quality-related parameters, but none of them, except the first one [6], are focused on personalized monitoring of indoor air conditions, which are critical to help individuals with respiratory illnesses.

In this work, an innovative and scalable WSN solution based on the ESP32 microcontroller and the Raspberry Pi 3 B+ is presented. This solution has a special focus on the monitoring of air quality parameters that directly affect people with asthma and COPD, providing different warning notifications when air conditions are critical to the user. A web-based application for advanced processing and its GUI are also presented.

III. SYSTEM DESCRIPTION

In order to create an air quality measuring system that envisions to reduce the risk of asthma attacks and COPD, a wireless sensor network with multiple measuring nodes, a real-time database, a smart lighting system and a web application for the end-user was considered. A simplified diagram of the system is presented in Fig. 1.

The sensor network contains several nodes with different types of sensors that allow the acquisition and measurement of air quality-related parameters and other variables.

Each node communicates with a coordinator node (a Raspberry Pi) using Bluetooth protocol. This short-range communication protocol is widely used in IoT systems. With its ability to connect different devices and by presenting a lower power consumption when compared to Wi-Fi, this protocol proves to be quite efficient on establishing a wireless connection between the sensor nodes and the coordinator node.

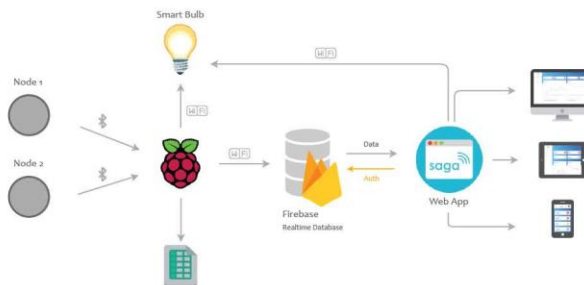


Fig. 1. System's Architecture

The coordinator node collects all the received data and sends it to Firebase, a Google's cloud hosted NoSQL Realtime database over the Internet, which was chosen due to its simplicity. Additionally, and to avoid losing data events, the acquired data is also saved on a local file on the Raspberry Pi 3 B+ SD card.

The system also has a smart ambient lighting system, changing its colour, intensity and frequency, to alert the user, according to previously determined codes, whenever the values measured by gas, temperature, and humidity sensors are potentially harmful. All this can be set by the user on a web application interface, according to personalized thresholds related to asthma. This interface is the system top layer, as it provides data analysis of the recorded data, giving the user a complete control over the entire system. It works on multiple platforms and it is compatible with most common operating systems, enabling it to be used by anyone through its personal computer, laptop, tablet or smartphone.

Throughout this section, a more detailed description of the system is provided. Firstly, hardware components and its implementation are described, followed by a brief description of the software used to develop this health monitoring system.

A. Hardware

Each sensor node consists of multiple sensors and a microcontroller: Node 1 is formed by a temperature and relative humidity sensor and a light intensity sensor (Light Dependent Resistor (LDR)).

For the temperature and relative humidity measurements, the Si7021 solid state sensor from Silicon Labs was used. It performs analog-to-digital conversions, signal processing, data calibration and it has an I²C communication interface. According to the manufacturer, this sensor performs relative humidity measurements with 3% accuracy and a measurement range of 0-80% RH, and temperature measurement accuracy of $\pm 0.4^{\circ}\text{C}$ for 10°C to 85°C measurement range. Due to its high accuracy and low power consumption, this sensor is quite suitable for measuring indoor thermal conditions.

A Light Dependent Resistor (LDR) is used to measure the indoor's light intensity levels which can also change the smart lighting power state. This inexpensive sensor changes its resistance, from around 400 Ω when exposed to 1000 Lux up to 1 M Ω when it is kept in the dark.

Node 2 includes a set of gas sensors. Since this system is intended to prevent the triggering of asthma crisis and COPD

exacerbations, they must detect Smoke, NO_x and CO, so the sensors used were the MQ-135, MQ-4 and MQ-9 sensors.

These sensors include a heating element and an electrochemical sensing unit expressed by a SnO₂ semiconductor. The heater is required because the sensitive

surface of the sensor is only reactive at certain higher temperatures. This surface has a low electrical conductivity when exposed to clean air, but it increases whenever it detects gases and particles in the air.

Each sensor can react to more than one type of gas, as specified in Table 1.

Table 1. Types of gas detected by each sensor

Sensor	Types of Gas
MQ-135	Air quality sensor with low selectivity (Ammonia (NH ₃), Nitrogen Oxides (NO _x), Alcohol, Benzene, Smoke and Carbon Dioxide (CO ₂))
MQ-4	Natural gas and Methane gas
MQ-9	Carbon Monoxide (CO), Methane and Liquefied Petroleum Gas (LPG)

Each WSN node is controlled by the ESP-32 microcontroller. This presents both Wi-Fi and Bluetooth wireless communication capabilities, being one of its greatest advantages when compared to the Arduino board (which would need an external Bluetooth module). It features a 32 bits dual core CPU, with a clock frequency that can go up to 240 MHz, and 520 kB of RAM.

For the coordinator node a Raspberry Pi 3 Model B+ is used. It works as a gateway between the final user and the sensing nodes, and it performs data analysis, control of actuators through a set of commands sent via Wi-Fi, and data transmission to an online database.

The actuator node incorporates the referred coded lighting subsystem to adapt the level, color or intensity variation of indoor lighting throughout the day, which then works as a smart and simple visual warning system. For testing purposes, the Yeelight LED Light Bulb (Color), from Xiaomi was used. This light bulb presents Wi-Fi connectivity and it can change between 16 million colors with a temperature range between 1700K - 6500K.

B. Software

The system software can be classified as embedded software and web application software. The ESP-32 is programmed with the Arduino IDE, using a C compiler. In each node, the board is set to perform the data acquisition from the measurement channels. Since the gas sensors have their output signal as voltage levels instead of gas concentration levels, their output was first normalized and calibrated. Since the gas sensor's voltage at their ADC output is a digital value from 0 to 4095, the calibration process required the conversion to gas concentration values using calibration curves provided by each sensor manufacturer.

After acquiring and processing the sensor's data, the microcontroller sends it to the Raspberry via Bluetooth.

By using a smart lighting system as the main alert mechanism, a warning mode was created to be performed by the smart bulb. This mode orders the smart bulb to perform a color transition cycle between two tonalities of red, which can be set to act as a common warning signal. This is only triggered when both humidity and temperature exceed a

chosen threshold value. For relative humidity, values between 40% and 60% are considered. Similarly to gas sensors, the MQ-135 humidity sensor will trigger an alert mechanism if a value of 100 ppm is exceeded.

As an additional improvement of indoor's lighting quality, the smart lighting system is also programmed to automatically change the color temperature and luminance levels throughout the day, to mimic natural light conditions. Whenever the indoor's light intensity, measured by an LDR, is higher than 700 lux, the smart lighting system turns off, for power saving purposes.

A Raspberry Pi was chosen as the WSN coordinator computation platform, and it is responsible to send the acquired data to an online database. Firebase Realtime Database was chosen for that purpose, due to its ease of access and available APIs.

IV. RESULTS

The system was tested in the laboratory, usually occupied by several people throughout the day (maximum 10 people). The sensor nodes were placed near the user's workplace, away from direct sunlight so the readings of temperature, humidity and gas were not influenced.

Calibration of the gas sensor was done with a chamber from Figaro with 235 x 180 x 210 mm of size, and an effective inner capacity of 5,400 ml. Different volumes of this substance were injected on this test chamber to find out a correlation between the gas concentration and the injected volume of gas. Tests were only made with Ethanol, since this is easier to obtain and safer than other types of gas.

The MQ-135 sensor was fully calibrated in this way. The different sensor responses regarding the different volumes of injected ethanol can be seen in Fig. 2. The readings are presented in parts per million (ppm) and the tests had a duration of 10 minutes. The blue line represents 0,54 ml of ethanol and the red line 0,6 ml. According to the test chamber's manufacturer, a volume of 0,54 ml equals to a concentration of 100 ppm.

As shown in Fig. 2, the gas concentration level stabilizes at 100 ppm for 0.54 ml after 4 min, which is the time this substance takes to effectively reach the sensor's surface.

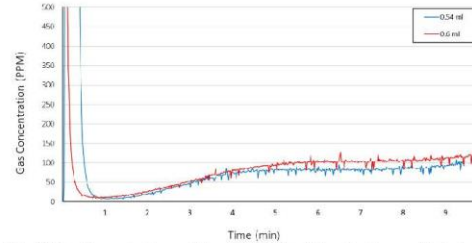


Fig. 2. Gas Concentration variation in PPM for different volumes of injected Ethanol (MQ-135 gas sensor)

In order to validate this correlation, the following formula was used [11]:

$$ppm = \frac{\text{Volume of Gas (ml)}}{0.0054} \quad (1)$$

Every gas sensor was calibrated by using the same principle, so the effective results obtained with the MQ-135 can be also verified on the other sensors.

Energy consumption of the sensor nodes was also monitored. Each node was powered up by a 10400 mAh power-bank. To reduce power consumption and extend the node's battery life, deep sleep modes were implemented on the ESP-32.

The measurements made on each node are presented in Fig.3.

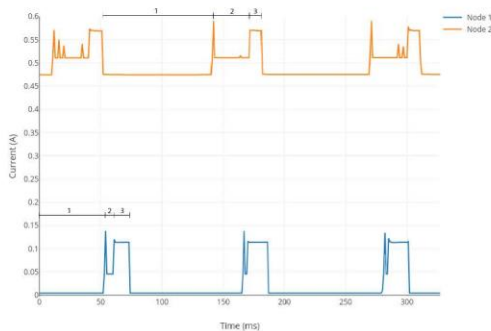


Fig. 3. Energy Consumption of each node while: (1)- on Deep Sleep Mode (2)- Waiting for connection (3)- Transmitting data

Each Bluetooth connection and data transmission are characterized by a sudden increase of the node's energy consumption. Node 1 presents an approximate value of only 4 mAh when on sleep mode, and 114 mAh when sending data over Bluetooth. Node 2, composed by three gas sensors with high energy consumption levels, presents values around 474 mAh when on deep sleep mode, 510 mAh when waiting for a Bluetooth connection and around 570 mAh when transmitting to the coordinator node. This gives the node an autonomy of approximately 20 hours.

As for the web application, it was designed to monitor the indoor air quality and to generate warning messages, with an additional safety status associated with each parameter. After the user performs an e-mail and password-based authentication, a dashboard with all values of temperature, humidity, smart bulb's temperature colour and gas concentration levels detected by each gas sensor is displayed. Given that different people may react to different types of triggering factors, the application provides the possibility of adjusting the threshold values used to signalize a likelihood of an asthma attack in a personalized manner.

To do so, the user needs to access his "User Profile" page where all the configurable values are displayed.

V. CONCLUSIONS AND FUTURE WORK

COPD and asthma are two common respiratory illnesses that are often triggered by certain air quality factors. To address this matter, a functional system that effectively monitors these elements and subsequently adopts a primary-prevention strategy was presented. The developed system is based on WSN and performs indoor air quality monitoring, consisting on multiple sensor nodes with temperature, relative humidity and gas sensors. The system implements different effective alert mechanisms and uses a unique web application for data analysis and system control. In the future, it is intended to expand the wireless sensor network with the addition of other sensor nodes for a full-house coverage. Different actuator nodes will be added to change indoor air conditions when needed.

ACKNOWLEDGMENTS

The work was supported by Fundação para a Ciência e Tecnologia, Project TailorPhy - PTDC/DTP-DES/6776/2014, Project UID/EEA/50008/2019 and Instituto de Telecomunicações.

REFERENCES

- [1] Ozlem Kar Kurt, Jिंगjing Zhang, and Kent E. Pinkerton, "Pulmonary Health Effects of Air Pollution", *Current opinion in pulmonary medicine*, vol 22(2), pp.138-143, 2016.
- [2] Galán, I., et al. "Short-Term Effects of Air Pollution on Daily Asthma Emergency Room Admissions." *European Respiratory Journal*, vol. 22, no. 5, 2003, pp. 802-808.
- [3] A. V. Arundel, E.M. Sterling, J. H. Biggin and T.D Sterling, "Indirect health effects of relative humidity in indoor environments", *Environmental health perspectives*, vol. 65, pp.351-61, 1986.
- [4] Stephanie Watson, "Humidity and Asthma: Effects of Humidity on Asthma & How to Prevent It," *Healthline*, 05-Apr-2018. [Online]. Available: <https://www.healthline.com/health/humidity-and-asthma> [Accessed: 11-Mar-2019].
- [5] Qureshi, Hammad et al. "Chronic obstructive pulmonary disease exacerbations: latest evidence and clinical implications." *Therapeutic advances in chronic disease*, vol. 5,5, pp. 212-27, 2014
- [6] O. Postolache, J. M. Pereira, P. S. Girão and G. Postolache, "Distributed Smart Sensing Systems for Indoor Monitoring of Respiratory Distress Triggering Factors". INTECH Open Access Publisher, 2011
- [7] F. Salamone, L. Belussi, L. Danza, T. Galanos, M. Ghellere and I. Meroni, "Design and Development of a Wearable Wireless System to Control Indoor Air Quality and Indoor Lighting Quality", 2017.
- [8] S. Abraham and X. Li, "A Cost-effective Wireless Sensor Network System for Indoor Air Quality Monitoring Applications," *Procedia Computer Science*, vol. 34, pp. 165-171, 2014.
- [9] J. Kim, C. Chu and S. Shin, "ISSAQ: An Integrated Sensing Systems for Real-Time Indoor Air Quality Monitoring", *IEEE Sensors Journal*, vol. 14, no. 12, pp. 4230-4244, 2014
- [10] N. Vidakis, M. A. Lasithiotakis, and E. Karapidakis, "Recodify- An Intelligent Environment and space hazard condition Monitoring System based on WSN and IoT technology," *Proceedings of the 22nd Pan-Hellenic Conference on Informatics - PCI 18*, 2018.
- [11] "SR-3 - Bench Top Test Chamber", *Product Information*, Figaro.

The 2nd article, entitled “**Indoor Air Quality System to Prevent the Triggering of Respiratory Distress**”, was presented at the 2nd International Symposium on Sensors and Instrumentation in Internet of Things Era (ISSI), in August 29-30, 2019, in Lisbon, Portugal.

The conference was organized by the IEEE Instrumentation and Measurement Society, ISCTE-IUL, Instituto de Telecomunicações (IT) and Shanghai Maritime University (SMU).

The scientific article received a Student Best Paper Award and will appear in IEEE Xplore.



ISSI 2019 2nd International Symposium on Sensing and Instrumentation in IoT Era | August 29-30 • Lisbon, Portugal

CALL FOR PAPERS

ISSI 2019 represents a forum where researchers, scientists, engineers and practitioners around the world will promote the advances in sensing and instrumentation for IoT. The symposium valorizes new and original research in IoT applications fields, such as smart cities, transportation, healthcare and farming.

The full version papers (4 to 6 pages) submitted to ISSI 2019 will be accepted based on peer review process. The accepted papers will be published in conference proceedings and will appear in *IEEE Xplore* and *EI Compendex*. Selected papers will be considered for publication in special issue of *Sensors*, SCI open Journal.

Topics of the symposium will include, but are not limited to:

- Smart Sensors and Wireless Sensor Networks for IoT;
- Test and Automated Instrumentation for IoT;
- Localization, Algorithms for Smart Sensor Network;
- Software Platforms and Middleware in Smart IoT Systems;
- IoT in Retail Logistics;
- IoT & Wearable Solutions for Healthcare;
- Big Data Processing in IoT Systems;
- Energy Harvesting and Scavenging for Wireless Sensors Networks and IoT;
- Standards for IoT and IoT Security;
- Industrial Internet of Things;
- Sensors and IoT for Smart Ports and Logistics;
- IoT for Healthcare;
- IoT Applications in Smart Cities;
- IoT Applications for Smart Homes;
- IoT in Smart Farming;
- IoT System Design Methodologies;

<https://sens-in-net.tech>

IMPORTANT DATES

March 17, 2019
Call for Special Sessions & Workshops

May 19, 2019
Papers Submission Deadline

June 15, 2019
Paper Acceptance Notification

July 7, 2019
Camera Ready Paper Submission

July 15, 2019
Registration

CONTACTS:

Octavian Postolache
ISCTE-IUL & IT, Portugal
E-mail: opostolache@lx.it.pt

IEEE INSTRUMENTATION & MEASUREMENT SOCIETY

instituto de telecomunicações **ISCTE IUL**
Instituto Universitário de Lisboa

上海海事大学
SHANGHAI MARITIME UNIVERSITY

ORGANIZERS

GENERAL CHAIRS

Octavian Postolache
ISCTE-IUL & IT, Portugal

Yongsheng Yang
Shanghai Maritime University, China

Subhas Mukhopadhyay
Macquarie University, Australia

TECHNICAL PROGRAM CHAIRS

Pedro Silva Girão
Universidade de Lisboa, Portugal

Joaquim Mendes
Universidade do Porto, Portugal

Francisco Martin
Universidad de Oviedo, Spain

Domenico Capriglione
Università degli Studi di Salerno, Italy

PUBLICATION CHAIRS

Sérgio Matos
ISCTE-IUL, Portugal

José Miguel Dias Pereira
Instituto Politécnico de Setúbal, Portugal

Daofang Chang
Shanghai Maritime University, China

Fang Yu
Shanghai Maritime University, China

LOCAL ORGANIZATION CHAIRS

Octavian Postolache
ISCTE-IUL & IT, Portugal

Francisco Cercas
ISCTE-IUL & IT, Portugal

Indoor Air Quality Monitoring System to Prevent the Triggering of Respiratory Distress

Mariana Jacob Rodrigues
Instituto de Telecomunicações, IT-IUL
ISCTE-IUL
Lisbon, Portugal
Mariana_Jacob@iscte-iul.pt

Octavian Postolache
Instituto de Telecomunicações, IT-IUL
ISCTE-IUL
Lisbon, Portugal
opostolache@lx.it.pt

Francisco Cercas
Instituto de Telecomunicações, IT-IUL
ISCTE-IUL
Lisbon, Portugal
francisco.cercas@lx.it.pt

Abstract— In this paper, an indoor air quality monitoring system based on a wireless sensor network (WSN) and compatible with the internet of things (IoT) is presented. By providing relevant information about indoor air conditions, the system may help to prevent the triggering of respiratory distresses, such as an asthma crisis, by highlighting critical air quality conditions. The sensor network contains several sensing nodes with temperature, humidity, gas and particulate matter sensors, and a set of actuators that will help improve indoor's thermal comfort and lighting quality. A Web-based application was developed to provide data analysis, system control and alert mechanisms for asthma attacks prevention. A smart lighting system was implemented to generate visual alert mechanisms and improve indoor's lighting comfort.

Keywords— indoor air quality, indoor lighting quality, environmental medicine, respiratory impairment, wireless sensor network (WSN), internet of things (IoT), web application

I. INTRODUCTION

Air pollution is one of the greatest environmental risks for human health and it can lead to a variety of health problems related to respiratory diseases. Chronic obstructive pulmonary diseases (COPD) and asthma are among the most common respiratory illnesses, but they can be prevented by monitoring certain air quality parameters. These parameters are generally air pollutants that are widely present in urban areas, such as particulate matter (PM), ozone (O_3), sulphur dioxide (SO_2), nitrogen oxides (NO_x) and carbon monoxide (CO) [1]. According to the study in [2] several pollutants present in the air are associated with asthma-related hospital emergencies, from which PM_{10} , NO_2 and O_3 are the major contributors that potentially aggravate this respiratory illness. Air pollution needs to be considered specially in indoor environments: according to the U.S Environmental Protection Agency (EPA) [3], indoor levels of pollutants can be 2 to 5 times higher than outdoors. Since population usually spends approximately 90% of their time inside buildings, these factors are of great concern. Some of these pollutants are created by indoor sources such as combustion sources, cleaning products, air conditioners (without maintenance) and building materials, and can potentially aggravate respiratory distress and asthma attacks.

In addition to these air pollutants, humidity can also trigger asthma exacerbations. A relative humidity between 40%-60% is ideal for indoor environments, as it minimizes most adverse health effects [4]. Values above 60% will turn the air harder to breath – humidity also makes the air stagnant and traps the pollutants and allergens, which can help trigger asthma attacks.

However, a poor indoor air quality does not only affect individuals who have respiratory disorders. Common symptoms may have an impact over a person's well-being such as headaches, fatigue, shortness of breath, coughing, dizziness, and many others. These types of symptoms can also be induced by the lack of some indoor environmental quality (IEQ) components, such as poor lighting quality and high sound intensity levels. A good lighting quality not only plays an important role in an individual's visual capacity, but also has many positive biological effects. Adequate lighting levels during the day and night can regulate circadian sleep-wake rhythms and vastly improve an individual's health, productivity and comfort. Therefore, the development of a system with smart lighting that automatically changes the colour temperature and illuminance levels of light throughout the day is of major importance.

The monitoring of these parameters, actuation and implementation of an alert mechanism is crucial to help preventing respiratory distress and improve IEQ levels. The main objective of this work is to present an indoor air quality monitoring system that measures the levels of pollutants present in the air, as well as the temperature and humidity levels in real-time. A smart lighting system will also be implemented to adapt both the level and the colour of indoor lighting throughout the day, as well as alerting the user when the air-quality parameters exceed an imposed threshold value. In order to provide data analysis, system control and an additional alert mechanism, a unique web application called "Saga" was also developed.

This paper is organized as follows: Section II presents the literature review, followed by Section III, where the system's description of the hardware and software is made. The obtained results are presented and discussed in Section IV, followed by Section V that summarises conclusions and future work.

II. RELATED WORK

There is a wide variety of indoor air quality monitoring systems with different distributed sensing solutions. An indoor and outdoor air quality monitoring system providing wireless data transmissions, accurate sensory measurements based on advanced processing algorithms and pollution detection is presented in [5].

Adopting a primary-prevention strategy for potential asthma attacks and COPD, authors in [6] developed a distributed smart sensing network for indoor air quality assessment based on semiconductor heated sensors and on three-electrode electrochemical sensors. A hybrid solution based on polynomial and artificial networks modelling was used for data processing purposes. A smartphone application was also developed to prevent asthma and COPD attacks through warnings, based on previously stored threshold values.

Salamone et al. [7] reported the design and implementation of a smart object that controlled the overall air quality using an air exchange system, as well as the lighting system, to optimize energy consumption and improve the user's comfort. Concentrations of CO₂ and luminosity levels were measured for that purpose. The final version of this smart object was built by following a "do-it-yourself" (DIY) approach.

Xinrong Li and Sherin Abraham [8] presented a wireless sensor network that used micro gas sensors, Xbee modules and an Arduino. The proposed system could simultaneously obtain six air quality-related parameters at different locations. A least-square estimation-based method was used for the sensor's data calibration.

Jung Kim et al. [9] developed a system that monitors the concentration levels of six types of gas - ozone (O₃), carbon monoxide (CO), nitrogen oxides (NO₂), sulphur dioxide (SO₂), volatile organic compound (VOC) and carbon dioxide (CO₂) and particulate matter (PM) - in real-time basis, providing overall air quality alerts.

Nikolas Vidakis et al. created Recodify [10], an embedded monitoring system that measures environmental parameters such as temperature, humidity, luminance and sound, as well as carbon monoxide, ozone levels and current consumption in real-time. A web application was also developed to support continuous monitoring, data visualization and node management, with a notification alert for when measured values are out of a specific range.

In this paper, we present an innovative and scalable WSN solution based on the ESP32 microcontroller, the core of every sensor node, and a Raspberry Pi 3 B+, which acts as the WSN coordinator. This solution has a special focus on the monitoring of air quality parameters that directly affect people with asthma and COPD, providing different warning notifications when air conditions are critical to the user. Indoor's thermal comfort, air quality and lighting quality are changed and improved through the implementation of actuator nodes, automatically controlled by the coordinator node. A web-based application providing full remote control over the system and real-time monitoring of the environment is also presented.

III. SYSTEM DESCRIPTION

In order to create an indoor air quality measuring system that envisions to reduce the risk of asthma attacks and COPD by monitoring respiratory distress triggering factors, a wireless sensor network with multiple measuring nodes, a real-time database, a set of actuators and a web application for the end-user was considered. To improve the indoor environmental quality (IEQ) levels, a smart light system was also implemented, alongside with the monitoring of indoor's sound intensity levels. A simplified diagram of the proposed system is presented in Fig. 1.

The sensor network contains several nodes with different types of sensors that allow the acquisition and measurement of air quality-related parameters and other variables.

Each node communicates with a coordinator node (a Raspberry Pi) using the Bluetooth protocol. This node collects all the received data and sends it to Firebase, a Google's cloud hosted NoSQL Realtime database, over the internet.

Additionally, and to avoid losing data events, the acquired data is saved on a local file, on the Raspberry Pi 3 B+ SD card.

The WSN has multiple actuator nodes, each one controlled by the coordinator node through Wi-Fi: a smart lighting system to adapt both the level and the colour of indoor lighting throughout the day and to alert the user when the values measured by gas, temperature and humidity sensors are potentially harmful (according with personalized thresholds stored on the database), a humidifier to increase humidity (moisture) levels, and finally a single-room ventilation unit to displace indoor pollutants, increase thermal comfort or dehumidify the environment. Then, a unique web application developed for this purpose is used to analyse the recorded data, to give the user manual control over the smart lighting system and other actuators, to allow the user to modify the threshold values related to asthma, and to implement an additional alert mechanism. The application works on multiple platforms and it is compatible with the most common operating systems, enabling it to be used by anyone through its personal computer, laptop, tablet or smartphone.

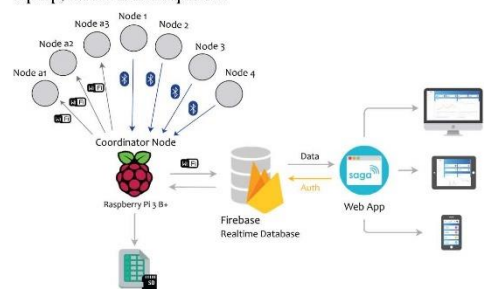


Fig. 1. System's Architecture

Throughout this section, a more detailed description of the system's main components is given. First, the hardware components and its implementation are described, followed by a complete description of the software elements used to develop this health monitoring system.

A. Hardware

Each sensor node (Node 1- 4) consists of multiple sensors and a microcontroller: Node 1 is formed by a temperature and relative humidity sensor, a light intensity sensor (Light Dependent Resistor (LDR)) and an electret microphone amplifier.

For the temperature and relative humidity measurements, the Si7021 solid state sensor from Silicon Labs was used. It performs analog-to-digital conversions, signal processing, data calibration and it has an I²C communication interface. It has low power consumption and performs relative humidity measurements, with $\pm 3\%$ accuracy and a measurement range of 0-80% RH, and temperature measurements accuracy of $\pm 0.4^\circ\text{C}$ for a 10°C to 85°C measurement range [11]. Due to its high accuracy and low power consumption, this sensor was chosen to measure the indoor thermal comfort during daily activities.

To measure indoor's light intensity, a Light Dependent Resistor (LDR) is used. The LDR is made of a material that changes its resistance according to the intensity of the light that illuminates it. Its resistance can go up to $1\text{ M}\Omega$ when kept in the dark and will drop significantly when exposed to light (400 Ω for 1000 Lux). Its final application will be described in the Software's section.

An electret microphone amplifier, model MAX9814 from Adafruit, is also used to measure sound levels.

Node 2 includes a set of gas sensors. In order to measure indoor gas concentrations, including those considered relevant to the triggering of asthma crisis and COPD exacerbation, such as NO_x, CO and Smoke [2], the MQ-135, MQ-4, and MQ-9 sensors are used. These sensors include a heating element and an electrochemical sensing unit expressed by a SnO₂ semiconductor. The heater is required because the sensor's sensitive surface is only reactive at certain temperatures. This surface has a low electrical conductivity when exposed to clean air. Whenever the sensing element detects gases and particles in the air, its electrical conductivity increases. Each sensor can react to more than one type of gas, as specified in Table 1.

Table 1. Types of Gas detected by each sensor

Sensor Type	Types of Gas
MQ-135	Air quality sensor with low selectivity (Ammonia (NH ₃), Nitrogen Oxides (NO _x), Alcohol, Benzene, Smoke and Carbon Dioxide (CO ₂))
MQ-4	Natural gas and Methane gas
MQ-9	Carbon Monoxide (CO), Methane and Liquefied Petroleum Gas (LPG)

The airborne particulate matter (PM) has a great impact on human health, especially in individuals with respiratory impairment. To measure PM concentrations, an additional WSN measurement node (Node 3) was considered. It includes a Shinyei PPD42NS particle counter that detects particles with $1\ \mu\text{m}$ or less in diameter. Its operation mode is based on the light-scattering principle, by determining the size of small particles in suspension. The sensor has a light chamber with a light emitting diode and a photo-diode detector. Once the

particles present in the air get inside the chamber, near-forward scattering properties of those particles are measured [12]. The sensor's output signal consists of Low Pulse Occupancy (LPO) measurements (the amount of time that the digital signal is held low, due to the presence of particles in the chamber), which are proportional to their concentration.

Finally, Node 4 has another Si7021 with temperature and relative humidity measurement capabilities. It will provide, alongside with Node 1, information about the spatial distribution of temperature and humidity.

Each WSN sensing node is characterized by the ESP-32 microcontroller. The node presents both Wi-Fi and Bluetooth wireless communication capabilities being one of its greatest advantages when compared to the Arduino board, which would need an external Bluetooth module. It features a 32 bits dual core CPU, with a clock frequency that can go up to 240 MHz, and 520 kB of RAM.[13].

For the coordinator node a Raspberry Pi 3 Model B+ is used. It works as a gateway between the final user and the sensing nodes, and performs data analysis, actuators control and data transmission to an online database.

Relatively to the actuator nodes, three nodes were added: Node a1, Node a2 and Node a3. Node a1 incorporates smart lighting to customize the level and color of indoor lighting to the user needs, and to signalize risky air conditions to users with respiratory impairments. The Yeelight LED Light Bulb (Color), from Xiaomi is used for that purpose. This light bulb presents Wi-Fi connectivity and it can change between 16 million colors with a temperature range between 1700K - 6500K.

The humidifier (Node a2) and ventilation unit's (Node a3) power states are remotely controlled by a TP-LINK Wi-Fi Smart Plug, model HS100.

B. Software

The system software can be classified as embedded software and web application software. The ESP-32 is programmed with the Arduino IDE, using a C compiler. In each node, the board is set to perform data acquisition from the measurement channels. The gas sensors voltage outputs are acquired and a digital value from 0 to 4095 is obtained at the ADC output. The conversion of the digital value to gas concentration levels is based on the gas sensor's calibration curves.

First, the analog value needs to be converted into voltage levels. The ESP32 ADCs have 12 bits resolution (unlike the ESP8266 and Arduino that only have 10 bits), therefore the total range of the ADCs readings go up to 4,095 (instead of 1,023 as on the ESP8266 and Arduino).

To perform the following steps of the sensor's calibration, the sensitivity calibration curve available in each sensor's datasheets [14][15][16] was used. Taking the MQ-135 sensitivity curve as an example, a formula based on the correlation between Rs/Ro and PPM was obtained. A y-axis and x-axis graph was created by picking the data points from the sensitivity characteristic of the sensor in the presence of Ethanol. By adding a power trendline to the resulting graph, the following expression was deduced:

$$c [\text{ppm}] = a_1 \times \left(\frac{R_s}{R_o}\right)^{-a_2} \quad (1)$$

where c is the concentration of gas in ppm, a_1 and a_2 are the coefficients of the obtained trendline equation and R_0 is the sensor resistance at 100 ppm of NH_3 or 50 ppm of alcohol in clean air. The value of R_s can be obtained by the following expression:

$$R_s = R_L \times \left(\frac{V_c}{V_{out}} - 1 \right) \quad (2)$$

with R_L as the load resistance. For this project, a R_L of 20 k Ω as specified in the sensor's datasheet was considered, alongside a V_c value of 5V. After primary processing of the sensor data, the microcontroller sends it to the Raspberry via Bluetooth.

The code for the Raspberry, the main core of this system, is written in Python and it is programmed to receive the data transmitted by each sensor node through Bluetooth.

The light intensity, gas, particulate matter, temperature and relative humidity readings are used to control the actuator's nodes according to previously specified thresholds. The smart lighting system is considered the main alert mechanism to prevent respiratory distress (asthma crisis and COPD) with the execution of warning signals: if the relative humidity or temperature values exceed an imposed threshold value, a command is sent via Wi-Fi to the Yeelight Light Bulb. This command orders the smart bulb to perform a color transition cycle between two tonalities of red, thus performing a warning signal. The same behavior is also applied for gas and particulate matter sensors readings. The pre-defined threshold values for temperature and humidity, based in [4], can be seen in Table 2.

Table 2. Threshold values of temperature and humidity used to prevent an asthma attack

Threshold	Measured Values	
	Temperature [°C]	Humidity [%]
Min	15	40
Max	30	60

In order to improve the smart lighting system while adapting both the level and the colour of indoor lighting throughout the day, a set of commands are sent to the smart bulb. Each command adjusts its colour temperature according to the time of the day, considering the colour temperature range of the smart bulb. The smart light's colour temperature variance throughout the day depends on the period of the day.

The WSN coordinator computation platform (Raspberry Pi) is also responsible for sending the acquired data to an online database. Firebase Realtime Database is used for that purpose, due to its ease of access and available APIs. In order to write data in the database, a Python interface is used with the Firebase's REST API. To make sure the sensor readings are always available, that same data is also saved locally on the Raspberry's SD card, on a LibreOffice calc spreadsheet.

As for the web application, it is designed to monitor the indoor air quality in real-time and warn the user if indoor air conditions are critical.

The user can also modify the temperature and humidity thresholds, as well as turning on/off the actuators. The application starts with a login page that requires an email and password authentication, as seen in Fig. 2.

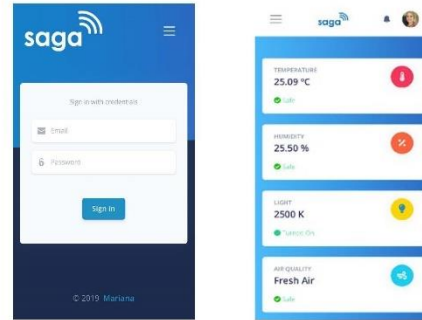


Fig. 2. Login form and Dashboard of the web application viewed on the smartphone version

Firebase SDK Authentication methods are used for that purpose. After a user is successfully logged in, a dashboard is displayed with the last reading made by each sensor node. The data displayed on the web application is retrieved from the Firebase Realtime database. The app was built using HTML 5, JavaScript, CSS and Bootstrap 4, jQuery and FusionCharts frameworks.

IV. RESULTS

The system was tested in the laboratory occupied by 10 people throughout the day. The sensor nodes were placed near the user's workplace and away from direct sunlight (see Fig. 6) so that the readings performed by the temperature, humidity and gas sensors were not influenced. The microcontrollers were programmed to send the data every 3 minutes to the coordinator node.

In order to test the gas sensor's calibration, the MQ-135 sensor was placed inside a gas sensor test chamber from Figaro with 235 x 180 x 210 mm of size, and with an effective inner capacity of 5,400 ml. The gas of interest is injected in the chamber and it is mixed with air by a built-in fan, so that the gas concentration is maintained uniform.

Ethanol was the injected substance, since it is easier to obtain and safer to use than the other types of gas. In this case, a 0.54 ml and 0.6 ml volume was injected.

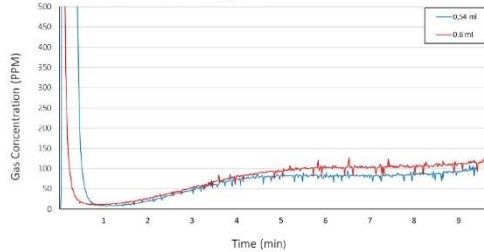


Fig. 3. Gas Concentration variation in PPM for different volumes of injected Ethanol (MQ-135 gas sensor)

The readings are presented in parts per million (PPM) and the tests lasted 10 minutes. According to the test chamber's

manufacturer, a volume of 0,54 ml alcohol injected by a syringe corresponds to a concentration of 100 ppm of gas.

As shown in Fig. 3, the gas concentration level stabilizes at 100 ppm for 0.54 ml after 4 min, which is the time this substance takes to effectively reach the sensor's surface. Every gas sensor was calibrated by using the same principle.

In order to validate this correlation, the following formula was used:

$$\text{ppm} = \frac{\text{Volume of Gas (ml)}}{0.0054} \quad (3)$$

A practical approach regarding the indoor's spatial distribution of temperature and relative humidity levels was considered. Therefore, Node 1 and Node 4 were placed at different locations of the room. The node's placement can be seen in Fig. 6. Temperature and relative humidity measurement were performed during 24h and can be seen in Fig. 4. In the figure, stage ① corresponds to the moment when the room is empty. Higher relative humidity levels are measured by the node close to the window (Node 1) during the night. At stage ②, the window's shutter is opened, which results in the rapid growth of temperature levels inside the room. At stage ③, windows were opened and, considering that outdoors temperature rounded the 30°C, the indoor's temperature levels increased even more. Relative humidity, as expected, presented low levels during the day and started to increase at around 18h00.

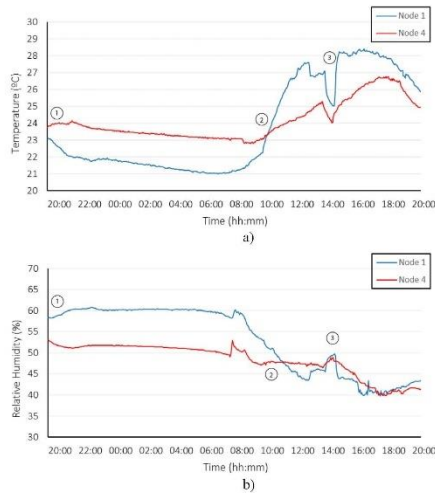


Fig. 4. Distributed temperature a) and relative humidity b) measurements during 24h.

Regarding the particulate matter measurements, the particles sensor was placed in a vertical position, in order to achieve the desired airflow expected by the designers. The samples were taken every 30s, as recommended by the manufacturers, and then averaged after 3 minutes.

The particles concentration is calculated by using a cubic polynomial derived from the characteristic graph that correlates the LPO time with the concentration of particles per 0.01 cubic

feet (pcs/283ml). Tests were made for this sensor for 14 hours continuously, as shown in Fig.5, where the average values demonstrate an indoor environment with very low pollution levels. A value below 600 pcs/0.01cf corresponds to low pollution levels, whereas values above 900 pcs/0.01cf correspond to high pollution levels.

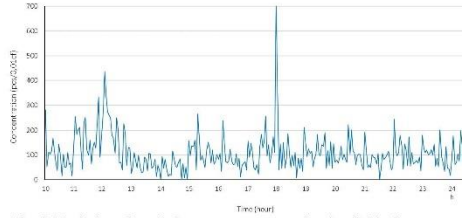


Fig. 5. Evolution of particulate matter concentration (pcs/0.01 cf) over time

To reduce power consumption and extend the WSN autonomy, deep sleep modes were implemented on the ESP-32 microcontroller. WSN's Node 1, for example, presented an energy consumption of about 82 mAh when active and without performing any background activity or Bluetooth transmission. After implementing this energy consumption optimization strategy, the energy consumption lowered to 8 mAh on deep sleep mode. For Bluetooth data transmissions, which only take about 4 seconds, the node's energy consumption reached 114 mAh. Node 3 and 4 have similar current consumptions. Node 2, however, consumes a greater amount of energy as expected. When all three gas sensors were operating with high energy consumption levels, a value of 474 mAh was presented when on sleep mode and approximately 570 mAh when transmitting data. Powered by a 10400 mAh power-bank, this node presented approximately 20 hours of autonomy.

As for the web application, after the user logs in, a Dashboard is displayed with the latest sensor readings saved on the database: temperature, relative humidity, the current light's temperature of the smart bulb, an air quality estimation based on the particulate matter concentrations and the values of gas concentrations in ppm. In order to develop an alert mechanism and inform the user about the different asthma and COPD attack triggering factors state, a small text revealing the safety status associated with each variable is presented below each reading: If temperature and humidity values exceed the threshold values assigned to these two parameters (Table 2), a red "Not Safe" message with an exclamation icon is displayed. If the values are within that range, a green "Safe" message takes place. For the light's indicator, its power state and the current colour temperature of the smart bulb are displayed.

As mentioned before, the user has the chance of changing the threshold values used to signalize a likelihood of an asthma attack. To do so, the user needs to access his "User Profile" page where all the configurable values are displayed.

Although the web app already serves as a warning signal, the smart lighting is used as the main alerting mechanism. Whenever the temperature, humidity or gas level's readings are out of the specified thresholds, the smart bulb performs a colour transition cycle between two tonalities of red as a warning signal, which can be noticeable straightaway.

The humidifier and ventilation unit power state are also induced by the temperature and humidity threshold values. If relative humidity is below the minimum value (dry environment), the coordinator node sends a command to the humidifier's smart plug, changing its power state. The same logic is used with the ventilation unit, for when the temperature readings exceed the maximum values.

The web application also triggers an alert message, followed by a message that explains its possible cause and it can only be dismissed if the user presses the OK button. If the readings are still out of the specified thresholds after 3 minutes, the same alert mechanism is triggered. The application has also an additional section with the room's floor plan, in which the user can visualize all sensor nodes locations and all data associated with each node, as shown in Fig. 6.

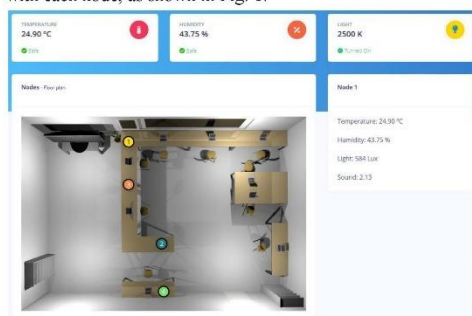


Fig. 6. Sensor nodes location and their respective data displayed on the web application.

Regarding the development of a smart lighting system to automatically change the light's colour temperatures throughout the day, its proper functioning was tested during a full working day. The colour temperature is set via the Raspberry Pi, which changes the bulb's properties by sending to it commands through Wi-Fi. A developed algorithm matches the light's colour temperature to a specific period of the day. The smart bulb only turned on to perform the warning signal or whenever the indoor's light intensity measured by the LDR sensor was below 700 lux. Otherwise, it was turned off for power saving purposes.

V. CONCLUSIONS AND FUTURE WORK

COPD and asthma are two common respiratory illnesses that are often triggered by certain air quality factors. To address this matter, a smart system that performs real-time monitoring and actuates as part of a primary-prevention strategy was presented. The developed system is based on a WSN and performs indoor air quality monitoring, consisting on multiple sensor nodes with temperature, relative humidity, gas and particulate matter sensors, and on several actuator nodes that enhance indoor air quality and indoor thermal comfort levels. The system implements different effective alert mechanisms and uses a unique web application for data analysis and system control. Considering the indoor's spatial distribution of temperature and relative humidity, tests were performed using two different

nodes placed at different locations of the room. Energy consumption levels were measured, and power saving strategies were implemented in each node to extend their autonomy. In future work, it is intended to expand the wireless sensor network with the addition of other sensor nodes and actuators for a full-house coverage.

ACKNOWLEDGEMENTS

The work was supported by Fundação para a Ciência e Tecnologia, Project TailorPhy - PTDC/DTP-DES/6776/2014, Project UID/EEA/50008/2019 and Instituto de Telecomunicações.

REFERENCES

- [1] Ozlem Kar Kurt, Jingjing Zhang, and Kent E. Pinkerton, "Pulmonary Health Effects of Air Pollution", *Current opinion in pulmonary medicine*, vol. 22(2), pp.138-143, 2016.
- [2] Galán, I., et al. "Short-Term Effects of Air Pollution on Daily Asthma Emergency Room Admissions." *European Respiratory Journal*, vol. 22, no. 5, 2003, pp. 802–808.
- [3] "Indoor Air Quality," EPA, 16-Jul-2018. [Online]. Available: <https://www.epa.gov/report-environment/indoor-air-quality> [Accessed: 11-Mar-2019].
- [4] A. V. Arundel, E.M. Sterling, J. H. Biggin and T.D Sterling, "Indirect health effects of relative humidity in indoor environments", *Environmental health perspectives*, vol. 65, pp.351-61, 1986.
- [5] O. Postolache, M. Dias Pereira, P. Silva Girão, "Smart Sensor Network for Air Quality Monitoring Applications", *Proceedings IEEE Instrumentation and Measurement Technology Conference (IMTC'2005)*, Vol. I, pp. 537-542, Ottawa, Canada, May 2005.
- [6] O. Postolache, J. M. Pereira, P. S. Girão and G. Postolache, "Distributed Smart Sensing Systems for Indoor Monitoring of Respiratory Distress Triggering Factors". *INTECH Open Access Publisher*, 2011.
- [7] F. Salamone, L. Belussi, L. Danza, T. Galanos, M. Ghellere and I. Meroni, "Design and Development of a Nearable Wireless System to Control Indoor Air Quality and Indoor Lighting Quality", 2017.
- [8] S. Abraham and X. Li, "A Cost-effective Wireless Sensor Network System for Indoor Air Quality Monitoring Applications," *Procedia Computer Science*, vol. 34, pp. 165–171, 2014.
- [9] J. Kim, C. Chu and S. Shin, "ISSAQ: An Integrated Sensing Systems for Real-Time Indoor Air Quality Monitoring", *IEEE Sensors Journal*, vol. 14, no. 12, pp. 4230-4244, 2014.
- [10] N. Vidakis, M. A. Lasithiotakis, and E. Karapidakis, "Recodify- An Intelligent Environment and space hazard condition Monitoring System based on WSN and IoT technology," *Proceedings of the 22nd Pan-Hellenic Conference on Informatics - PCI 18*, 2018.
- [11] "Si7021 Datasheet." *Silicon Laboratories*, 2016. Available:<https://www.silabs.com/documents/public/datasheets/Si7021-A20.pdf>, 2019
- [12] E. Austin, I. Novosselov, E. Seto, and M. G. Yost, "Laboratory Evaluation of the Shinyei PPD42NS Low-Cost Particulate Matter Sensor," *Plos One*, vol. 10, no. 9, Sep. 2015.
- [13] "ESP32 Series Datasheet", *Espressif*, 2019. Available:https://www.espressif.com/sites/default/files/documentation/esp32_datasheet_en.pdf
- [14] "Technical Data MQ-135 Gas Sensor", *Hanwei Eletronics*. Available:https://www.electronicoscaldas.com/datasheet/MQ-135_Hanwei.pdf
- [15] "MQ-4 Semiconductor Sensor for Natural Gas", *Hanwei Eletronics*. Available: <https://www.pololu.com/file/0J311/MQ4.pdf>
- [16] "Semiconductor Sensor for CO/Combustible Gas", *Hanwei Eletronics*. Available:<http://www.huoyuelectronics.com/Attachment/MQ-9/MQ9.pdf>

Appendix B

Best Paper Award



Appendix C

Gas Sensors Datasheets

HANWEI ELECTRONICS CO.,LTD

MQ-135

<http://www.hwsensor.com>

TECHNICAL DATA

MQ-135 GAS SENSOR

FEATURES

Wide detecting scope
Stable and long life

Fast response and High sensitivity
Simple drive circuit

APPLICATION

They are used in air quality control equipments for buildings/offices, are suitable for detecting of NH₃,NO_x, alcohol, Benzene, smoke,CO₂,etc.

SPECIFICATIONS

A. Standard work condition

Symbol	Parameter name	Technical condition	Remarks
V _c	Circuit voltage	5V±0.1	AC OR DC
V _H	Heating voltage	5V±0.1	ACOR DC
R _L	Load resistance	can adjust	
R _H	Heater resistance	33 Ω ± 5%	Room Tem
P _H	Heating consumption	less than 800mw	

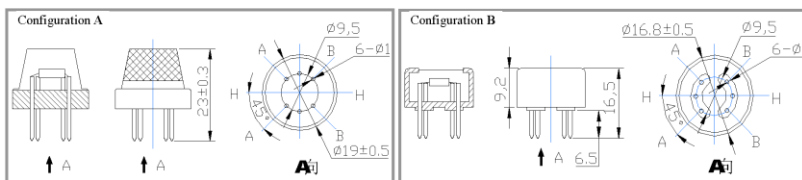
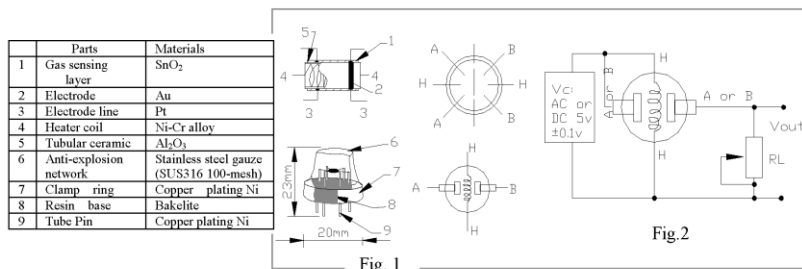
B. Environment condition

Symbol	Parameter name	Technical condition	Remarks
Tao	Using Tem	-10℃-45℃	
Tas	Storage Tem	-20℃-70℃	
R _H	Related humidity	less than 95%Rh	
O ₂	Oxygen concentration	21%(standard condition)Oxygen concentration can affect sensitivity	minimum value is over 2%

C. Sensitivity characteristic

Symbol	Parameter name	Technical parameter	Ramark 2
R _s	Sensing Resistance	30K Ω -200K Ω (100ppm NH ₃)	Detecting concentration scope: 10ppm-300ppm NH ₃ 10ppm-1000ppm Benzene 10ppm-300ppm Alcohol
α (200/50) NH ₃	Concentration Slope rate	≤0.65	
Standard Detecting Condition	Temp: 20℃±2℃ Humidity: 65%±5%	V _c :5V±0.1 V _H : 5V±0.1	
Preheat time	Over 24 hour		

D. Structure and configuration, basic measuring circuit



Structure and configuration of MQ-135 gas sensor is shown as Fig. 1 (Configuration A or B), sensor composed by micro AL₂O₃ ceramic tube, Tin Dioxide (SnO₂) sensitive layer, measuring electrode and heater are fixed into a crust made by plastic and stainless steel net. The heater provides necessary work conditions for work of

TEL: 86-371-67169070 67169080

FAX: 86-371-67169090

E-mail: sales@hwsensor.com

sensitive components. The enveloped MQ-135 have 6 pin ,4 of them are used to fetch signals, and other 2 are used for providing heating current.

Electric parameter measurement circuit is shown as Fig.2

E. Sensitivity characteristic curve

Fig.2 sensitivity characteristics of the MQ-135

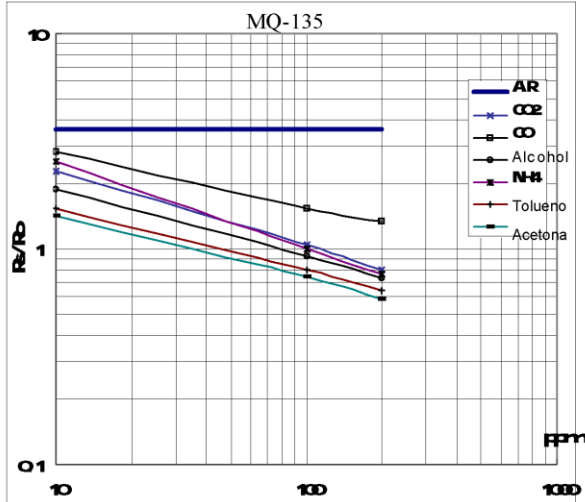


Fig.3 is shows the typical sensitivity characteristics of the MQ-135 for several gases.

in their: Temp: 20°C,
Humidity: 65%,
O₂ concentration 21%
RL=20k Ω

R₀: sensor resistance at 100ppm of NH₃ in the clean air.
R_s:sensor resistance at various concentrations of gases.

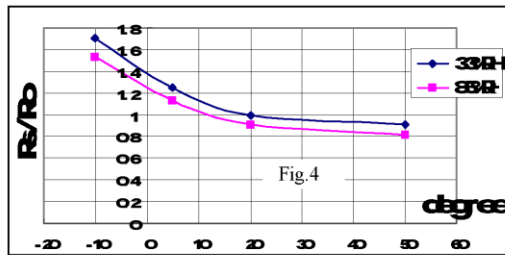


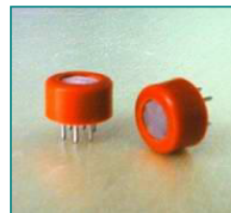
Fig.4 is shows the typical dependence of the MQ-135 on temperature and humidity.

R₀: sensor resistance at 100ppm of NH₃ in air at 33%RH and 20 degree.
R_s: sensor resistance at 100ppm of NH₃ at different temperatures and humidities.

SENSITIVITY ADJUSTMENT

Resistance value of MQ-135 is difference to various kinds and various concentration gases. So,When using this components, sensitivity adjustment is very necessary. we recommend that you calibrate the detector for 100ppm NH₃ or 50ppm Alcohol concentration in air and use value of Load resistancethat(R_L) about 20 K Ω (10K Ω to 47 K Ω).

When accurately measuring, the proper alarm point for the gas detector should be determined after considering the temperature and humidity influence.



MQ-4 Semiconductor Sensor for Natural Gas

Sensitive material of MQ-4 gas sensor is SnO₂, which with lower conductivity in clean air. When the target combustible gas exist, The sensor's conductivity is more higher along with the gas concentration rising. Please use simple electrocircuit, Convert change of conductivity to correspond output signal of gas concentration.

MQ-4 gas sensor has high sensitivity to Methane, also to Propane and Butane. The sensor could be used to detect different combustible gas, especially Methane, it is with low cost and suitable for different application.

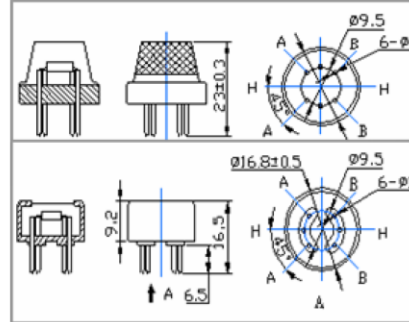
Character

- * Good sensitivity to Combustible gas in wide range
- * High sensitivity to Natural gas
- * Long life and low cost
- * Simple drive circuit

Application

- * Domestic gas leakage detector
- * Industrial Combustible gas detector
- * Portable gas detector

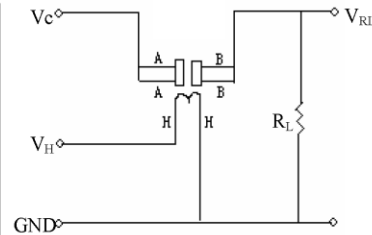
Configuration



Technical Data

Model No.		MQ-4	
Sensor Type		Semiconductor	
Standard Encapsulation		Bakelite (Black Bakelite)	
Detection Gas		Natural gas/ Methane	
Concentration		300-10000ppm (Natural gas / Methane)	
Circuit	Loop Voltage	V _c	≤24V DC
	Heater Voltage	V _H	5.0V±0.2V AC or DC
	Load Resistance	R _L	Adjustable
Character	Heater Resistance	R _H	31Ω±3Ω (Room Tem.)
	Heater consumption	P _H	≤900mW
	Sensing Resistance	R _s	2KΩ-20KΩ(in 5000ppm CH ₄)
	Sensitivity	S	R _s (in air)/R _s (5000ppm CH ₄)≥5
	Slope	α	≤0.6(R _{5000ppm} /R _{3000ppm} CH ₄)
Condition	Tem. Humidity	20℃±2℃; 65%±5%RH	
	Standard test circuit	V _c : 5.0V±0.1V; V _H : 5.0V±0.1V	
	Preheat time	Over 48 hours	

Basic test loop



The above is basic test circuit of the sensor. The sensor need to be put 2 voltage, heater voltage (V_H) and test voltage (V_C). V_H used to supply certified working temperature to the sensor, while V_C used to detect voltage (V_{RL}) on load resistance (R_L) whom is in series with sensor. The sensor has light polarity, V_c need DC power. V_C and V_H could use same power circuit with precondition to assure performance of sensor. In order to make the sensor with better performance, suitable R_L value is needed: Power of Sensitivity body (P_s):

$$P_s = V_c^2 \times R_s / (R_s + R_L)^2$$

$$\text{Resistance of sensor}(R_s): R_s = (V_c / V_{RL} - 1) \times R_L$$

Sensitivity Characteristics

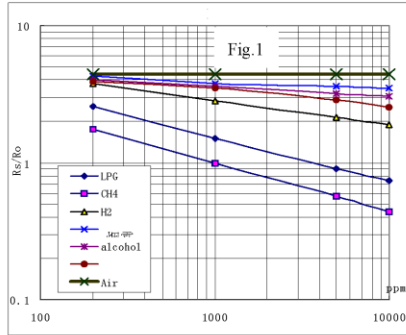


Fig. 1 shows the typical sensitivity characteristics of the MQ-4, ordinate means resistance ratio of the sensor (Rs/Ro), abscissa is concentration of gases. Rs means resistance in different gases, Ro means resistance of sensor in 1000ppm Methane. All test are under standard test conditions.

P.S.: Sensitivity to smoke is ignite 10pcs cigarettes in 8m³ room, and the output equals to 200ppm Methane

Influence of Temperature/Humidity

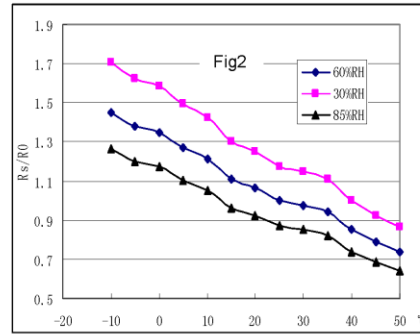
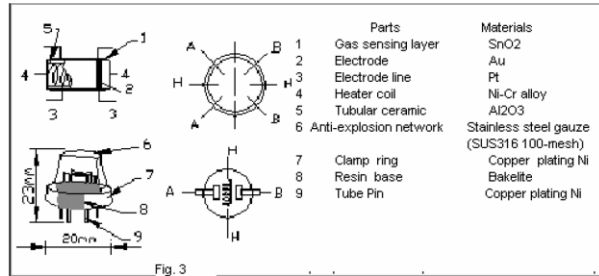


Fig.2 shows the typical temperature and humidity characteristics. Ordinate means resistance ratio of the sensor (Rs/Ro), Rs means resistance of sensor in 1000ppm Methane under different tem. and humidity. Ro means resistance of the sensor in environment of 1000ppm Methane, 20°C/65%RH

Structure and configuration



Structure and configuration of MQ-4 gas sensor is shown as Fig. 3, sensor composed by micro AL2O3 ceramic tube, Tin Dioxide (SnO2) sensitive layer, measuring electrode and heater are fixed into a crust made by plastic and stainless steel net. The heater provides necessary work conditions for work of sensitive components. The enveloped MQ-4 have 6 pin, 4 of them are used to fetch signals, and other 2 are used for providing heating current.

MQ-9 Semiconductor Sensor for CO/Combustible Gas

Sensitive material of MQ-9 gas sensor is SnO₂, which with lower conductivity in clean air. It make detection by method of cycle high and low temperature, and detect CO when low temperature (heated by 1.5V). The sensor's conductivity is more higher along with the gas concentration rising. When high temperature (heated by 5.0V), it detects Methane, Propane etc combustible gas and cleans the other gases adsorbed under low temperature. Please use simple electrocircuit, Convert change of conductivity to correspond output signal of gas concentration.

MQ-9 gas sensor has high sensitivity to Carbon Monoxide, Methane and LPG. The sensor could be used to detect different gases contains CO and combustible gases, it is with low cost and suitable for different application.

Character

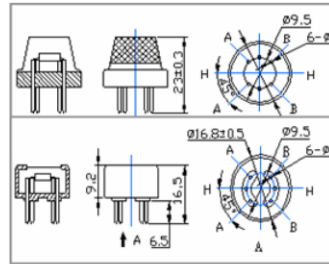
- * Good sensitivity to CO/Combustible gas
- * High sensitivity to Methane, Propane and CO
- * Long life and low cost
- * Simple drive circuit

Application

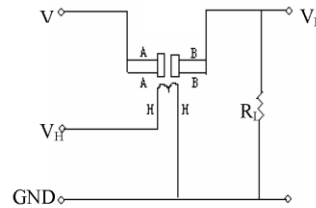
- * Domestic gas leakage detector
- * Industrial gas detector
- * Portable gas detector

Technical Data

Configuration



Basic test loop



The above is basic test circuit of the sensor. The sensor need to be put 2 voltage, heater voltage (VH) and test voltage (VC). VH used to supply certified working temperature to the sensor, while VC used to detect voltage (VRL) on load resistance (RL) whom is in series with sensor. The sensor has light polarity, Vc need DC power. VC and VH could use same power circuit with precondition to assure performance of sensor. In order to make the sensor with better

Model No.		MQ-9	
Sensor Type		Semiconductor	
Standard Encapsulation		Bakelite	
Detection Gas		CO and combustible gas	
Concentration		10-1000ppm CO 100-10000ppm combustible gas	
Circuit	Loop Voltage	Vc	≤10V DC
	Heater Voltage	VH	5.0V±0.2V AC or DC (High) 1.5V±0.1V AC or DC (Low)
	Heater Time	TL	60±1S (High) 90±1S (Low)
	Load Resistance	RL	Adjustable
Character	Heater Resistance	RH	31Ω±3Ω (Room Tem.)
	Heater consumption	PH	≤350mW
	Sensing Resistance	RS	2KΩ-20KΩ (in 100ppm CO)
	Sensitivity	S	RS(in air)/RS(100ppm CO) ≥5
	Slope	α	≤0.6 (R300ppm/R100ppm CO)
Condition	Tem. Humidity	20°C±2°C; 65%±5%RH	
	Standard test circuit	Vc: 5.0V±0.1V; VH (High) : 5.0V±0.1V; VH (Low) : 1.5V±0.1V	
	Preheat time	Over 48 hours	

performance, suitable RL value is needed:

Power of Sensitivity body (Ps): $Ps = Vc^2 \times Rs / (Rs + RL)^2$

Tel: 86-371-67169070/80 Fax: 86-371-67169090

Email: sales@hwsensor.com

Resistance of sensor(R_s): $R_s=(V_c/V_{RL}-1)\times R_L$

Sensitivity Characteristics

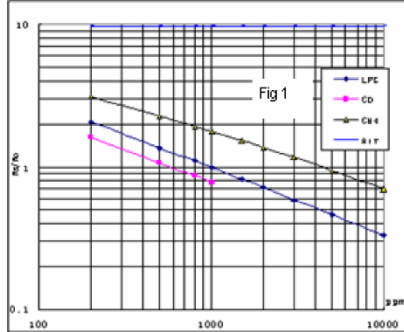


Fig. 1 shows the typical sensitivity characteristics of the MQ-9, ordinate means resistance ratio of the sensor (R_s/R_o), abscissa is concentration of gases. R_s means resistance in different gases, R_o means resistance of sensor in 1000ppm LPG. All test are under standard test conditions.

Influence of Temperature/Humidity

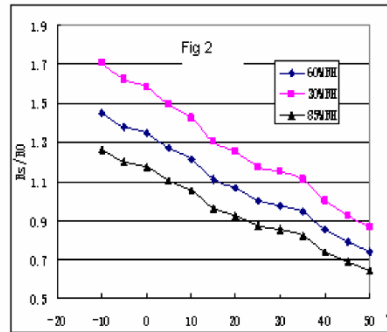
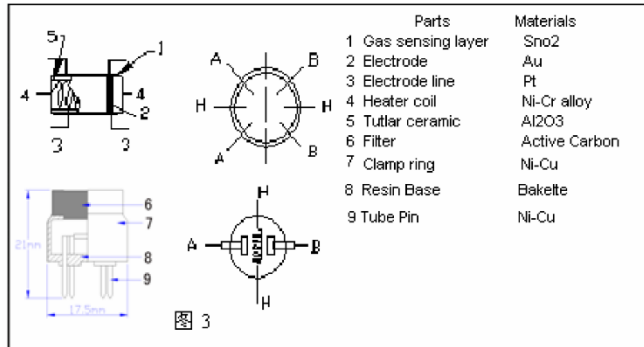


Fig.2 shows the typical temperature and humidity characteristics. Ordinate means resistance ratio of the sensor (R_s/R_o), R_s means resistance of sensor in 1000ppm Propane under different tem. and humidity. R_o means resistance of the sensor in environment of 1000ppm Propane, 20°C/65%RH

Structure and configuration



Structure and configuration of MQ-9 gas sensor is shown as Fig. 3, sensor composed by micro AL2O3 ceramic tube, Tin Dioxide (SnO2) sensitive layer, measuring electrode and heater are fixed into a crust made by plastic and stainless steel net. The heater provides necessary work conditions for work of sensitive components. The enveloped MQ-7 have 6 pin, 4 of them are used to fetch signals, and other 2 are used for providing heating current.